Peroxisome proliferators-activated receptor (PPAR) regulation in cardiac metabolism and disease

Hamid el Azzouzi

The research described in this thesis was performed at the Hubrecht Institute of the Royal Netherlands Academy of Arts and Sciences (KNAW), within the Graduate School of Developmental Biology, Utrecht, the Netherlands.

Hubrecht Institute of the Royal Netherlands Academy of Arts and Science (KNAW), Uppsalalaan, 83584 CT Utrecht, the Netherlands

Voor mijn ouders

Printed by: F&N Boekservice, Amsterdam
Cover and layout: © Ibra

ISBN:

Peroxisome proliferators-activated receptor (PPAR) regulation in cardiac metabolism and disease

Peroxisome proliferators-geactiveerde receptor (PPAR) regulatie in hartspier metabolisme en ziekte
(met een samenvatting in het Nederlands)

Proefschrift

ter verkrijging van de graad van doctor aan de Universiteit Utrecht
op gezag van de rector magnificus, prof. dr. J.C. Stoof,
ingevolge het besluit van het college voor promoties
in het openbaar te verdedigen
op dinsdag 13 januari 2009 des middags te 12.45 uur

door

Hamid el Azzouzi

Promotor

Prof. dr. H.C. Clevers

Co-promotoren

dr. L.J. de Windt
dr. M. van Bilsen

Het verschijnen van dit proefschrift werd mede mogelijk gemaakt door de steun van de Nederlandse Hartstichting en Interuniversitair Cardiologisch Instituut Nederland (ICIN).
Addtionele financiële ondersteuning werd verleend door J.E. Jurriaanse stichting.

Contents

PREFACE

Despite significant progress in the prevention and treatment of cardiovascular diseases, heart failure is still a leading cause of morbidity and mortality in industrial countries. A number of pathological conditions of the myocardium are accompanied by a reduction in fatty acid metabolism. During the development of cardiac hypertrophy, myocardial fatty acid oxidation (FAO) decreases and glucose utilization increases. In recent years, evidence has accumulated that this decrease in fatty acid utilization is due to, at least in part, a downregulation of genes that are involved in the catabolism of cardiac fatty acids. The peroxisome proliferator activated receptors (PPARs) are transcription factors in the family of steroid hormone receptors. PPARs have been demonstrated to bind to and be activated by fatty acids as well as a number of biological active fatty acid derivatives. During this transition, the reduced nuclear level of PPARα suggests that this phenomenon may be responsible for downregulation of cardiac FAO genes in the hypertrophied heart. Hence, understanding the mechanisms that regulate the activity of PPAR is crucial to determine the precise contribution of altered FAO at the genesis and progression of heart failure.

In **chapter 1** we review evidence of the versatile nature and many homeostatic functions of fatty acids, one of our more common dietary substrates. Many still associate these compounds with their role in the development of atherogenesis, but fatty acids also are the main resource for energy production in the healthy heart muscle. The balance between health and disease is tilted the wrong way when genetic mutations lead to the disruption of this continuous flow of energy, while also a balance exists between glucose and fatty acid utilization for cardiac energy metabolism, and utilizing one substrate to the exclusion of the other appears to favor the pathogenesis of cardiac disease. Fatty acids can further act as a double-edged sword in their capacity to either induce or prevent myocardial electrical remodeling, depending upon the dietary fatty acid species supplied to the heart. And finally, the gene expression profile of a cardiomyocyte may well be influenced by the supply of fatty acids provided on a day-to-day basis. The goal of this review is to distil complexities of fatty acid metabolism described in the literature and discuss the potential this complexity offers us for novel approaches in the daily treatment and management of myocardial disease.

Considerable evidence has established the importance of PPARs in myocardial lipid homeostasis and cardiovascular function. Yet, the PPAR isoform specific gene expression profile in the heart has not been fully delineated. In chapter 2 this caveat in the literature was experimentally addressed and a heart muscle gene expression profile of all PPAR isoforms was uncovered. To this end, we constructed murine ventricular clones allowing stable expression of siRNAs to specifically knockdown each of the PPAR isoforms. By combining gene profiling and computational PPRE analysis following PPAR isoform activation in normal versus PPAR deficient heart muscle cells we have, for the first time, determined the PPAR isoform-specific endogenous targets in the heart. One isoform-specific target gene was selected for further analysis. Electromobility shift and chromatin immunoprecipitation assays demonstrated the existence of an evolutionary conserved PPRE consensus-binding site

in an igf1 enhancer. In line, Wy-14643 mediated PPARα activation in the wild-type mouse heart resulted in upregulation of igf1 transcript abundace and provided protection against cardiomyocyte apoptosis following ischemia/reperfusion or biomechanical stress. Inhibition of the IGF1/PI3K pathway or PPARα-deficiency abrogated these effects, demonstrating a novel mechanism underlying the cardioprotective effects of PPARα in heart muscle.

Studies embarking on mitogen-activated protein kinase (MAPK) signaling cascades in the heart have indicated PPARα as a downstream effector that can be regulated through phosphorylation. The response of the postnatal heart to growth and stress stimuli includes activation of a network of signal transduction cascades, including the stress activated protein kinases such as p38 mitogen-activated protein kinase (MAPK), c-Jun NH2-terminal kinase (JNK) and the extracellular signal-regulated kinase (ERK1/2) pathways. In response to acute pressure overload stimulation induced by aortic banding, the mitogen-activated protein kinase kinase (MAPKK) MEK1 has been shown to be activated. Despite its importance, little is known about the relationship between MEK1-ERK1/2 pathway and cardiac PPAR signaling. In chapter 3 we show that activation of the MEK1-ERK1/2 pathway leads to specific inhibition of PPARα transcriptional activity. Furthermore we show, for the first time, that this inhibitory effect is mediated by MEK1, and not by its downstream effector kinase ERK1/2, through a mechanism involving direct binding to PPARα and subsequent stimulation of PPARα export out of the nucleus.

PPARβ/δ is an abundant member of the peroxisome proliferator-activated receptors (PPARs) family, a nuclear receptor family of ligand activated transcription factors. Limited information is available on the function of PPARβ/δ in the adult myocardium. In chapter 4 we addressed this scientific caveat using genetically modified mice to address the question whether altered fatty acid oxidation lies at the genesis and progression of heart failure. To circumvent the embryonic lethality associated with postnatal deletion of PPARβ/δ, we triggered conditional PPARβ/δ loss through the use of a tamoxifen-inducible Cre recombinase in the postnatal murine myocardium. Targeted PPARβ/δ deletion in adult mice provoked premature death within one week accompanied by rapid and dramatic biventricular enlargement, dramatic atrial enlargement, escorted by myocyte hypertrophy, myofiber disarray, ventricular fibrosis and strong induction of fetal gene transcripts and indications of severe disruption of fatty acid oxidation. Overall, these results indicate that PPARβ/δ loss suffices to impact both adult myocardial morphology and function.

The transcription factor myocyte enhancer factor 2 (MEF2) is transcriptional partner for PPAR in the heart. In addition, MEF2 is also a downstream target for several hypertrophic signaling pathways in the heart. In chapter 5, we demonstrated the transcriptional synergy between PPAR and MEF2, and further investigated the potential benefits of MEF2 inhibition in a mouse model of chronic pressure overloading. Therefore, we subjected wildtype and transgenic mice expressing a dominant negative form of MEF2 (DN-MEF2 Tg) in the heart to transverse aortic constriction (TAC). Histological analysis revealed no major differences in cardiac remodeling between DN-MEF2 Tg and wildtype mice after TAC. Surprisingly, echocardiographic analysis revealed that

DN-MEF2 Tg mice displayed an exaggerated decrease in cardiac function compared to control animals. Analysis of the mitochondrial respiratory chain showed that DN-MEF2 Tg mice displayed lower expression of NADH dehydrogenase subunit 6 (ND6), part of the large Complex I enzyme, only following pressure overload. The reduced expression of ND6 in DN-MEF2 Tg mice after pressure overload resulted in an increase in cell death secondary to overproduction of reactive oxygen species (ROS). These data suggest that a PPAR/MEF2 transcriptional complex is required for proper mitochondrial function and its inhibition predisposes the heart to impaired mitochondrial function, overproduction of ROS, enhanced cell death and cardiac dysfunction following pressure overload.

Chapter 6 reviews our findings and extrapolates the results described in this thesis to the current knowledge on the phenomenon that under pathological situations myocardial fatty acid oxidation decreases and glucose utilization increases, and to give direction to future research.

chapter

CHAPTER 1

Cardiac fatty acid homeostasis in health and diseasse

Hamid el Azzouzi, Leon J. De Windt

Published in part as:

De Windt LJ, Cox K, Hofstra L, Doevendans P. Molecular and genetic aspects of cardiac fatty acid homeostasis in health and disease. Eur Heart J. 2002;23:774-787.

Cardiac fatty acid metabolism

Fatty acids are simple molecules belonging to the lipid family and their basic biochemical structure consists of a hydrophilic (or water-soluble) group attached to one end of a hydrophobic (water-insoluble) hydrocarbon chain. Figure 1(a) depicts an example of palmitic acid, a common dietary fatty acid consisting of 16 carbon (C) atoms with all the carbons saturated with hydrogen (H) atoms. Palmitic acid is therefore referred to as a saturated fatty acid. Many important, naturally occurring fatty acids are unsaturated such as palmitoleic acid, meaning that the carbon atom chain contains one or more double bonds (Fig. 1(b)). These unsaturated bonds have important effects on the molecular structure of fatty acids, for each double bond inserts a bend in the hydrocarbon chain of the molecule, which will influence the melting point of the fatty acid. Ultimately, the fluidity of the membrane structure strongly depends upon the relative content of unsaturated to saturated fatty acid species in the membrane (Fig. 1(c)).

Fatty acids are delivered to the myocardium complexed to albumin or as fatty acyl esters, present in chylomicrons and very low density lipoprotein (VLDL) (1). Following transport to the mitochondria by a series of membrane transport proteins and intracellular binding proteins, the carboxylic group of fatty acids is converted to a coenzyme A (CoA) group to increase the solubility of fatty acids in the hydrophylic environment of the cytosol, or shuttled esterified to glycerol and remains in a small pool of triglyceride stores (2,3). Part of the resulting fatty acyl-CoA structures are subsequently converted into energy in the form of ATP for the multiple energy demanding processes in the cardiomyocyte at the level of the sarcomere for force generation or at the sarcolemma and sarcoplasmatic reticulum for intracellular ion homeostasis (2,4).

When used to generate ATP, fatty acids are catalytically broken down in mitochondria and peroxisomes by the -oxidation reaction. To this end, the fatty acyl-CoA esters are transported into the mitochondrial matrix via a carnitine-dependent shuttle mechanism (Fig. 2). The translocation of activated fatty acids across the mitochondrial membrane involves the combined action of three enzymes: carnitine palmitoyltransferase I (CPT I) at the outer mitochondrial membrane; carnitine:acylcarnitine translocase (CT) and carnitine palmitoyltransferase II (CPT II), which are both located at the inner mitochondrial membrane (Fig. 2). Once inside the mitochondrial matrix, the fatty acyl-CoA esters enter the -oxidation, four sequential reactions that result in the cleavage of two carbon atoms from the amino terminal end of the fatty acyl-CoA molecule, generating one molecule of acetyl CoA, a fatty acyl-CoA two carbons shorter, and reducing equivalents after each turn of the cycle (Fig. 2). The shorter fatty acyl-CoA is subsequently returned to the -oxidation spiral. The other product, acetyl CoA, can enter the citric cycle where it is oxidized further to generate NADH and FADH2 as endproducts. The latter two compounds are used to generate ATP via oxidative phosphorylation (Fig. 2) (2,4).

(a)

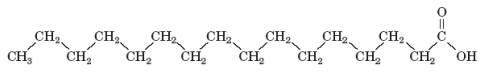

Palmitic acid = 16:0 = $CH_3(CH_2)_{14}COOH$

(b)

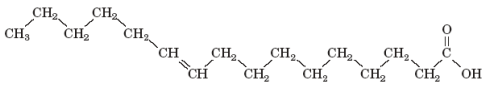

Palmitoleic acid = 16:1cΔ9 = $CH_3(CH_2)_7CH{=}CH(CH_2)_7COOH$

(c)

Palmitic acid	Abbreviation	Structure	Melting point (°C)
Palmitic acid	16:0	$CH_3(CH_2)_{14}COOH$	63·1
Stearic acid	18:0	$CH_3(CH_2)_{16}COOH$	69·6
Oleic acid	18:1cΔ9	$CH_3(CH_2)_7CH{=}CH(CH_2)_7COOH$	16
Linoleic acid	18:2cΔ9,12	$CH_3(CH_2)_4CH{=}CHCH_2CH{=}CH(CH_2)_7COOH$	5
Arachidonic acid	20:4cΔ5,8,11,14	$CH_3(CH_2)_4CH{=}CHCH_2CH{=}$ $CHCH_2CH{=}CH(CH_2)_3COOH$	–50

Figure1. Structure of fatty acids. (a) The basic chemical structure of a fatty acid exemplified by the chemical structure of a common dietary saturated fatty acid, palmitic acid. A fatty acid consists of a long hydrophobic (water insoluble) hydrocarbon chain (CH2 or CH3) linked to a hydrophilic head group (COOH). This fatty acid species is called saturated because it lacks a double bond in the hydrocarbon chain. (b) Chemical structure of an unsaturated fatty acid, palmitoleic acid, which only differs from its saturated counterpart palmitic acid by one double bond in the hydrocarbon chain between carbon atoms at positions 9 and 10 counted from the COOH group. Double bonds have a major impact on the molecular structure of the fatty acid species as it introduces a bend into the hydrocarbon chain, which ultimately influences the melting point of the fatty acid species. (c) List of most common saturated and unsaturated fatty acid species present in the human myocardium with their respective chemical abbreviation, structure formula and melting point. Note that the relative melting point of fatty acid species lowers as the number of double bonds increases.

Shift in energy metabolism – diabetes

Recent studies indicate that disrupted cardiac physiology arises not only from primary defects in energy metabolism, but that fatty acid metabolism contributes secondarily to the pathogenesis of more common disorders such as diabetic cardiomyopathy. It is well

established that patients with insulin dependent diabetes mellitus (IDDM) are particularly susceptible for heart failure (5). Experimental evidence suggests that the chronic cardiac metabolic changes in the IDDM patient largely contribute to the deteriorated state of the heart, independent from the various vascular effects associated with the disease. Diabetic patients have increased adipose tissue lipolysis and subsequently have higher circulating fatty acid levels. The rate of lipolysis within the diabetic heart is also increased, in concert with an expanded myocardial triacylglycerol pool. These factors, in addition to the reduced uptake of glucose across the sarcolemma, will lead to an almost complete reliance on fatty acids of both endogenous and exogenous sources for cardiac ATP generation and has been correlated to a direct inhibitory effect on glucose oxidation (6-9).

One explanation for the impaired glucose utilization by fatty acids in type II diabetes is through a reduction of glucose transport capacity, in particularly GLUT-4 activity (7,8), through increased glycogen deposition or through indirect activation of the pyruvate dehydrogenase complex. Additionally, concomitant intracellular accumulation of potentially toxic intermediates of fatty acid oxidation has been demonstrated to modify ion channel activity and properties (10,11), interfere with adenine nucleotide pathways and reduce myocardial ATP levels. These detrimental effects will ultimately lead to cardiac dysfunction through a disturbance in intracellular calcium (Ca2+) handling, intracellular Ca2+ overload and activation of Ca2+ dependent proteases and toxic Ca2+ deposition in mitochondria and depletion of ATP stores (12,13).

Studies performed in streptotozin-induced diabetic animals indicate that activation of the pyruvate dehydrogenase complex by dichloroacetate administration resulted in a switch from a reliance on fatty acids to glucose oxidation for energy production. An improvement in cardiac performance was observed, at least in the early stages of chronic diabetes (14). Pharmacological intervention with other drugs such as etomoxir, which specifically block CPT-I (and indirectly fatty acid oxidation), have also demonstrated to improve cardiac function in a number of experimental studies using diabetic animals models (15,16).

Collectively, these promising results in animal models have provided greater insight into IDDM-related cardiac dysfunction. Furthermore, from a clinical point of view, the future development and testing of drugs that stimulate cardiac glucose utilization at the expense of fatty acids might provide a new avenue for a more favorable cardiac energy metabolism and improved myocardial performance in patients with diabetic cardiomyopathy.

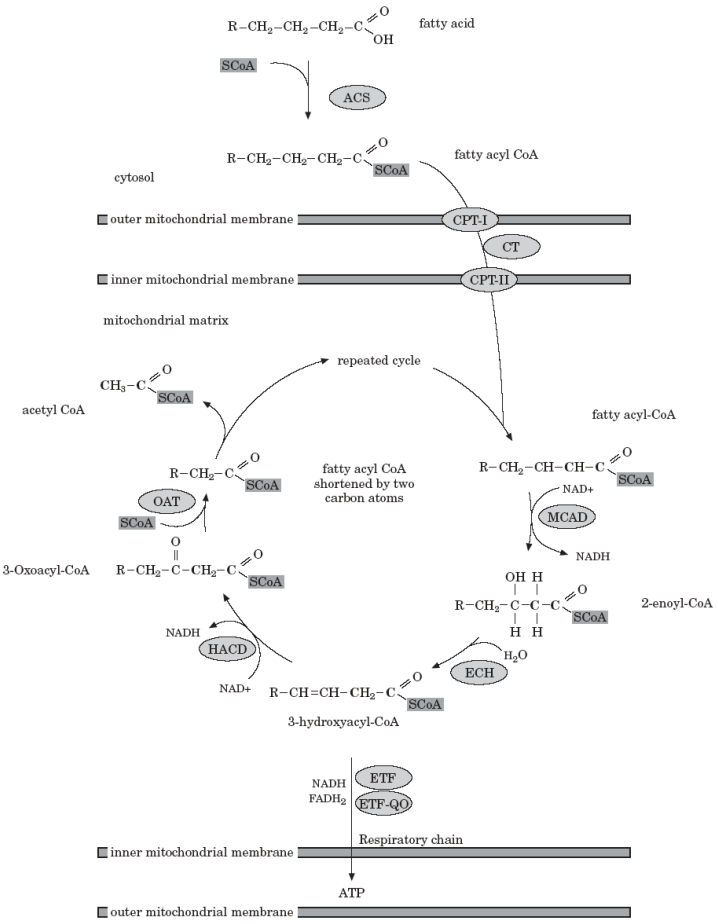

Figure 2. Mitochondrial fatty acid transport and β-oxidation cycle. Fatty acids are imported across mitochondria membranes into the mitochondrial matrix by the cooperative effort of specialized shuttle enzymes CPT-I, CT and CPT-II. The -oxidation cycle itself is catalyzed by a series of four enzymes in the mitochondrial matrix. At the same relative position of MCAD within the β-oxidation cycle, SCAD, LCAD and VLCAD are also positioned depending on the length of the chain of the fatty acid that is being oxidized. Each turn of the cycle shortens the fatty acid chain by two carbon atoms (shown in red) and generates one molecule of acetyl CoA and one molecule each of NADH and FADH2. The electrons carried by these coenzymes will be subsequently transferred to the electron transfer flavoproteins (ETF) and ETF-dehydrogenase (ETF-QO) which shuttle electrons to coenzyme Q in the respiratory chain in the mitochondrial inner membrane, to generate energy in the form of ATP. ACS=acyl-CoA synthase; CPT-I=carnitine palmitoyl transferase I; CT=carnitine:acylcarnitine translocase; CPT-II=carnitine palmitoyltransferase II; MCAD=medium chain acyl-CoA dehydrogenase; SCAD=short-chain acyl-CoA dehydrogenase; LCAD=long chain acyl-CoA dehydrogenase; VLCAD=very long chain acyl-CoA dehydrogenase; ECH=enoyl-CoA hydratase; HACD=hydroxyacyl-CoA dehydrogenase; OAT=keto-acyl thiolase.

Shift in energy metabolism – ischemic heart disease and heart failure

During oxygen deprivation as occurs in acute myocardial infarction (AMI) or during cardiac bypass surgery, both glucose and fatty acid oxidation are interrupted as a result of hypoxia (17,18). During periods of hypoxia affected regions of the heart are completely dependent on glyocolysis (or anaerobic metabolism) for ATP production.

As a result ATP levels fall rapidly as the energy yield of 1 mole glucose converted to lactate is only 5% of that yielded from the completed oxidation of 1 mole palmitate in the mitochondrial -oxidation. However, fatty acid activation (creation of fatty acyl CoA esters) continues to take place in the cytosol and, as a consequence, the level of fatty acyl esters of CoA and acylcarnitine species rise and are detectable 2 min after the onset of experimental global ischemia (19). The reinstitution of coronary blood flow (reperfusion) e.g. by thrombolytic or percutaneous intervention after AMI or after release of the cross-clamp during bypass surgery, will lead to a rapid return of both oxygen consumption and overall respiration chain activity to pre-ischemic levels.

Paradoxically, despite the return of oxidative metabolism and oxygen consumption during reperfusion, which is an absolute requirement for ultimate survival of the ventricular tissue, severe post-ischemic depression of contractile function is commonly observed. Because intracellular Ca2+ concentrations rise during ischemia and further increases after reperfusion, activation of Ca2+ transport processes, aimed at normalizing the intracellular Ca2+ homeostasis, may contribute to the rise in energy expenditure. Evidence consistent with this hypothesis was demonstrated in isolated rat hearts rendered globally ischemic, which demonstrated improved contractile function following addition of NiCl2 or ruthenium red during reperfusion to inhibit trans-sarcolemmal Ca2+ transport and Ca2+ transport at the inner mitochondrial membrane (20-23). These results indicate that the oxidative rate during reperfusion might arise from processes aimed at normalizing the intracellular ion homeostasis.

Although the accumulation of fatty acid intermediates during ischemia and changes in energy expenditure during reperfusion clearly contribute to the deterioration in mechanical function, it appears that the rise in fatty acid catabolism in the post-ischemic period has detrimental effects on the myocardium (22). It has been observed that fatty acid oxidation accounts for most of cellular oxidative metabolism during reperfusion, while glucose oxidation remains lower as compared to pre-ischemic levels. This metabolic alteration may be due to the higher plasma fatty acid levels, which are generally observed following AMI or cardiac surgery (24). An alternative explanation for the higher post-ischemic fatty acid oxidation, however, relates to the increase in cardiac AMP to ATP conversion due to limited ATP generation during ischemia. This accumulation of AMP results in phosphorylation and activation of 5'-AMP-activated protein kinase (AMPK).

Activated AMPK phosphorylates serine residues in acetyl-CoA carboxylase (ACC) during reperfusion resulting in the inhibition of ACC. Inactivation of ACC re-

sults in decreased malonyl-CoA levels and release of the malonyl-CoA inhibition of CPT-I. Elevated CPT-I activity in turn results in increased mitochondrial fatty acid uptake and oxidation, leading to inhibition of the pyruvate dehydrogenase complex and glucose oxidation.

The concomitant decrease in glucose oxidation causes impaired coupling of glycolysis to mitochondrial glucose oxidation and increased proton production from glycolytically derived ATP. Indeed, recent studies indicate that elevated proton production contributes to decreased functional recovery of hearts rendered experimentally ischemic. Efforts to pharmacologically stimulate glucose oxidation over fatty acid oxidation during reperfusion have emphasized the detrimental effects of loss of glucose oxidation capacity of the post-ischemic myocardium. Stimulation of the pyruvate dehydrogenase complex by administration of dichloroacetate or by using perfusion solutions with high concentrations of glucose (which increases intracellular pyruvate), have been shown to improve post-ischaemic haemodynamic recovery (24). Similar improvement was observed by inhibition of fatty acid oxidation by administering compounds as etomoxir (inhibitor of CPT-I), ranolazine and l-carnitine during reperfusion, all of which inhibit fatty acid -oxidation and favor glucose oxidation. Beneficial effects were also observed in clinical studies using a reperfusion solution containing high glucose, insulin and potassium, although these effects have not always been reproduced (25). Clearly, the beneficial effects of enhancing glucose oxidation during reperfusion at the expense of fatty acid oxidation merits further investigation, both in animal studies and in clinical trials. The ultimate goal would be to achieve an adjuvant therapy that would improve clinical mortality and morbidity in patients experiencing AMI by pharmacological stimulation of cardiac glucose oxidation over fatty acid oxidation e.g. during the acute reperfusion phase.

Fatty acids as regulators of cardiac gene expression

As mentioned above, a number of pathological conditions of the myocardium are accompanied by a reduction in fatty acid metabolism. In recent years, evidence has accumulated that this decrease in fatty acid utilization is due to, at least in part, a downregulation of genes that are involved in the catabolism of cardiac fatty acids.

It was soon realized that the expression patterns of these genes resulted from the influence of fatty acid metabolites directly on gene expression patterns. In fact, feeding rats a diet enriched with PUFAs increased CPT-I expression and activity in cardiac and skeletal muscle (26). Moreover, primary cardiomyocyte cultures incubated with certain fatty acid species at physiological levels displayed specific upregulation of mRNA levels of a transsarcolemmal fatty acid transporter (FAT), hearttype fatty acid binding protein, ACS and LCAD (27). One example of how fatty acids are thought to influence transcriptional activity of certain target genes is described below. The peroxisome proliferator activated receptors (PPARs) are transcription factors in the family of steroid hormone receptors. PPARs have been demonstrated to bind to and be activated by fatty acids as well as a num-

ber of biological active fatty acid derivatives (28).

Activated PPARs heterodimerize with the retinoic acid receptor X protein and bind to canonical peroxisome proliferator response elements in the promoter of target genes. Peroxisomes are essential organelles that have as one role the processing and oxidation of very long chain fatty acids. Analysis of the cis-regulatory elements in genes responsive to PPAR activation revealed a consensus DNA site consisting of a direct repeat of two hexameric half-sites (AGG(A/T)CA), separated by one nucleotide. In addition to genes involved in peroxisome function, these peroxisome proliferator-cis-regulatory DNA elements or PPREs have been identified in other genes directly involved in fatty acid metabolism or transport, such as acyl-CoA oxidase, acyl-CoA synthetase, medium-chain acyl-CoA dehydrogenase, the liver-type fatty acid binding protein and apolipoprotein A-II[127,128]. PPARs do not act alone. For their activation they need to dimerize with retinoic-X-receptors (RXR), which are activated by the vitamin A derivative 9-cis-retinoic acid (29). Consistent with this view, 9-cis-retinoic acid and fatty acid ligands can act together to synergistically activate the transcription of the peroxisomal gene acyl-CoA oxidase. Currently, multiple isoforms of PPARs with differing ligand selectivity and tissue distribution have been identified (30) and are currently under investigation as to the role of fatty acid-PPAR-RXR mediated influence on gene expression in the heart.

Peroxisome proliferator-activated receptor α (PPARα) is a nuclear receptor which is believed to act as a sensor of fatty acid and other metabolites to enable the cell to adapt to environmental changes through regulation of a large number of processes such as inflammation, differentiation and metabolism (31). PPARα is expressed in metabolically active tissues such as the liver, brown fat, kidney, skeletal muscle and heart (32). Transgenic mice with forced overexpression of PPARα in cardiac muscle display increased fatty acid oxidation rates, accumulation of triacylglycerides, decrease in glucose metabolism and eventually develop cardiomyopathy (33). In turn, mice deficient for PPARα have elevated free fatty acid levels as a consequence of inadequate fatty acid oxidation, rendering them hypoglycemic as a result of their reliance on glucose (34).The natural ligands for PPARα are fatty acids, such as medium and long chain fatty acids and eicosinoids. Synthetic ligands for PPAR comprise hypolipidemic, anti-inflammatory and insulin-sensitizing drugs. In the presence of a ligand, PPARs adopt an active conformation by forming an obligate heterodimer with the retinoid X receptor (RXR). Recruitment of additional co-activators leads to binding to peroxisome proliferator response elements (PPRE) in target genes, provoking PPAR-dependent gene expression.

During the development of cardiac hypertrophy, myocardial fatty acid oxidation (FAO) rats decrease and glucose utilization increases (35). During this transition, the reduced nuclear level of PPARα suggest that this phenomenon may be responsible for down-regulation of cardiac FAO genes in the hypertrophied heart (36). Hence, understanding the mechanisms that regulate the activity of PPARα is crucial to determine the precise contribution of altered FAO at the genesis and progression of heart failure. Apart from the classical ligand-dependant regulation, several studies have reported the modulation

of PPARα activity by phosphorylation. For example, insulin treatment induces phosphorylation, at the serine residues 12 and 21 in the transactivation domain, and subsequent activation of PPARα (37). PKA activators have also been shown to modulate the activity of PPARα through phosphorylation of several subdomains, including the DNA-binding domain and the ligand binding domain (38).

The response of the postnatal heart to growth and stress stimuli includes activation of a network of signal transduction cascades, including the stress activated protein kinases such as p38 mitogen-activated protein kinase (MAPK), c-Jun NH2-terminal kinase (JNK) and the extracellular signal-regulated kinase (ERK1/2) pathways (39). Studies embarking on MAPK signaling in the heart have indicated PPARα as a downstream effector that can be regulated through phosphorylation (40). Moreover, members of the p38 kinase family have been shown to phosphorylate PPARα in ligand dependant manner and results in enhanced transcriptional activity (40). Transgenic mice with cardiac-restricted expression of an activated form of MEK1 developed concentric hypertrophy with preserved cardiac function (41), indicating an important role for MEK1-ERK1/2 signaling pathway during cardiac hypertrophy. It is interesting to note that activation of the MEK1-ERK1/2 pathway led to inhibition of PPARγ transcriptional activity in cells (42,43), indicating a diverse effect of the different MAPK pathways on PPAR activity.

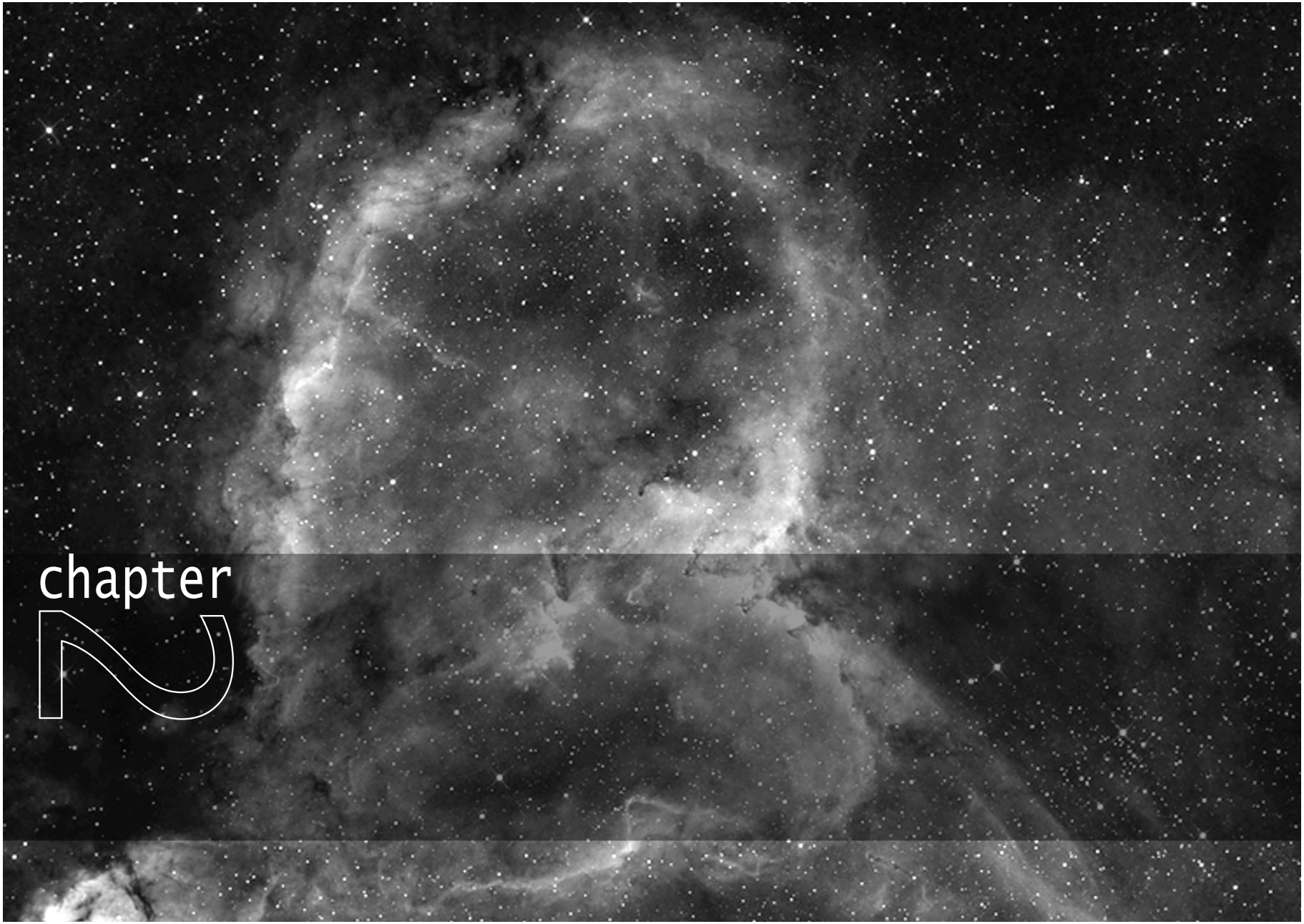
chapter
2

CHAPTER 2

PPAR gene profiling uncovers insulin-like growth factor-1 (IGF1) as a PPARα target gene in cardioprotection.

Hamid el Azzouzi, Stefanos Leptidis, Meriem Bourajjaj, Roel van der Nagel,
Marc van Bilsen, Leon J. De Windt

Submitted as:

Hamid el Azzouzi, Stefanos Leptidis, Meriem Bourajjaj, Roel van der Nagel,
Marc van Bilsen, Leon J. De Windt. PPAR gene profiling uncovers insulin-like growth factor-1 (IGF1) as a PPARα target gene in cardioprotection.

ABSTRACT

Peroxisome proliferators-activated receptors (PPARs) are members of the nuclear receptor family of ligand activated transcription factors and consist of the three isoforms, PPARα, PPARβ/δ and PPARγ. Considerable evidence has established the importance of PPARs in myocardial lipid homeostasis and cardiovascular function. Yet, the PPAR isoform specific gene expression profile in the heart has not been fully delineated. Here, we constructed murine ventricular clones allowing stable expression of siRNAs to specifically knockdown each of the PPAR isoforms. By combining gene profiling and computational PPRE analysis following PPAR isoform activation in normal versus PPAR deficient heart muscle cells we have, for the first time, determined the PPAR isoform-specific endogenous targets in the heart. Unexpectedly, electromobility shift and chromatin immunoprecipitation assays demonstrated the existence of an evolutionary conserved PPRE consensus-binding site in an *igf1* enhancer. In line, Wy-14643 mediated PPARα activation in the wild-type mouse heart resulted in upregulation of igf1 transcript abundace and provided protection against cardiomyocyte apoptosis following ischemia/reperfusion or biomechanical stress. Inhibition of the IGF1/PI3K pathway or PPARα-deficiency abrogated these effect, demonstrating a novel mechanism underlying the cardioprotective effects of PPARα in heart muscle.

INTRODUCTION

Long-chain fatty acids (FA) coordinately induce the expression of a panel of genes involved in cellular FA metabolism in cardiac muscle, thereby promoting FA oxidation in this organ (Gilde et al., 2003). These effects are likely mediated by peroxisome proliferator-activated receptors (PPARs), members of the nuclear receptor family of ligand activated transcription factors (21, 22). Given their function as essential transcriptional mediators of adipogenesis, lipid metabolism, insulin sensitivity, and glucose homeostasis, PPARs are increasingly recognized as key players in inflammatory cells and in cardiovascular diseases (CVD) such as hypertension, atherosclerosis, cardiac hypertrophy, and congestive heart failure (Boudina and Abel, 2007; Madrazo and Kelly, 2008; Smeets et al., 2007). In the presence of ligands, PPARs adopt an active conformation by forming an obligate heterodimer with the retinoid X receptor (RXR). Recruitment of additional co-activators provokes binding to peroxisome proliferator response elements (PPRE) in target genes, allowing PPAR-dependent gene expression (Guerre-Millo et al., 2001). Despite the high levels of homologies at the protein level, the three PPAR isoforms, PPARα, PPARβ/δ and PPARγ, exert different functions relying on differentially distribution in distinct tissues, isoform specific phosphorylation, selective interactions with their specific ligand and co-activators, and, likely, isoform-selective target gene activation (Boudina and Abel, 2007; Madrazo and Kelly, 2008; Smeets et al., 2007).

PPARα and PPARγ are characterized by their capacity to influence lipid metabolism, glucose homeostasis, cell proliferation, differentiation and apoptosis, as well as the inflammatory response (Boudina and Abel, 2007; Madrazo and Kelly, 2008; Smeets et al., 2007). PPARα activation mediates different effects such as the stimulation of lipid oxidation and anti-inflammatory effect by squelching the inflammatory transcription factor NF-κB (Ding et al., 2006; Hasegawa et al., 2005). Mice overexpressing PPARα in cardiac muscle display an increased fatty acid oxidation rates, accumulation of triacylglycerides, decrease in glucose metabolism and eventually develop cardiomyopathy (Finck et al., 2003; Finck et al., 2002). Not surprisingly, mice lacking PPARα have elevated free fatty acid levels as a consequence of inadequate fatty acids oxidation rendering them hypoglycemic as a result of their reliance on glucose (Guerre-Millo et al., 2001). Elucidation of the role of PPARγ in cardiac muscle has been hampered by its low abundance and the absence of significant effects of PPAR ligands such as ciglitazone and rosiglitazone on regulation of target genes (Gilde et al., 2003). Nevertheless, transgenic mice overexpressing PPARγ in the heart displayed increased cardiac FFA uptake without a concomitant reduction in glucose uptake, and ultimately developed severe heart failure (Ding et al., 2007).

Less is known about PPARβ/δ function in the heart. Heart muscle-restricted deletion of PPARβ/δ resulted in progressive myocardial lipid accumulation, cardiac hypertrophy and congestive heart failure (Cheng et al., 2004). Based upon the analysis of the PPARβ/δ null mouse model, PPARβ/δ deficiency leads to multiple developmental and metabolic abnormalities including frequent embryonic lethality, impaired wound healing

and skin abnormalities due to altered inflammatory responses in the skin (Barak et al., 2002; Peters et al., 2000). Studies in skeletal muscle cells have indicated a role for PPARβ/δ in the regulation of fatty acid oxidation where uncoupling proteins such as UCP-2 and UCP-3 were upregulated by PPARβ/δ (Chevillotte et al., 2001; Zhu et al., 1993). Selective overexpression of PPARβ/δ in the mouse heart provoked an increase in myocardial glucose utilization with no myocardial lipid accumulation and normal cardiac function (Burkart et al., 2007; He et al., 1999).

Whilst the above findings suggest that PPARs fulfill a necessary function in myocardial lipid homeostasis and cardiac function, the PPAR isoform-selective gene profiles in cardiac muscle responsible for their pleiotropic biological responses remain ill defined. To circumvent the non-specificity of PPAR synthetic ligands, we combined PPAR subtype selective siRNA knockdown with computational PPRE analysis to determine the PPAR isoform-specific endogenous targets in the heart muscle. PPARα activation also induced a unique, anti-apoptotic gene ontology which utilized activation of an endogenous insulin-like growth factor-1 (IGF1)/ phosphatidylinositol 3-kinase (PI3K) route. Electromobility shift and chromatin immunoprecipitation assays demonstrated the existence of an evolutionary conserved PPRE consensus-binding site in an *igf1* enhancer. Additionally, PPARα activation in the murine heart, through Wy-14643 administration, provoked induction of *igf1* expression and subsequent protection against ischemia/reperfusion induced apoptosis. Pharmacological inhibition of the igf1/PI3K pathway or a null allele for PPARα abrogated this effect. Finally, PPARα-deficient mice displayed impaired induction of *igf1* following ischemic insults or pressure induced overloading and a higher incidence of cardiomyocyte apoptosis, which contributed to deterioration of cardiac function.

MATERIALS AND METHODS

Animals. PPARα KO animals were purchased from Charles Rivers's lab. All protocols were performed according to institutional guidelines and approved by local Animal Care and Use Committees.

Cell culture and recombinant adenoviruses. Isolation and culture of neonatal rat ventricular cardiomyocytes was performed as described before in detail.(van Rooij et al., 2002) NKL-TAg cells were cultured and mortalized by AdCre infection as described previously. (Rybkin et al., 2003) (van Oort et al., 2006)

Generation of stable cardiac cell lines. To generate NKL-TAg clones harboring stably integrated constructs, NkL-TAg cells were transfected using FUGENE 6 reagent (Roche), with a vector expressing the PPAR iso-type specific siRNA, pcDNA4/TO-(siPPARα; siPPARβ/δ; siPPARγ), and selected in the presence of 500 μg/μl zeocin to generate stable cell lines.

Histological analysis and immunofluorescence microscopy. For histological analysis, hearts were arrested in diastole, perfusion-fixed with 4% paraformaldehyde, embedded in paraffin and sectioned at 5 μm. Paraffin sections were stained with hematoxylin and eosin (H&E) for routine histological analysis; Sirius Red for the detection of fibrillar collagen. Slides were visualized using a Nikon Eclipse E600 microscope or a Zeiss Axiovert 135 (immunofluorescence).

Transthoracic Echocardiography. Echocardiographic measurements were performed on mice anesthetized with isoflurane as described before32, 8 weeks after starting transaortic banding. In M-mode, the following parameters were obtained: AWthd, anterior wall thickness in diastole; LVIDd, left ventricular internal diameter in diastole; PWthd, posterior wall thickness in diastole; AWths, anterior wall thickness in systole; LVIDs, left ventricular internal diameter in systole; PWths, posterior wall thickness in systole; PWths, posterior wall thickness in systole; LVmass, left ventricular mass and FS, fractional shortening.

Quantitative RT-PCR. One microgram of total RNA was used as template for Superscript reverse transcriptase II (Promega). For real time-PCR, a BioRad iCycler (Biorad) and SYBR Green was used in combination with specific primer sets designed to detect transcripts (primer sequences available upon request)

Cardiac Ischemia Reperfusion. Two month-old mice were anaesthetized with isoflurane, intubated and connected to a rodent respirator (model 683; Harvard Apparatus, South Natick, MA) on room air with a tidal volume of 0.2 ml and a respiratory rate of 180 breaths /min. Following a left thoracotomy, the left anterior descending coronary artery was li-

gated to induce ischemia for 30 min after which blood flow was re-established. For the delineation of the area-at-risk (AAR), 5% Evans blue dye was injected into the apex after the indicated reperfusion times as described previously. Hearts were removed and stained with triphenyltetrazolium chloride (TTC) to quantify infarct sizes. The area-at-risk was expressed as a percentage of the LV, and the area of infarct (IA) as a percentage of the AAR.

TUNEL staining. TUNEL assays were performed as described previously,(van Empel et al., 2005b) using the In Situ Cell Death Detection TMR-Red Kit (Roche) and using an antibody against α-actinin (Sigma) and TO-PRO3 (Molecular Probes) on 10 μm frozen, apical cross-sections of hearts.

Flow cytometry. Flow cytometry was performed on isolated neonatal rat ventricular cardiomyocytes either treated or not with the apoptosis inducer H2O2 (500μM for 3h), cells were then washed with ice-cold PBS, trypsinized, and resuspended in binding buffer containing 10 mM HEPES, pH 7.4, 140 mM NaCl, 2.5 mM CaCl2. Cells were double stained with Annexin V conjugated with R-phycoerythrin conjugate (Annexin V-PE, BD Pharmingen) and propidium iodide (PI; 2.5 mg/ml, Molecular Probes) and analyzed using the CellQuest™ Flow Cytometry System from BD Biosciences.

Transverse Aortic Banding. Transverse aortic banding (TAC) or sham surgery was performed in WT and PPARα KO mice. The aorta was subjected to a defined, 27 gauge constriction between the first and second truncus of the aortic arch as described in detail previously (18). Pressure gradients between the proximal and distal sites of the transverse aortic constriction, were determined by Doppler echocardiography (van Empel et al., 2006).

Statistical analysis. The results are presented as mean values ± standard error of the mean (SEM). Statistical analyses were performed using InStat 3.0 software (GraphPad Software Inc.) and consisted of ANOVA followed by Tukey's post-test or Student's paired T-test when group differences were detected at the 5% significance level.

Supplemental data. Supplemental data include an Expanded Agilent microarray analyses.

RESULTS

Generation of cardiac cell lines stably expressing PPAR subtype-specific siRNAs.

To determine whether the distinct cardiovascular functions of PPAR isoforms are related to activation of distinctive, isoform-selective target gene profiles, we first set up a method to determine PPAR subtype-specific target genes in the cardiomyocyte. To this end, we resorted to the use of a previously developed ventricular muscle cell line, NKL-TAg (Rybkin et al., 2003). NKL-TAg cells actively proliferate without apparent senescence, while introduction of Cre recombinase results in elimination of a loxP flanked SV40 large T-antigen (TAg), provoking permanent exit from the cell cycle and cardiogenic differentiation with expression of cardiac markers. We also designed expression vectors harboring expressing one PPAR subtype-specific shRNA. Transient co-transfection of V5-tagged PPAR isoform with the corresponding siRNA in NkL-TAg cells showed efficient knockdown of the corresponding PPAR isoform (Fig. 1a).

Next, we generated NkL-TAg clones stably expressing shRNAs against PPARα, -β/δ or -γ using zeocin as a selectable marker. To control for cell-based variations, we selected two stably expressing siRNA clones for each PPAR isoform. By RT-PCR (Fig. 1e), AdCre-mortalized and differentiated siRNA clones expressed transcripts from the cardiogenic transcription factors nkx2.5 and gata4; cardiac ion channels were expressed regulating the calcium transient (atp2a2 and ryr2) and the transient outward K+ current (kncip2). Sarcomeric components were also detected including a-myosin heavy chain (myh6), myosin light chain-1a (myl4), desmin and sarcomeric actin (actc) at levels comparable to parental differentiated NKL-TAg cells and cardiac muscle (Fig. 1e), demonstrating the maintenance of cardiac muscle identity of differentiated shRNA expressing clones, even after stable integration events. Real time PCR demonstrated at least 70% knockdown of the endogenous PPAR isoforms in each clone (Fig. 1b).

As a functional verification of the clones, parental, wildtype NkL-TAg cells and the siRNA clones were transiently transfected with a luciferase reporter driven by a mCPT promoter harboring a functional PPRE (Baldan et al., 2004). The data show that activation of either PPARα, -β/δ or -γ using their synthethic ligands in the respective PPARα, -β/δ or -γ siRNA clones was substantially suppressed with respect to mCPT-Luc activity, indicating functional PPAR-isotype selective knockdown in the selected clones (Fig. 1c).

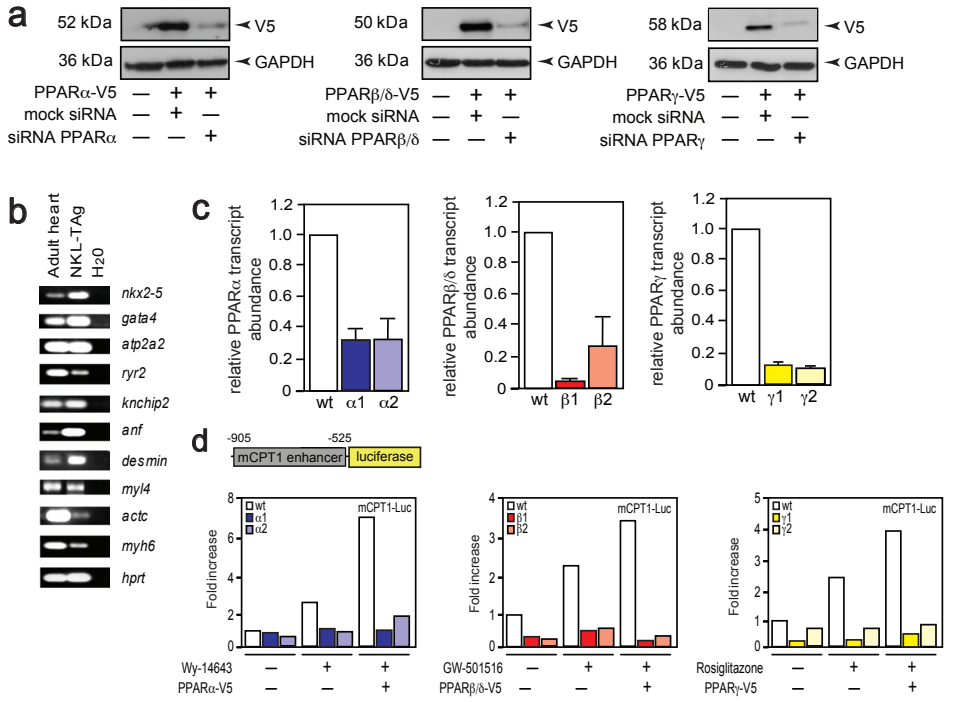

Figure 1. Generation of cardiac cell lines stably expressing PPAR subtype-specific siRNAs. (a) Western blot analysis using anti-V5 antibody on lysates of NkL-Tag cells transiently co-transfected with the selected siRNA showing specific knockdown of the indicated PPAR isoform. (b) RT-PCR identification for cardiac markers in NkL-Tag cells compared to adult mouse heart tissue, including transcripts for HPRT. (c) Real time RT-PCR quantitative analysis of endogenous ppara, ppard, pparg transcripts (encoding PPARα, PPARβ/δ, PPARγ), indicating efficient, stable siRNA knockdown of the endogenous transcript. (d) Luciferase measurements on siRNA clones, transiently transfected with a mCPT promoter driven reporter as a functional verification of efficient PPAR-isotype knockdown in each clone.

Subtype-specific expression profile of PPAR target genes in cardiac muscle.

Following this proof-of-principle that our PPAR isoform-specific siRNA clones adopt a cardiac muscle fate and provide stable knockdown of each respective PPAR subtype, we designed experiments to profile endogenous PPAR isoform-specific target genes. PPARα, -β/δ or -γ was activated in differentiated wildtype NkLTAg cells and their corresponding siRNA clones using the specific synthetic ligands, Wy-14643, GW5015160 or Rosiglitazone, respectively, for 24 hrs. Agilent mouse chips harboring 22,000 transcripts wereused to identify the early gene expression pattern evoked by PPAR-isoform specific activation.

As depicted in the schematic representation (Fig. 2a), in this setup, genes that were diferentially expressed in the respective PPAR isotype siRNA clones were considered ligand activated but nonspecific for PPAR activity. Accordingly, these genes were subtracted from the expression profiles obtained in the corresponding ligand activated, wildtype NkLTAg cells. 502, 620, and 277 genes (0.23, 0.28 and 0.13% of all genes present on the arrays) were differentially expressed following PPARα, -β/δ or -γ activation, respectively, with a fold change in expression ≥ 2 ($P < 0.01$) (Fig. 2b,c). Detection of upstream PPREs using Fatigo matrices revealed that over 80% of the reported genes contained at least one evolutionary conserved PPRE, a direct repeat of the consensus half-site motif (AGGNCA) spaced by a single nucleotide (DR-1). The resulting expression profiles were depicted in a heat map and in a Venn-diagram format (Fig. 2b, c).

Next, to validated the gene profiles for each PPAR isoform, we performed RT-PCR to verify differential expression in (un)stimulated wildtype cells and siRNA clones (Fig. 2d). For PPARα activation, acyl-CoA thioesterase 1 (*cte1*) and insulin-like growth factor-1 (*igf1*) were upregulated following Wy-14643 stimulation, but not in the siRNA clones, which further validates our unbiased array approach (Fig. 2d). Likewise, for PPARβ/δ, aldehyde oxidase 1 (*aox1*) and muscle and heart-type fatty acid binding protein 3 (*fabp3*) were specifically induced following GW5015160 stimulation, but not in the PPARβ/δ siRNA clones (Fig. 2d). Finally, rosiglitazone induced lipoprotein lipase (lpl) induction and downregulation of baculoviral IAP repeat-containing 5 (*birc5*, also known as survivin), but not in the PPARγ siRNA clones (Fig. 2d).

Strikingly, we found that PPARβ/δ and PPARγ shared a more closely related and overlapping number of transcripts than PPARα in the cardiomyocyte. In addition, whereas PPARβ/δ and PPARγ showed considerable resembles in their target genes, PPARα also regulated a distinct ontology profile of target genes in the cardiomyocyte (Fig. 2e). Gene ontology classifications of the target genes revealed for all the three PPAR isoforms an overrepresentation of genes involved in metabolism regulation, cell cycle, adhesion, apoptosis and immune response (Table 1). By RT-PCR we verified two target genes for each of the expression areas indicated in the Venn-diagram (Fig. 2e). Conclusively, using an unbiased array approach and including a setup with stringent criteria, we have defined the specific target genes and gene ontologies for each PPAR isoform in heart muscle.

PPARα activation induces *igf1* gene expression.

Gene ontology classifications revealed an overrepresentation of target genes involved in metabolism regulation (60%) Interestingly, PPARα also display a relative overrepresentation of genes involved in apoptosis and cellular survival. In line, it has been reported that activation of PPARα by its respective ligands in cardiac muscle can attenuate cardiomyocytic apoptosis and heart muscle injury (Yeh et al., 2006; Yue et al., 2003).

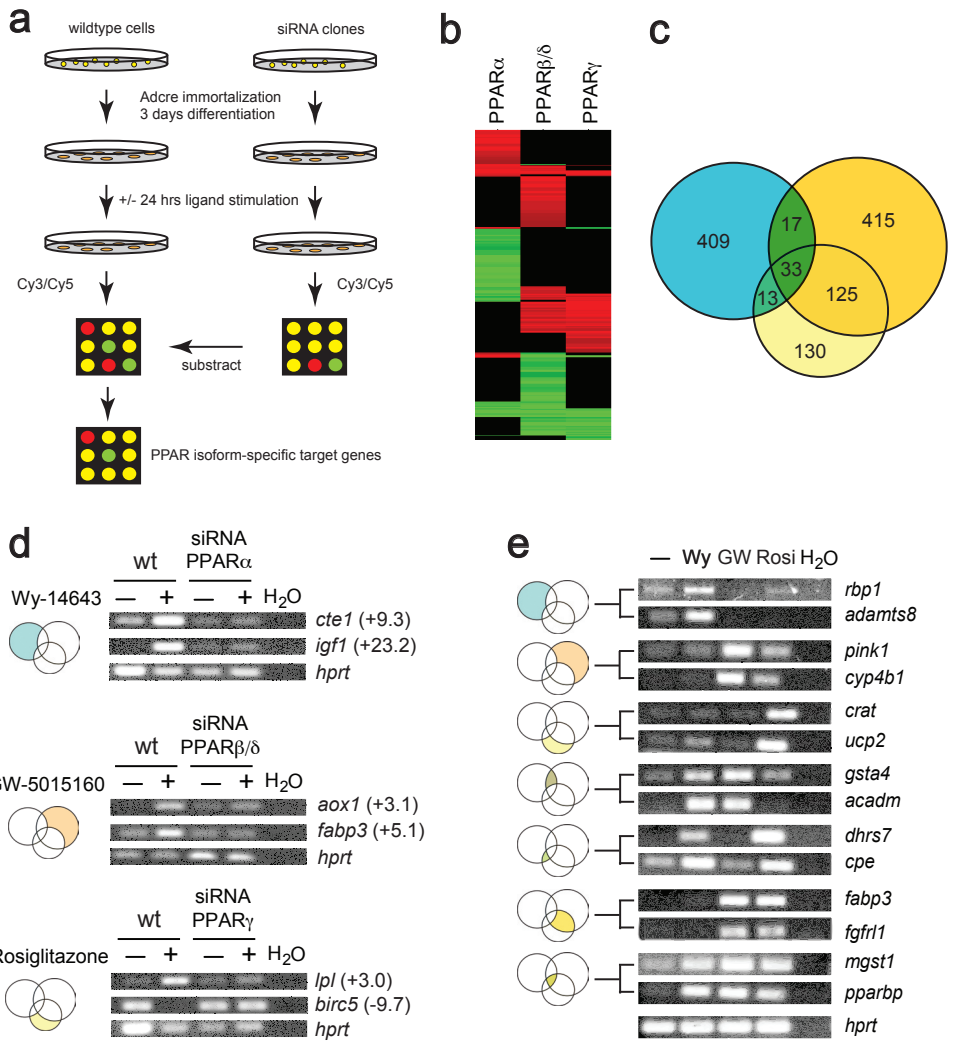

Figure 2. Genome-wide expression profile of PPAR target genes in cardiac muscle. (a) Schematic representation of the genome-wide array setup. (b) Cardiac RNA was collected from 3 separate siRNA clones and 3 separate WT and subjected to expression profiling using the Agilent 22k mouse whole genome microarray slides (Palo Alto) arrays. RT-PCR analyses of differentially expressed PPAR isoform-specific target genes are depicted. (c) Heat map representation of the resulting expression profiles, colors represent gene expression levels as indicated, with black equal to 0 (no change), bright red equal to 3.0 (3.0-fold increased expression), and bright green equal to -3.0 (-3.0 decreased expression). (d) The micro-array expression profiles depicted in a Venn-diagram format, signifying the number of overlapping target genes between the three PPAR isoforms. (e) RT-PCR validation of microarray results for mRNA levels of indicated genes.

By RT-PCR, we confirmed differential regulation of this gene ontology by PPARα activation in primary rat cardiomyocytes. The results indicate a downregulation of pro-apoptotic target genes such as caspase-3 and caspase-7 and the upregulation of the anti-apoptotic target gene *igf-1* upon Wy-14643 stimulation (Fig. 3a). *Igf1* has been identified as a potent growth factor providing protection against apoptosis and prolong cell survival in several cell types, including cardiac muscle (Buerke et al., 1995a; Wang et al., 1998) , suggesting a plausible genetic mechanism for the potential anti-apoptotic function of PPARα in the heart.

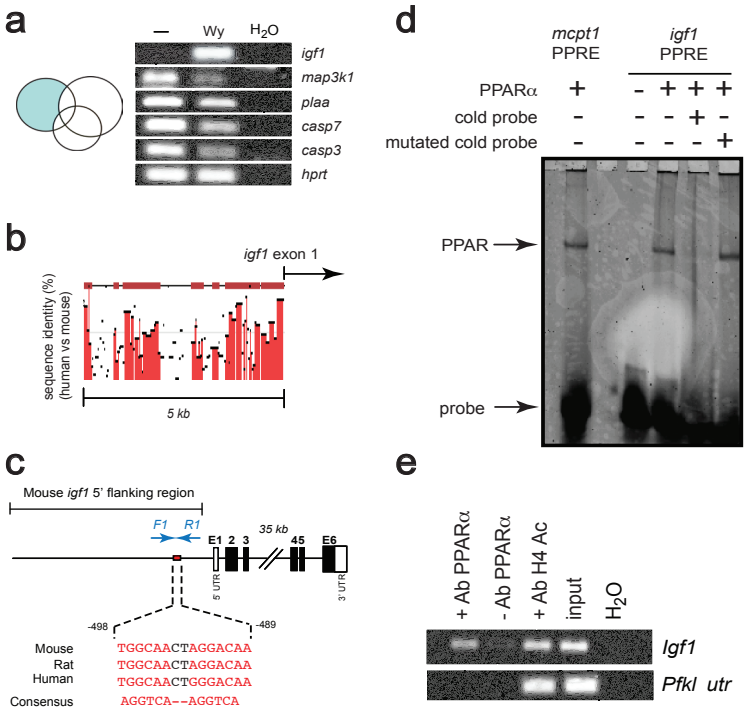

Figure 3. PPARα induces an anti-apoptotic profile in cardiomyocyte with *igf-1* as direct target gene. (a) RNA was collected from 3 separate isolation of primary rat cardiomyocytes either treated with PPARα agonist, Wy-14643, or untreated. Depicted is RT-PCR analysis of apoptosis related PPARα isoform-specific target genes. (b, c) Comparison of the *igf-1* genomic regions between mouse and human. Percentage conservation of a 5' 10.0 kb genomic region upstream of *igf-1* first exon is shown along with a schematic presentation of a ± 2.5 kb 5' flanking region in mouse igf-1 and location of potential PPRE conserved in human, mouse and rat. (d) Gel mobility shift assay was performed using fluorescent probes of PPARα consensus sequences (m-CPT) or PPRE-like site from the *igf-1* promoter. (e) Chromatin immunoprecipitation assays were performed on Differentiated NkL-Tag cells were either or not treated with Wy-14643 for 24hr to activate PPAR and soluble chromatin was immunoprecipitated with a specific antibody for PPARα. Associated DNA was purified and RT-PCR analysis was performed using specific primers to the igf-1 promoter flanking the PPRE, or a non-coding genomic region 3' of the pfkl gene.

In order to mechanistically define the PPARα responsiveness of *igf1*, we searched for evolutionary conserved enhancers that regulate in vivo transcription of the igf1 gene. Comparison of genomic sequences across species using rVISTA revealed that a 2.5 kb genomic region immediately upstream of the first exon of *igf1* was conserved between human and mouse, apart from discontinued more distal regions that also displayed high cross-species conservation (Fig. 3b). A potential PPRE in the *igf1* enhancers was nearly identical and conserved in human, mouse and rat (Fig. 3b). To confirm the binding of PPARα to the *igf1* enhancers, we performed electromobility shift assays and demonstrate that a probe including one putative element (*igf1* PPRE) formed a retardation complex with ligand-activated PPARα (Fig.3c lane 4). The specificity of binding was studied by competition assays. Addition of excess unlabeled *igf1* PPRE eliminated the specific complex (Fig. 3c lane 5), while a labeled, mutated probe could not inhibit complex formation between PPARα with the wild-type probe (Fig. 3c lane 6).

To confirm in-vivo binding of PPARα to the *igf1* enhancer, we performed chromatin immunoprecipitation (ChIP) assays. Differentiated wild-type NkL-Tag cells were either or not treated with Wy-14643 for 24hr to stimulate PPARα activity. The resultant soluble chromatin fractions were immunoprecipitated using a PPARα-specific antibody and associated DNA purified. Using specific primers to the *igf1* promoter flanking the PPRE, a PCR product was detected in input material and in PPARα-immunoprecipitated chromatin (Fig. 3d). This association was specific for PPARα, since enrichment was not obtained when using beads alone, or when using primers to an unrelated intergenic region, in this case a fragment 20 kB upstream of *pfkl* (Fig. 3d). When using an antibody for H4-acetylated histone, as a postive controle, enrichment of the PCR product was obtained, indicating the open character of chromatin at this locus. Taken together, these results indicate that PPARα signaling regulates the *igf1* gene by direct transcriptional activation, and unambiguously show the presence of endogenous PPARα proteins on the proximal *igf1* promoter in vivo, establishing *igf1* as direct target gene of PPARα signaling in cardiac muscle.

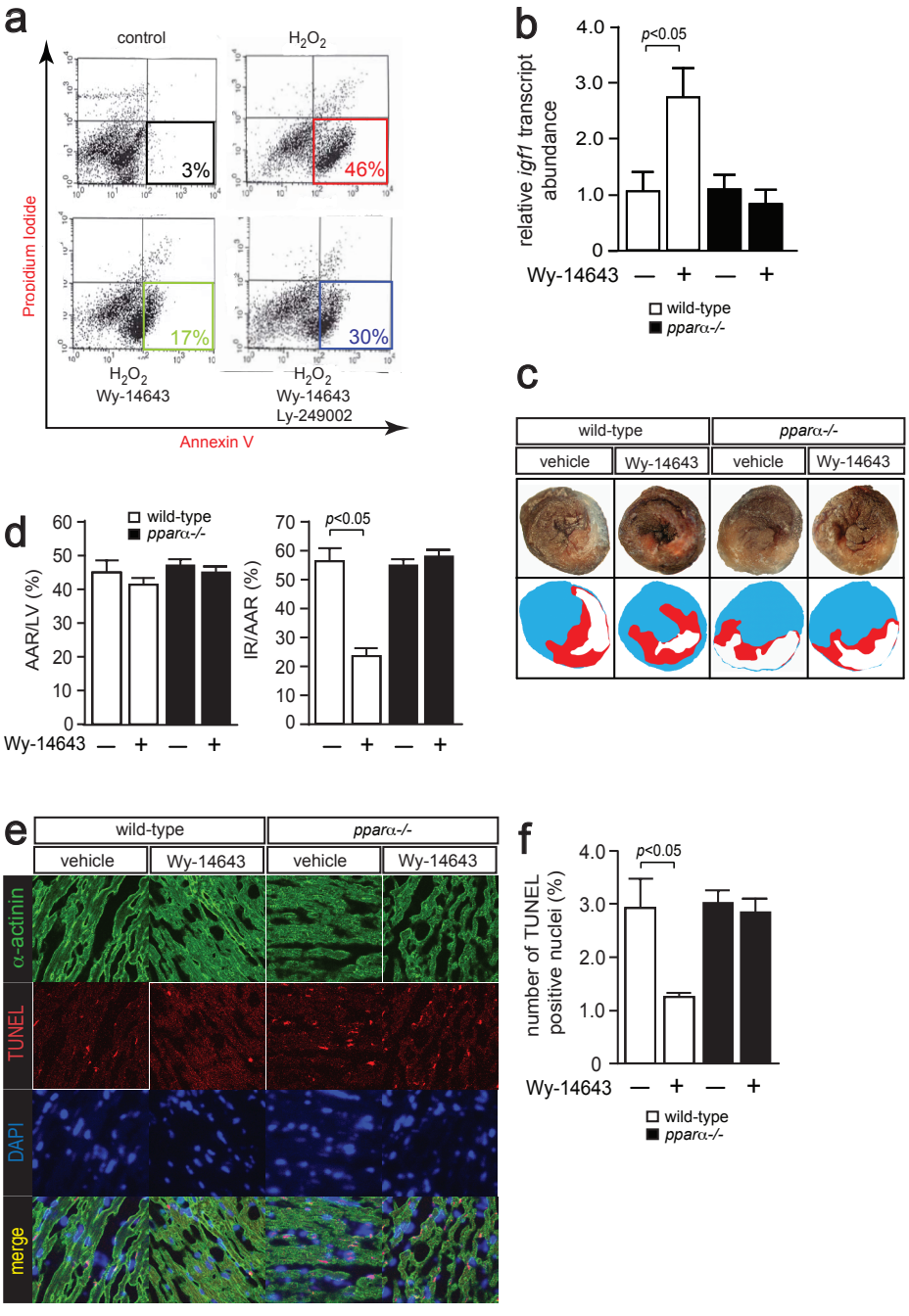
a
control
H2O2
3%
46%
17%
30%
Propidium Iodide
H2O2
Wy-14643
H2O2
Wy-14643
Ly-249002
Annexin V
b
relative igf1 transcript abundance
p<0.05
4.0
3.0
2.0
1.0
0
Wy-14643 — + — +
wild-type
pparα-/-
c
wild-type
pparα-/-
vehicle
Wy-14643
vehicle
Wy-14643
d
wild-type
pparα-/-
AAR/LV (%)
IR/AAR (%)
p<0.05
Wy-14643 — + — +
e
wild-type
pparα-/-
vehicle
Wy-14643
vehicle
Wy-14643
α-actinin
TUNEL
DAPI
merge
f
number of TUNEL positive nuclei (%)
p<0.05
Wy-14643 — + — +
wild-type
pparα-/-

PPARα activation inhibits apoptosis via an IGF-1/PI3K pathway in vivo.

Accumulating evidence suggests that oxidative stress triggers cardiac cell death and the pathogenesis of a number of cardiovascular diseases, such as ischemic heart disease, heart failure, and atherosclerosis (Crow et al., 2004; Griendling and FitzGerald, 2003a; Griendling and FitzGerald, 2003b). While other growth factors seem unable to suppress apoptosis of cardiac muscle cells at pharmacological levels, IGF-1 has been observed to have profound anti-apoptotic properties even at physiological concentrations (Wang et al., 1998). Activation of the IGF-1 receptor in cardiac muscle leads to activation of the phosphatidylinositol 3-kinase (PI3K) axis, which also has been linked to anti-apoptotic responses and protection from cardiac reperfusion injury in vivo (Dolcet et al., 1999).

To test whether the anti-apoptotic effect of PPARα in cardiomyocytes is mediated via a functional IGF-1/PI3k pathway, primary rat cardiomyocytes were both left untreated, or treated with Wy-14643 for 24hr and subjected to H202 to induce apoptosis. To detect early loss of apoptotic-associated alterations in membrane asymmetry of phospholipids and signs of nuclear apoptosis, cells were stained with Annexin-V and propidium iodide (PI) and analyzed using flow cytometry. H202 treatment produced a nearly 50% increase in the proportion of Annexin-V/PI positive cells compared to control conditions, whereas activation of PPARα profoundly reduced H202 induced apoptosis (Fig. 4a). Cells co-treated with LY294002, a selective PI3K inhibitor, significantly reduced Wy-14643-induced rescue of H202 induced apoptosis (Fig. 4a), implicating the downstream activation of the PI3K pathway following PPARα activation in cardiomyocyte survival signaling. Further analysis of whether Wy-14643 stimulation also leads to protection of heart muscle apoptosis in vivo, cohorts of two month-old wild-type and pparα-deficient mice were treated with Wy-14643 or vehicle for four consecutive days.

Figure 4. (a) Representative pictures from flow cytometry experiments on primary rat cardiomyocytes, untreated or stimulated with Wy-14643 in combination with co-treatments with H2O2 (500μM for 2h) or LY294002 (10 μM) 30min prior to H2O2 addition. Percentage of AnnexinV-PE/ PI double-positive population is shown in the lower corner, signifying less apoptotic cells were found only after activation of PPARα in combination with an intact PI3k pathway. (b) Real time PCR analysis for Igf-1, which is increased after Wy-14643 stimulation in the WT hearts but not in PPARα KO (n=3 per group). (c) Representative image of cross-sections of 2- to 3-month-old WT and PPARα KO mice hearts subjected to ischemia/reperfusion (I/R), stimulated either with Wy-14643 or vehicle. In red, the AAR is depicted, in white the IA, and in blue, the areas of the heart not perfused by the LAD. (d) AAR, expressed as SEM of percentage of total LV, was comparable in WT and PPARα mice. The IA/AAR ratio demonstrated significant differences between WT and PPARα KO only after Wy-14643 stimulation (n=5 and n=6, respectively). (e) Representative image of TUNEL labeling of WT and PPARα KO hearts stimulated either with Wy-14643 or vehicle and subjected to I/R. (f) Bar graph indicates mean±SEM of the percentage of TUNEL positive cardiomyocytes after ischemic insult (n=3 per group), which showed significant Wy-14643 stimulation dependent rescue in WT hearts and not in PPARα KO.

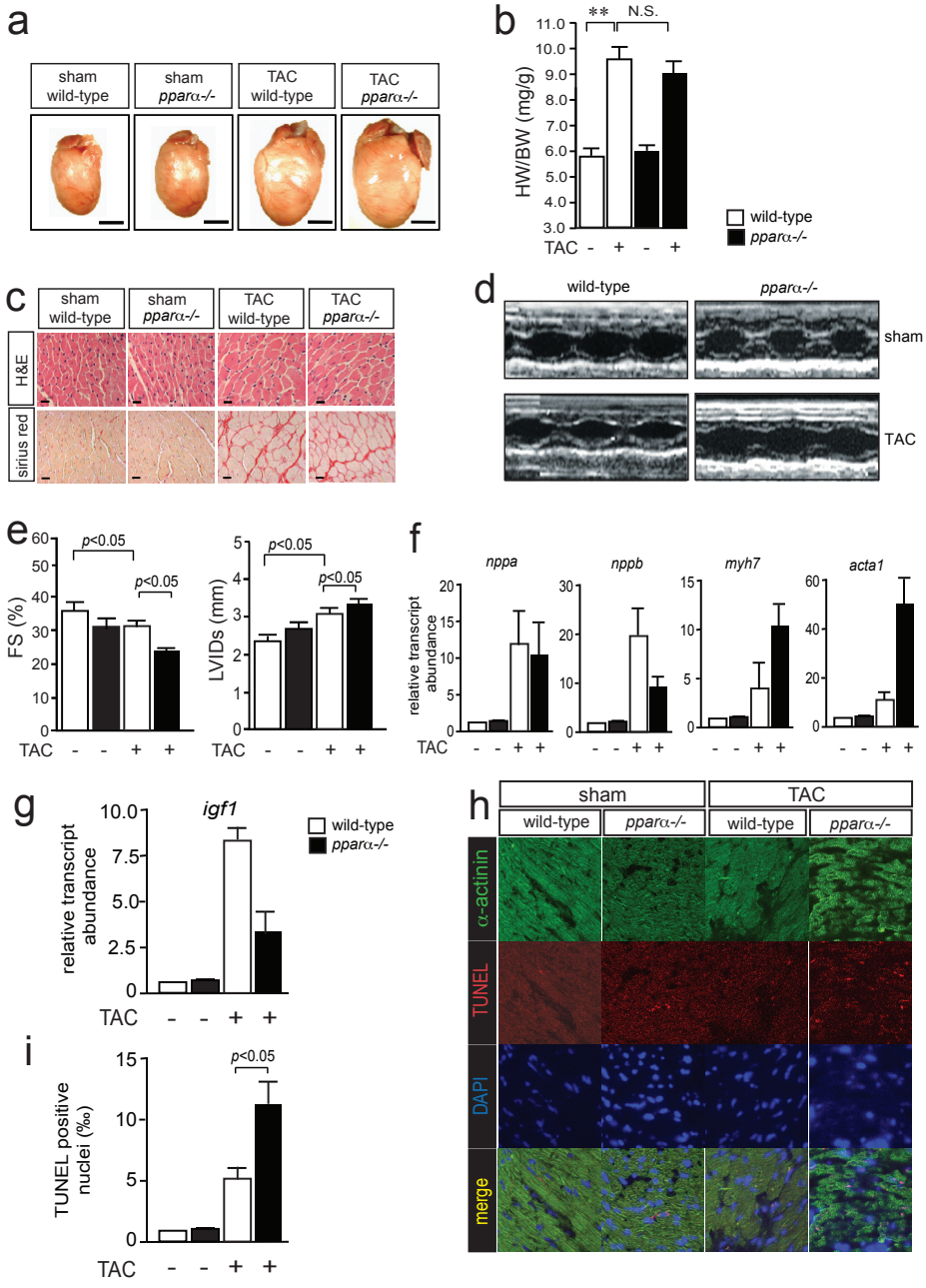
a
sham wild-type
sham pparα-/-
TAC wild-type
TAC pparα-/-
b
**
N.S.
HW/BW (mg/g)
11.0
10.0
9.0
8.0
7.0
6.0
5.0
4.0
3.0
TAC - + - +
wild-type
pparα-/-
c
sham wild-type
sham pparα-/-
TAC wild-type
TAC pparα-/-
H&E
sirius red
d
wild-type
pparα-/-
sham
TAC
e
p<0.05
p<0.05
FS (%)
60
50
40
30
20
10
0
TAC - - + +
p<0.05
p<0.05
LVIDs (mm)
5
4
3
2
1
0
TAC - - + +
f
nppa
nppb
myh7
acta1
relative transcript abundance
20
15
10
5
0
30
20
10
0
15
10
5
0
60
40
20
0
TAC - - + +
g
igf1
relative transcript abundance
10.0
7.5
5.0
2.5
0
TAC - - + +
wild-type
pparα-/-
i
p<0.05
TUNEL positive nuclei (‰)
15
10
5
0
TAC - - + +
h
sham
TAC
wild-type
pparα-/-
wild-type
pparα-/-
α-actinin
TUNEL
DAPI
merge

Next, mice were subjected to transient occlusion of the left anterior descending coronary artery (LAD) for 30 min (ischemia) followed by 24h reperfusion (I/R) to provoke widespread cardiac cell death. After the reperfusion period, the LAD was religated, hearts perfused with Evans blue dye, removed and incubated in TTC to quantify area-at-risk (AAR) and infarct area (IA), respectively. The AAR/total left ventricular area (LV) ratio did not differ between the four groups (Fig. 4d), indicating that there were no genotype dependent differences in the perfused areas between the experimental groups. Interestingly, the infarct area was substantially reduced following Wy-14643 treatment in wild-type mice, whereas Wy-14643 had no effect in pparα null mice, indicating the obligate requirement of PPARα in Wy-14643 mediated cardioprotection (Fig. 4d,c).

To establish whether the Wy-14643 mediated reduction in infarct size was related to reduction in programmed cardiac muscle cell death, the levels of apoptotic cells within the viable left ventricle and septum were assessed by TUNEL labeling. As indicated by the numbers of TUNEL/α-actinin/DAPI triple positive myocytes, Wy-14643 treatment sig nificantly reduced the incidence of apoptotic cell death in wild-type mice but not in pparα-deficient mice (Fig. 4e,f). Finally, real time RT-PCR indicated that igf1 transcripts were upregulated after Wy-14643 treatment in wild-type and not in pparα null mice, demonstrating that Wy-14643-mediated cadioprotection was accompanied by in vivo induction of *ifg-1* in a PPARα dependent manner (Fig. 4b). Combined, these data confirm that PPARα activation in cardiac muscle provides protection against cardiac muscle apoptosis via activation of an IGF-1/PI3K pathway.

Figure 5. (a) Representative gross morphology of hearts dissected from 4 months-old mice of indicated genotypes after 8 weeks of sham or TAC surgery, demonstrating a profound cardiac enlargement after pressure overload (bar 5 mm). (b) Heart weight/body weight ratios of 4 months-old WT and PPARα KO, after 8 weeks of sham or TAC surgery, indicates a significant increase in cardiac mass after pressure overload (n=5 per group) N.S., not significant; **, indicates $P < 0.01$. (c) Representative histological images of hearts from mice of indicated genotypes after 8 weeks of sham or TAC surgery (bar 0.2 mm). H&E-stained images reveal remarkable myocyte hypertrophy and myofiber disarray in mice subjected to TAC surgery. Sirius red staining indicates massive interstitial and perivascular fibrosis in hearts of WT and PPARα KO subjected to TAC surgery. (d) Representative M-mode images of WT and PPARα KO mice after 8 weeks of sham or TAC surgery, indicating decreased contractility and increased left ventricular internal dimensions after pressure overload. (e) Bar graph representations of fractional shortening (FS) and left ventricular internal diameter at systole (LVIDs), indicating increased functional and geometrical deterioration after TAC in PPARα KO mice compared to WT mice subjected to TAC (n=5-8 per group). (f) Quantitative RT-PCR analysis of nppa (atrial natriuretic factor), nppb (brain natriuretic peptide) and myh7 (beta-myosin heavy chain) α-ska (alpha-skeletal actin) in hearts of WT and PPARα KO mice after 8 weeks of sham or TAC surgery. Error bars are mean ± SEM of n=3. (g) Quantitative RT-PCR analysis of *igf-1* in hearts of WT and PPARα KO mice after 8 weeks of sham or TAC surgery, indicating significant upregulation of *igf-1* transcripts in WT mice after pressure overload. (h) Representative image of TUNEL labeling of WT and PPARα KO hearts after 8 weeks of sham or TAC surgery. (i) Bar graph indicates mean±SEM of the percentage of TUNEL positive cardiomyocytes in hearts of WT and PPARα KO mice subjected to sham or TAC surgery (n=3 per group), showing enhanced apoptosis in PPARα KO hearts subjected to pressure overload.

PPARα protects against pressure-induced myocardial cell death.

Biomechanical stress activates signaling cascades including oxidative stress (Lorell and Carabello, 2000), predisposes cardiac muscle to late-onset apoptosis (Hirota et al., 1999; Sadoshima et al., 2002; van Empel et al., 2005b; Zhang et al., 2000), and provokes progressive left ventricular remodeling and heart failure (Hirota et al., 1999; Zhang et al., 2000). To determine whether *igf1* induction downstream of PPARα activation also protects from apoptosis in response to biomechanical stress, transverse aortic banding (TAC), a surgical technique whereby the transverse aorta is partially constricted to mimic chronic hypertensive disease, was performed on cohorts of wild-type and pparα-deficient mice.

To ensure equal loading conditions on all experimental groups, pressure gradients were measured non-invasively (Fig. 5a). Eight weeks after pressure overload, gross morphology showed no differences between sham-operated wild-type and pparα-deficient mice (Fig. 5b, c). Both experimental groups showed substantial cardiac enlargement upon biomechanical stress (HW/BW ratios 9.4 ± 0.8 and 8.9 ± 0.7 mg/g, respectively; N.S.; Fig. 5b, c), indicating that the cardiac hypertrophic response to pressure overload is not affected in the absence of PPARα.

Using M-mode echocardiography, we studied pressure overload-induced hemodynamic behavior at 8 weeks after TAC. Representative images of M-mode recordings of all experimental groups are displayed in Figure 5d. A more pronounced increase in left ventricular internal diameter (LVID) (Fig. 5d, e) and a proportional decrease in systolic contractility (FS) were evident in pparα-deficient mice compared to wild-type mice following pressure overload (Fig. 5f), indicative of accelerated progressive LV dilation and heart failure.

Reactivation of fetal gene expression is a hallmark of pathological hypertrophy and heart failure. To this end, transcripts levels for nppa (atrial natriuretic factor), nppb (brain natriuretic peptide), myh7 (beta-myosin heavy chain) and acta1 (alpha-skeletal actin) were analyzed and found significantly upregulated upon pressure overload in pparα null mice compared to their wild-type counterparts (Fig. 5g). Next, H&E- and Sirius red-stained cardiac sections did not show signs of histopathology in sham operated wild-type and pparα-deficient mice (Fig. 5h, i). In contrast, cardiomyocyte hypertrophy, myocyte disarray, and extensive areas of interstitial and perivascular fibrosis were evident in both pressure overloaded wild-type and pparα-deficient hearts, but more these changes were more pronounced in pressure overloaded pparα null hearts (Fig5 h, i).

Pressure overload predisposes loss of excessively stressed myocytes in the hypertrophied heart, further fueling the histopathological changes and functional deterioration of the failing heart (Hunt et al., 2005). TUNEL labeling showed a significant increase of TUNEL/α-actinin/DAPI positive myocytes after pressure overload in pparα-deficient hearts compared to wild-type hearts (Fig. 5i), indicating that the PPARα-deficient myocardium has a higher incidence of stress-induced myocyte apoptosis. Finaly, real time RT-

PCR demonstrated that *igf1* was significantly upregulated in the pressure overloaded wild-type heart, but not in pparα knockout mice, revealing a PPARα dependent activation of igf1 upon pressure overload (Fig. 5j). Taken together, these data confirm igf1 as a genuine in vivo target of PPARα during pressure overload and the involvement of a PPARα-IGF1 signaling pathway in the protection of cardiomyocytes under hemodynamic loading conditions.

DISCUSSION

Despite major therapeutic advances, heart failure remains a leading cause of morbidity and mortality worldwide, which rivals or exceeds that of many forms of cancers. Additionally, evidence is emerging that derangements in cardiac fuel metabolism, related to insulin resistance or diabetes, contribute to the development of diabetic cardiac dysfunction. Indeed, diabetes predisposes to heart failure, particularly in combination with other comorbid conditions such as hypertension and coronary artery disease. Numerous studies have identified decreased cardiac energy levels and flux as a consistent feature of HF, and have focused considerable attention on metabolic modulations as a therapeutic modality for HF (Braissant et al., 1996; Brun et al., 1996). Although regulation of metabolism is modulated by a variety of influences, transcriptional regulation of genes involved in metabolism by the PPAR family of transcription factors has been intensively investigated. As PPARs are activated by lipid moieties, they provide attractive targets for therapeutic interventions. Despite their putative role in HF, only a few studies have sought to mutually compare PPAR subtype-specific activation of endogenous genes in the heart (Nielsen et al., 2006).

Microarray profiling and genome wide identification of PPREs using stimulation with isoform-selective synthetic ligands have suggested the existence of a considerable number of PPAR-regulated genes, which have not previously been described as PPAR target genes (Keen et al., 2004; Tamura et al., 2006). While useful, selective activation of PPAR isoforms by their synthetic ligands is seriously hampered by their overlapping specificity (ref). These ligands have been shown to differentially induce unspecific activation of other PPAR isoforms, or even act PPAR independent (Seimandi et al., 2005). Because of lack of evidence whether the different physiological function among the different PPAR isotypes is due to intrinsic biochemical properties or to differences in the cellular milieu in which PPARs are expressed, we combined selective, PPAR-isoform dependent siRNA-mediated knockdown in a cardiomyocte cell line as a template to determine cardiac myocyte specific target genes of the individual PPAR isoforms. The advantage of this in vitro system is the ability to eliminate background gene expression in non-cardiomyocytes to yield optimal sensitivity and specificity of direct effects of PPAR activation in cardiomyocytes.

Genome-wide predictions previously uncovered that among conserved elements, 4.5% of all genes contain a predicted PPRE, suggesting a wide range of target genes for the PPAR family members (Lemay and Hwang, 2006). In our array results, more than 80% of target genes contained a conserved PPRE, indicating the high specificity of the system we used. Apart from well-known target genes, our data also uncovered a series of novel target genes, regulated by one single PPAR isoform or co-regulated by two or even all three PPAR isoforms in cardiac muscle.

Although our approach has yielded a significant amount of interesting PPAR subtype-specific unknown target genes in the cardiomyocyte, we noted that PPARα regulated a subset of genes that suggest activation of survival pathways and antagonism against apoptotic cell death of the cardiomyocyte, compared to the gene profiles regulated by PPARβ/δ and PPARγ. The results indicated downregulation of pro-apoptotic target genes such as *casp3* and *casp7* and the upregulation of the anti-apoptotic target gene *igf1* upon Wy-14643 stimulation. Apoptotic loss of myocardium itself can increase hemodynamic stress through ventricular dilation and wall thinning, and is therefore hypothesized to play an important role in the downward functional spiral that ultimately leads to overt heart failure (Diwan and Dorn, 2007; van Empel et al., 2005a). An emerging body of evidence suggests that PPARα agonists protect the heart from apoptosis (Yeh et al., 2005), although the mechanisms involved in this cardioprotection were deemed multifactorial and not well understood.

Here we show that splice transcripts *igf1* encoding splice isoform 1 was significantly upregulated after PPARα activation through direct transcriptional activation, as shown by chromatin immunoprecipitation and electromobility shift assays. *Igf1* has been shown to decrease myocyte apoptosis after myocardial infarction in mice (Li et al., 1999), and in ischemia-reperfusion injury in rats and cultured rat myocytes (Buerke et al., 1995b). Our findings also demonstrate that PPARα activation in the mouse heart, through Wy-14643 administration, resulted in upregulation of *igf1* expression and subsequent protection against ischemia/reperfusion-induced apoptosis. Although ischemic injury results in cardiomyocyte loss through programmed cell death and necrosis, many studies have confirmed that apoptosis is the key contributor to myocyte loss, accompanying many forms of myocardial disease without identifiable necrosis (MacLellan and Schneider, 1997).

Apart from stimuli secondary to direct massive myocardial injury, primary hemodynamic overload, as observed under conditions of chronic hypertension and aortic stenosis, also leads to cardiomyocyte loss through apoptosis. Although apoptosis during pressure overload is a relatively less common feature than in the setting of myocardial ischemia-reperfusion injury, the effects of continuing loss of functional units are tremendous for cardiac function. The heart adapts to the loss of cardiomyocytes through structural changes and re-expression of fetal genes, including pro-apoptotic genes that are essential for development of the fetal heart, but proof to have ruinous effects on long-term cardiac function (Esposito et al., 2002; Sano and Schneider, 2002).

We therefore setout to distinguish whether PPARα may equally well protect the heart during pressure overload injury in terms of increasing the survivability of the cardiomyocyte. Transverse aortic banding (TAC) showed to readily increase *igf1* expression wildtype hearts. Remarkably, pressure overload induced expression of *igf1* was completely abrogated in mice lacking PPARα, indicating the requirement of PPARa isoform for regulating *igf1* in vivo. Quantification of the incidence of apoptotic cardiomyocytes, using in vivo TUNEL labeling, substantiated an increase of apoptotic cell death in hearts with pressure overload. Taken together, this study mechanistically links PPARa activation, induction of *igf1* gene expression, cardiomyocyte drop-out, ventricular remodeling and functional deterioration at the transition point from compensated pressure overload hypertrophy to decompensated heart failure.

In conclusion, by combining large-scale gene expression analysis using microarrays and computational approaches, we revealed the PPAR subtype-specific endogenous targets in the heart muscle. Primary analysis of these results present a novel mechanism motivating the anti-apoptotic properties of PPARα signaling in the heart muscle, suggesting a pharmaceutical value for select activation of the PPARα isoform in heart failure.

ACKNOWLEDGEMENTS

The authors are grateful to Jeroen Korving, Jennifer Megan Meerding and Pantelis Hatzis for technical assistance. This work was supported by grants 912-04-054, 912-04-017 and a VIDI award 917-86-372 from the Netherlands Organization for Health Research and Development (ZonMW) and by the European Union Contract No. LSHM-CT-2005-018833/EUGeneHeart (to L.J.D.W.).

REFERENCES

Baldan, A., Relat, J., Marrero, P. F., and Haro, D. (2004). Functional interaction between peroxisome proliferator-activated receptors-alpha and Mef-2C on human carnitine palmitoyltransferase 1beta (CPT1beta) gene activation. Nucleic Acids Res 32, 4742-4749.

Barak, Y., Liao, D., He, W., Ong, E. S., Nelson, M. C., Olefsky, J. M., Boland, R., and Evans, R. M. (2002). Effects of peroxisome proliferator-activated receptor delta on placentation, adiposity, and colorectal cancer. Proc Natl Acad Sci U S A 99, 303-308.

Boudina, S., and Abel, E. D. (2007). Diabetic cardiomyopathy revisited. Circulation 115, 3213-3223.

Braissant, O., Foufelle, F., Scotto, C., Dauca, M., and Wahli, W. (1996). Differential expression of peroxisome proliferator-activated receptors (PPARs): tissue distribution of PPAR-alpha, -beta, and -gamma in the adult rat. Endocrinology 137, 354-366.

Brun, R. P., Tontonoz, P., Forman, B. M., Ellis, R., Chen, J., Evans, R. M., and Spiegelman, B. M. (1996). Differential activation of adipogenesis by multiple PPAR isoforms. Genes Dev 10, 974-984.

Buerke, M., Murohara, T., and Lefer, A. M. (1995a). Cardioprotective effects of a C1 esterase inhibitor in myocardial ischemia and reperfusion. Circulation 91, 393-402.

Buerke, M., Murohara, T., Skurk, C., Nuss, C., Tomaselli, K., and Lefer, A. M. (1995b). Cardioprotective effect of insulin-like growth factor I in myocardial ischemia followed by reperfusion. Proc Natl Acad Sci U S A 92, 8031-8035.

Burkart, E. M., Sambandam, N., Han, X., Gross, R. W., Courtois, M., Gierasch, C. M., Shoghi, K., Welch, M. J., and Kelly, D. P. (2007). Nuclear receptors PPARbeta/delta and PPARalpha direct distinct metabolic regulatory programs in the mouse heart. J Clin Invest 117, 3930-3939.

Cheng, L., Ding, G., Qin, Q., Huang, Y., Lewis, W., He, N., Evans, R. M., Schneider, M. D., Brako, F. A., Xiao, Y., et al. (2004). Cardiomyocyte-restricted peroxisome proliferator-activated receptor-delta deletion perturbs myocardial fatty acid oxidation and leads to cardiomyopathy. Nat Med 10, 1245-1250.

Chevillotte, E., Rieusset, J., Roques, M., Desage, M., and Vidal, H. (2001). The regulation of uncoupling protein-2 gene expression by omega-6 polyunsaturated fatty acids in human skeletal muscle cells involves multiple pathways, including the nuclear receptor peroxisome proliferator-activated receptor beta. J Biol Chem 276, 10853-10860.

Crow, M. T., Mani, K., Nam, Y. J., and Kitsis, R. N. (2004). The mitochondrial death pathway and cardiac myocyte apoptosis. Circ Res 95, 957-970.

Ding, G., Cheng, L., Qin, Q., Frontin, S., and Yang, Q. (2006). PPARdelta modulates lipopolysaccharide-induced TNFalpha inflammation signaling in cultured cardiomyocytes. J Mol Cell Cardiol 40, 821-828.

Ding, G., Fu, M., Qin, Q., Lewis, W., Kim, H. W., Fukai, T., Bacanamwo, M., Chen, Y. E., Schneider, M. D., Mangelsdorf, D. J., et al. (2007). Cardiac peroxisome proliferator-activated receptor gamma is essential in protecting cardiomyocytes from oxidative damage. Cardiovasc Res 76, 269-279.

Diwan, A., and Dorn, G. W., 2nd (2007). Decompensation of cardiac hypertrophy: cellular mechanisms and novel therapeutic targets. Physiology (Bethesda) 22, 56-64.

Dolcet, X., Egea, J., Soler, R. M., Martin-Zanca, D., and Comella, J. X. (1999). Activation of phosphatidylinositol 3-kinase, but not extracellular-regulated kinases, is necessary to mediate brain-derived neurotrophic factor-induced motoneuron survival. J Neurochem 73, 521-531.

Esposito, G., Rapacciuolo, A., Naga Prasad, S. V., Takaoka, H., Thomas, S. A., Koch, W. J., and Rockman, H. A. (2002). Genetic alterations that inhibit in vivo pressure-overload hypertrophy prevent cardiac dysfunction despite increased wall stress. Circulation 105, 85-92.
Finck, B. N., Han, X., Courtois, M., Aimond, F., Nerbonne, J. M., Kovacs, A., Gross, R. W., and Kelly, D. P. (2003). A critical role for PPARalpha-mediated lipotoxicity in the pathogenesis of diabetic cardiomyopathy: modulation by dietary fat content. Proc Natl Acad Sci U S A 100, 1226-1231.
Finck, B. N., Lehman, J. J., Leone, T. C., Welch, M. J., Bennett, M. J., Kovacs, A., Han, X., Gross, R. W., Kozak, R., Lopaschuk, G. D., and Kelly, D. P. (2002). The cardiac phenotype induced by PPARalpha overexpression mimics that caused by diabetes mellitus. J Clin Invest 109, 121-130.
Gilde, A. J., van der Lee, K. A., Willemsen, P. H., Chinetti, G., van der Leij, F. R., van der Vusse, G. J., Staels, B., and van Bilsen, M. (2003). Peroxisome proliferator-activated receptor (PPAR) alpha and PPARbeta/delta, but not PPARgamma, modulate the expression of genes involved in cardiac lipid metabolism. Circ Res 92, 518-524.
Griendling, K. K., and FitzGerald, G. A. (2003a). Oxidative stress and cardiovascular injury: Part I: basic mechanisms and in vivo monitoring of ROS. Circulation 108, 1912-1916.
Griendling, K. K., and FitzGerald, G. A. (2003b). Oxidative stress and cardiovascular injury: Part II: animal and human studies. Circulation 108, 2034-2040.
Guerre-Millo, M., Rouault, C., Poulain, P., Andre, J., Poitout, V., Peters, J. M., Gonzalez, F. J., Fruchart, J. C., Reach, G., and Staels, B. (2001). PPAR-alpha-null mice are protected from high-fat diet-induced insulin resistance. Diabetes 50, 2809-2814.
Hasegawa, H., Takano, H., Zou, Y., Qin, Y., Hizukuri, K., Odaka, K., Toyozaki, T., and Komuro, I. (2005). Pioglitazone, a peroxisome proliferator-activated receptor gamma activator, ameliorates experimental autoimmune myocarditis by modulating Th1/Th2 balance. J Mol Cell Cardiol 38, 257-265.
He, T. C., Chan, T. A., Vogelstein, B., and Kinzler, K. W. (1999). PPARdelta is an APC-regulated target of nonsteroidal anti-inflammatory drugs. Cell 99, 335-345.
Hirota, H., Chen, J., Betz, U. A., Rajewsky, K., Gu, Y., Ross, J., Jr., Muller, W., and Chien, K. R. (1999). Loss of a gp130 cardiac muscle cell survival pathway is a critical event in the onset of heart failure during biomechanical stress. Cell 97, 189-198.
Hunt, S. A., Abraham, W. T., Chin, M. H., Feldman, A. M., Francis, G. S., Ganiats, T. G., Jessup, M., Konstam, M. A., Mancini, D. M., Michl, K., et al. (2005). ACC/AHA 2005 Guideline Update for the Diagnosis and Management of Chronic Heart Failure in the Adult: a report of the American College of Cardiology/American Heart Association Task Force on Practice Guidelines (Writing Committee to Update the 2001 Guidelines for the Evaluation and Management of Heart Failure): developed in collaboration with the American College of Chest Physicians and the International Society for Heart and Lung Transplantation: endorsed by the Heart Rhythm Society. Circulation 112, e154-235.
Keen, H. L., Ryan, M. J., Beyer, A., Mathur, S., Scheetz, T. E., Gackle, B. D., Faraci, F. M., Casavant, T. L., and Sigmund, C. D. (2004). Gene expression profiling of potential PPARgamma target genes in mouse aorta. Physiol Genomics 18, 33-42.
Lemay, D. G., and Hwang, D. H. (2006). Genome-wide identification of peroxisome proliferator response elements using integrated computational genomics. J Lipid Res 47, 1583-1587.
Li, B., Setoguchi, M., Wang, X., Andreoli, A. M., Leri, A., Malhotra, A., Kajstura, J., and Anversa, P. (1999). Insulin-like growth factor-1 attenuates the detrimental impact of nonocclusive coronary artery constriction on the heart. Circ Res 84, 1007-1019.

Lorell, B. H., and Carabello, B. A. (2000). Left ventricular hypertrophy: pathogenesis, detection, and prognosis. Circulation 102, 470-479.
MacLellan, W. R., and Schneider, M. D. (1997). Death by design. Programmed cell death in cardiovascular biology and disease. Circ Res 81, 137-144.
Madrazo, J. A., and Kelly, D. P. (2008). The PPAR trio: Regulators of myocardial energy metabolism in health and disease. J Mol Cell Cardiol.
Nielsen, R., Grontved, L., Stunnenberg, H. G., and Mandrup, S. (2006). Peroxisome proliferator-activated receptor subtype- and cell-type-specific activation of genomic target genes upon adenoviral transgene delivery. Mol Cell Biol 26, 5698-5714.
Peters, J. M., Lee, S. S., Li, W., Ward, J. M., Gavrilova, O., Everett, C., Reitman, M. L., Hudson, L. D., and Gonzalez, F. J. (2000). Growth, adipose, brain, and skin alterations resulting from targeted disruption of the mouse peroxisome proliferator-activated receptor beta(delta). Mol Cell Biol 20, 5119-5128.
Rybkin, II, Markham, D. W., Yan, Z., Bassel-Duby, R., Williams, R. S., and Olson, E. N. (2003). Conditional expression of SV40 T-antigen in mouse cardiomyocytes facilitates an inducible switch from proliferation to differentiation. J Biol Chem 278, 15927-15934.
Sadoshima, J., Montagne, O., Wang, Q., Yang, G., Warden, J., Liu, J., Takagi, G., Karoor, V., Hong, C., Johnson, G. L., et al. (2002). The MEKK1-JNK pathway plays a protective role in pressure overload but does not mediate cardiac hypertrophy. J Clin Invest 110, 271-279.
Sano, M., and Schneider, M. D. (2002). Still stressed out but doing fine: normalization of wall stress is superfluous to maintaining cardiac function in chronic pressure overload. Circulation 105, 8-10.
Seimandi, M., Lemaire, G., Pillon, A., Perrin, A., Carlavan, I., Voegel, J. J., Vignon, F., Nicolas, J. C., and Balaguer, P. (2005). Differential responses of PPARalpha, PPARdelta, and PPARgamma reporter cell lines to selective PPAR synthetic ligands. Anal Biochem 344, 8-15.
Smeets, P. J., Planavila, A., van der Vusse, G. J., and van Bilsen, M. (2007). Peroxisome proliferator-activated receptors and inflammation: take it to heart. Acta Physiol (Oxf) 191, 171-188.
Tamura, K., Ono, A., Miyagishima, T., Nagao, T., and Urushidani, T. (2006). Profiling of gene expression in rat liver and rat primary cultured hepatocytes treated with peroxisome proliferators. J Toxicol Sci 31, 471-490.
van Empel, V. P., Bertrand, A. T., Hofstra, L., Crijns, H. J., Doevendans, P. A., and De Windt, L. J. (2005a). Myocyte apoptosis in heart failure. Cardiovasc Res 67, 21-29.
van Empel, V. P., Bertrand, A. T., van der Nagel, R., Kostin, S., Doevendans, P. A., Crijns, H. J., de Wit, E., Sluiter, W., Ackerman, S. L., and De Windt, L. J. (2005b). Downregulation of apoptosis-inducing factor in harlequin mutant mice sensitizes the myocardium to oxidative stress-related cell death and pressure overload-induced decompensation. Circ Res 96, e92-e101.
van Empel, V. P., Bertrand, A. T., van Oort, R. J., van der Nagel, R., Engelen, M., van Rijen, H. V., Doevendans, P. A., Crijns, H. J., Ackerman, S. L., Sluiter, W., and De Windt, L. J. (2006). EUK-8, a superoxide dismutase and catalase mimetic, reduces cardiac oxidative stress and ameliorates pressure overload-induced heart failure in the harlequin mouse mutant. J Am Coll Cardiol 48, 824-832.
van Oort, R. J., van Rooij, E., Bourajjaj, M., Schimmel, J., Jansen, M. A., van der Nagel, R., Doevendans, P. A., Schneider, M. D., van Echteld, C. J., and De Windt, L. J. (2006). MEF2 activates a genetic program promoting chamber dilation and contractile dysfunction in calcineurin-induced heart failure. Circulation 114, 298-308.
van Rooij, E., Doevendans, P. A., de Theije, C. C., Babiker, F. A., Molkentin, J. D., and de Windt, L. J. (2002). Requirement of nuclear factor of activated T-cells in calcineurin- mediated cardiomyo-

cyte hypertrophy. J Biol Chem 277, 48617-48626.
Wang, L., Ma, W., Markovich, R., Chen, J. W., and Wang, P. H. (1998). Regulation of cardiomyocyte apoptotic signaling by insulin-like growth factor I. Circ Res 83, 516-522.
Yeh, C. H., Chen, T. P., Lee, C. H., Wu, Y. C., Lin, Y. M., and Lin, P. J. (2006). Cardiomyocytic apoptosis following global cardiac ischemia and reperfusion can be attenuated by peroxisome proliferator-activated receptor alpha but not gamma activators. Shock 26, 262-270.
Yeh, C. H., Lin, Y. M., Wu, Y. C., and Lin, P. J. (2005). Inhibition of NF-kappa B activation can attenuate ischemia/reperfusion-induced contractility impairment via decreasing cardiomyocytic proinflammatory gene up-regulation and matrix metalloproteinase expression. J Cardiovasc Pharmacol 45, 301-309.
Yue, T. L., Bao, W., Jucker, B. M., Gu, J. L., Romanic, A. M., Brown, P. J., Cui, J., Thudium, D. T., Boyce, R., Burns-Kurtis, C. L., et al. (2003). Activation of peroxisome proliferator-activated receptor-alpha protects the heart from ischemia/reperfusion injury. Circulation 108, 2393-2399.
Zhang, D., Gaussin, V., Taffet, G. E., Belaguli, N. S., Yamada, M., Schwartz, R. J., Michael, L. H., Overbeek, P. A., and Schneider, M. D. (2000). TAK1 is activated in the myocardium after pressure overload and is sufficient to provoke heart failure in transgenic mice. Nat Med 6, 556-563.
Zhu, Y., Alvares, K., Huang, Q., Rao, M. S., and Reddy, J. K. (1993). Cloning of a new member of the peroxisome proliferator-activated receptor gene family from mouse liver. J Biol Chem 268, 26817-26820.

Supplemental data. An Expanded Agilent microarray

Gene	Description	PPARα
Adamts8	a disintegrin-like and metalloprotease (reprolysin type) with thrombospondin type 1 motif, 8	33,3
Gstt3	glutathione S-transferase, theta 3	23,7
Igf1	insulin-like growth factor 1	23,2
Crabp1	cellular retinoic acid binding protein I	16,3
Kcnn2	potassium intermediate/small conductance calcium-activated channel, subfamily N, member 2	15,2
Lass4	longevity assurance homolog 4	14,8
Dfna5h	deafness, autosomal dominant 5 homolog	12,1
Cte1	cytosolic acyl-CoA thioesterase 1	9,3
Hist1h1d	histone 1, H1d	8,7
Khdrbs3	KH domain containing, RNA binding, signal transduction associated 3	8,6
Ces3	carboxylesterase 3	8,4
Pappa	pregnancy-associated plasma protein-A mRNA	7,9
Msx2	homeo box, msh-like 2	6,8
Pgam2	phosphoglycerate mutase 2	6,4
Lims2	LIM and senescent cell antigen like domains 2	6,2
Akp2	alkaline phosphatase 2	6,1
Cspg4	chondroitin sulfate proteoglycan 4	5,9
Gypc	glycophorin C	5,8
Mmp2	matrix metalloproteinase 2	5,7
Prodh	proline dehydrogenase	5,6
Bace2	beta-site APP-cleaving enzyme 2	5,3
H2-Ke6	H2-K region expressed gene 6	5,0
Bscl2	Bernardinelli-Seip congenital lipodystrophy 2 homolog	5,0
Tmeff2	transmembrane protein with EGF-like and two follistatin-like domains 2	4,9
S3-12	plasma membrane associated protein, S3-12	4,8
Jam3	junction adhesion molecule 3	4,7
Ocil	osteoclast inhibitory lectin	4,7
Rbp1	retinol binding protein 1	4,5
Ggtla1	gamma-glutamyltransferase-like activity 1	4,5
Renbp	renin binding protein	4,4
Tcn2	transcobalamin 2	4,4
Cables1	Cdk5 and Abl enzyme substrate 1	4,4
Ogn	osteoglycin	4,3
Serpine1	serine (or cysteine) proteinase inhibitor, clade E, member 1	4,2
Idb3	inhibitor of DNA binding 3 (Idb3), mRNA	4,2
Mmp3	matrix metalloproteinase 3	4,1
C1qtnf5	C1q and tumor necrosis factor related protein 5	4,0
Pdk4	pyruvate dehydrogenase kinase, isoenzyme 4	3,9
Ces1	carboxylesterase 1	3,8
Semcap2	semaF cytoplasmic domain associated protein 2	3,8
Fmo5	flavin containing monooxygenase 5	3,7
Aplp1	amyloid beta (A4) precursor-like protein 1	3,7
Chst7	carbohydrate (N-acetylglucosamino) sulfotransferase 7	3,7
P2rx5	purinergic receptor P2X, ligand-gated ion channel, 5	3,7
Psen2	presenilin 2	3,6
Fhl1	four and a half LIM domains 1	3,6
Aldh1a1	aldehyde dehydrogenase family 1, subfamily A1	3,5
Usmg4	upregulated during skeletal muscle growth 4	3,5
Twist1	twist gene homolog 1	3,5
Tgfb1i1	transforming growth factor beta 1 induced transcript 1	3,4
Myom2	myomesin 2	3,3
Cd59a	CD59a antigen	3,3
Ctgf	connective tissue growth factor	3,2
Ly6c	lymphocyte antigen 6 complex, locus C	3,2
Ptp4a3	protein tyrosine phosphatase 4a3	3,2
Bace2	beta-site APP-cleaving enzyme 2	3,2
Lsp1	lymphocyte specific 1	3,1
Defb2	defensin beta 2	3,0
Jam2	junction adhesion molecule 2	3,0
Ppap2b	phosphatidic acid phosphatase type 2B	3,0
Slfn2	schlafen 2	3,0
Gyg1	glycogenin 1	3,0
Gsta3	glutathione S-transferase, alpha 3	3,0
Klc3	kinesin light chain 3	2,8
Lrfn3	leucine rich repeat and fibronectin type III domain containing 3	2,8
Mfn2	mitofusin 2	2,8
Creld1	cysteine-rich with EGF-like domains 1	2,7
Xdh	xanthine dehydrogenase	2,7
Smpd2	sphingomyelin phosphodiesterase 2	2,7
Msra	methionine sulfoxide reductase A	2,7
Rin3	Ras and Rab interactor 3	2,7

Maged2	melanoma antigen, family D, 2	2,7
Gng13	guanine nucleotide binding protein 13, gamma	2,6
Plcg2	phospholipase C, gamma 2	2,6
Map3k12	mitogen activated protein kinase kinase kinase 12	2,6
Emilin2	elastin microfibril interfacer 2	2,6
Cog8	component of oligomeric golgi complex 8	2,6
Tuba1	tubulin, alpha 1	2,6
Ly6i	lymphocyte antigen 6 complex, locus I	2,6
Bckdha	branched chain ketoacid dehydrogenase E1, alpha polypeptide	2,6
Dok1	docking protein 1	2,6
H2-M2	strain P/J MHC class Ib antigen	2,6
Cnn2	calponin 2	2,6
Prdx5	peroxiredoxin 5	2,6
Stxbp2	syntaxin binding protein 2	2,6
H2-T23	histocompatibility 2, T region locus 23	2,6
Popdc3	popeye domain containing 3	2,5
Nagk	N-acetylglucosamine kinase	2,5
Hspb8	heat shock 27kDa protein 8	2,5
Apba3	amyloid beta (A4) precursor protein-binding, family A, member 3	2,5
Slamf9	SLAM family member 9	2,5
Kcnj14	potassium inwardly-rectifying channel, subfamily J, member 14	2,5
Gstk1	glutathione S-transferase kappa 1	2,5
Khk	ketohexokinase	2,4
Tnnt2	troponin T2, cardiac	2,4
G6pc3	glucose 6 phosphatase, catalytic, 3	2,4
Prrx1	paired related homeobox 1	2,4
Arpc4	actin related protein 2/3 complex, subunit 4	2,4
Nosip	nitric oxide synthase interacting protein	2,4
Tusc2	tumor suppressor candidate 2	2,3
Pde4a	phosphodiesterase 4A, cAMP specific (Pde4a), mRNA	2,3
Fbxo6b	F-box only protein 6b	2,3
Glrx1	glutaredoxin 1 (thioltransferase)	2,3
Mapk13	mitogen activated protein kinase 13	2,3
Klhl13	kelch-like 13 (Drosophila)	2,3
Eif4g3	eukaryotic translation initiation factor 4 gamma, 3	2,3
Nte	neuropathy target esterase	2,3
Kelchl	kelch-like (D. melanogaster)	2,3
Ankrd1	ankyrin repeat domain 1 (cardiac muscle)	2,3
Polrmt	polymerase (RNA) mitochondrial (DNA directed)	2,3
Extl1	exostoses (multiple)-like 1	2,3
Prcc	papillary renal cell carcinoma (translocation-associated)	2,3
F8a	factor 8-associated gene A	2,3
Fah	fumarylacetoacetate hydrolase	2,3
Def8	differentially expressed in FDCP 8	2,2
Zdhhc1	zinc finger, DHHC domain containing 1	2,2
Mpra	membrane progestin receptor alpha	2,2
Xab2	XPA binding protein 2	2,2
Fbxo46	F-box protein 46	2,2
Agpat2	1-acylglycerol-3-phosphate O-acyltransferase 2	2,2
Fuk	fucokinase (Fuk), transcript variant 1	2,2
Man2b2	mannosidase 2, alpha B2	2,2
Taf1c	TATA box binding protein (Tbp)-associated factor, RNA polymerase I, C	2,2
Dhodh	dihydroorotate dehydrogenase	2,2
Efs	embryonal Fyn-associated substrate	2,2
Etfb	electron transferring flavoprotein, beta polypeptide	2,1
Slc1a7	solute carrier family 1 (glutamate transporter), member 7	2,1
Rgl1	ral guanine nucleotide dissociation stimulator,-like 1	2,1
Elp3	elongation protein 3 homolog (S. cerevisiae)	2,1
Ngfb	nerve growth factor, beta	2,1
Ldh2	lactate dehydrogenase 2, B chain	2,1
Btd	biotinidase	2,1
Naglu	alpha-N-acetylglucosaminidase (Sanfilippo disease IIIB)	2,1
Rdh5	retinol dehydrogenase 5	2,1
Pold4	polymerase (DNA-directed), delta 4	2,1
Folr1	folate receptor 1 (adult)	2,1
Numbl	numb-like	2,0
Col4a2	procollagen, type IV, alpha 2	2,0
Cryab	crystallin, alpha B	2,0
Eif4ebp1	eukaryotic translation initiation factor 4E binding protein 1	2,0
Fbxl6	F-box and leucine-rich repeat protein 6	2,0
Clca2	chloride channel calcium activated 2 (Cl	2,0
Pdlim4	PDZ and LIM domain 4	2,0
Fhod1	formin homology 2 domain containing 1	2,0
Lrig1	leucine-rich repeats and immunoglobulin-like domains 1	2,0
Pcbd	6-pyruvoyl-tetrahydropterin synthase/dimerization cofactor of hepatocyte nuclear factor 1 alpha	2,0

Leprel2	leprecan-like 2	2,0
Col4a5	procollagen, type IV, alpha 5	2,0
Mmp11	matrix metalloproteinase 11	2,0
Mras	muscle and microspikes RAS	2,0
Suox	sulfite oxidase	2,0
Pfn1	profilin 1	2,0
Oplah	5-oxoprolinase (ATP-hydrolysing)	2,0
Sdf2l1	stromal cell-derived factor 2-like	-2,0
Stam2	signal transducing adaptor molecule (SH3 domain and ITAM motif) 2	-2,0
Prpsap2	phosphoribosyl pyrophosphate synthetase-associated protein 2	-2,0
Uap1	UDP-N-acetylglucosamine pyrophosphorylase 1	-2,0
Spon2	spondin 2, extracellular matrix protein	-2,0
Thrap6	thyroid hormone receptor associated protein 6	-2,0
Cd1d1	CD1d1 antigen	-2,0
Aqp1	aquaporin 1	-2,0
Kifap3	kinesin-associated protein 3	-2,0
Prei3	preimplantation protein 3	-2,0
Gfpt1	glutamine fructose-6-phosphate transaminase 1	-2,0
Lztfl1	leucine zipper transcription factor-like 1	-2,0
Gjb4	gap junction membrane channel protein beta 4	-2,0
Lypla1	lysophospholipase 1	-2,0
Stk38	serine/threonine kinase 38	-2,0
Cyp2s1	cytochrome P450, family 2, subfamily s, polypeptide 1	-2,1
Sephs1	selenophosphate synthetase 1	-2,1
Cdh13	cadherin 13	-2,1
Ugt1a9	UDP glycosyltransferase 1 family polypeptide A9	-2,1
Olfr368	olfactory receptor 368	-2,1
Nfatc1	nuclear factor of activated T-cells, cytoplasmic, calcineurin-dependent 1	-2,1
Gtpbp4	GTP binding protein 4	-2,1
Ccrn4l	CCR4 carbon catabolite repression 4-like	-2,1
Anapc10	anaphase promoting complex subunit 10	-2,1
Runx1	runt related transcription factor 1	-2,1
Ptgis	prostaglandin I2 (prostacyclin) synthase	-2,1
Bcar3	breast cancer anti-estrogen resistance 3	-2,1
Krt1-19	keratin complex 1, acidic, gene 19	-2,1
Mtif2	mitochondrial translational initiation factor 2	-2,1
Cova1	cytosolic ovarian carcinoma antigen 1	-2,1
Apobec1	apolipoprotein B editing complex 1	-2,1
Usp47	ubiquitin specific protease 47	-2,1
Stxbp3	syntaxin binding protein 3	-2,2
Clk4	CDC like kinase 4	-2,2
Extl2	exotoses (multiple)-like 2	-2,2
Wdr9	WD repeat domain 9	-2,2
Adrb1	adrenergic receptor, beta 1	-2,2
Slc12a2	solute carrier family 12, member 2	-2,2
Irak1bp1	interleukin-1 receptor-associated kinase 1 binding protein 1	-2,2
Mafb	v-maf musculoaponeurotic fibrosarcoma oncogene family, protein B	-2,2
Hmgb2l1	high mobility group box 2-like 1	-2,2
Hccs	holocytochrome c synthetase	-2,2
Ncoa6ip	nuclear receptor coactivator 6 interacting protein	-2,2
Armcx3	armadillo repeat containing, X-linked 3	-2,2
Oact2	O-acyltransferase (membrane bound) domain containing 2	-2,2
Rab1	RAB1, member RAS oncogene family	-2,2
Ltbp2	latent transforming growth factor beta binding protein 2	-2,2
Mapk8ip3	mitogen-activated protein kinase 8 interacting protein 3	-2,2
Rnf128	ring finger protein 128	-2,2
Tfg	Trk-fused gene	-2,2
Usp54	ubiquitin specific protease 54	-2,2
Myohd1	myosin head domain containing 1	-2,2
Herc3	hect domain and RLD 3	-2,2
Cmkor1	chemokine orphan receptor 1	-2,2
Cul5	cullin 5	-2,2
Cul1	cullin 1	-2,2
Nphp1	nephronophthisis 1 (juvenile) homolog (human)	-2,2
Dst	dystonin	-2,2
Kif1b	kinesin family member 1B (Kif1b), transcript variant 1	-2,3
Blzf1	basic leucine zipper nuclear factor 1	-2,3
Vim	vimentin	-2,3
Mgat3	mannoside acetylglucosaminyltransferase 3	-2,3
Csnk1g3	casein kinase 1, gamma 3	-2,3
Gig1	glucocorticoid induced gene 1	-2,3
Rpl4	ribosomal protein L4	-2,3
Fzd3	frizzled homolog 3 (Drosophila)	-2,3
Rnf12	ring finger protein 12	-2,3
Idb2	inhibitor of DNA binding 2	-2,3

Sema3e	sema domain, immunoglobulin domain (Ig), short basic domain, secreted, (semaphorin) 3E	-2,3
Plaa	phospholipase A2, activating protein	-2,3
Catnbip1	catenin beta interacting protein 1	-2,3
Tgfbr2	transforming growth factor, beta receptor II (Tgfbr2), transcript variant 1	-2,3
Gltp	glycolipid transfer protein	-2,4
Zzz3	zinc finger, ZZ domain containing 3	-2,4
Pard6g	par-6 partitioning defective 6 homolog gamma	-2,4
Zfyve16	zinc finger, FYVE domain containing 16	-2,4
Crlf3	cytokine receptor-like factor 3	-2,4
Nrd1	nardilysin, N-arginine dibasic convertase, NRD convertase 1	-2,4
Epim	epimorphin	-2,4
Trim33	tripartite motif protein 33	-2,4
Sox11	SRY-box containing gene 11	-2,4
Zfhx1b	zinc finger homeobox 1b	-2,4
Mtf2	metal response element binding transcription factor 2	-2,4
Nup107	nucleoporin 107	-2,4
Ugp2	UDP-glucose pyrophosphorylase 2	-2,4
Rassf2	Ras association (RalGDS/AF-6) domain family 2	-2,5
C1d	nuclear DNA binding protein	-2,5
Clic5	chloride intracellular channel 5	-2,5
Phca	phytoceramidase, alkaline	-2,5
Myc	myelocytomatosis oncogene	-2,5
Zfpm2	zinc finger protein, multitype 2	-2,5
Adam1a	a disintegrin and metalloproteinase domain 1a	-2,5
Crsp9	cofactor required for Sp1 transcriptional activation, subunit 9	-2,5
Cklfsf8	chemokine-like factor super family 8	-2,5
Birc1b	baculoviral IAP repeat-containing 1b	-2,5
Nck1	non-catalytic region of tyrosine kinase adaptor protein 1	-2,5
Foxp1	forkhead box P1	-2,5
Mtmr1	myotubularin related protein 1	-2,5
Rabep1	rabaptin, RAB GTPase binding effector protein 1	-2,6
Ofd1	oral-facial-digital syndrome 1 gene homolog	-2,6
Camk2d	calcium/calmodulin-dependent protein kinase II, delta	-2,6
Ywhae	tyrosine 3-monooxygenase/tryptophan 5-monooxygenase activation protein	-2,6
Drctnnb1a	down-regulated by Ctnnb1, a	-2,6
Vcl	vinculin	-2,6
Acate2	acyl-Coenzyme A thioesterase 2, mitochondrial	-2,6
Orc2l	origin recognition complex, subunit 2-like	-2,6
Sbds	Shwachman-Bodian-Diamond syndrome homolog	-2,6
Pspc1	paraspeckle protein 1	-2,6
Gcnt1	glucosaminyl (N-acetyl) transferase 1, core 2	-2,6
Odz3	odd Oz/ten-m homolog 3	-2,6
Pdir	protein disulfide isomerase-related	-2,7
Coro2a	coronin, actin binding protein 2A	-2,7
Rad50	RAD50 homolog	-2,7
Hyal1	hyaluronidase 1	-2,7
Akap9	A kinase (PRKA) anchor protein	-2,7
Slc7a3	solute carrier family 7 (cationic amino acid transporter, y+ system), member 3	-2,7
Cetn4	centrin 4	-2,7
Ddx52	DEAD (Asp-Glu-Ala-Asp) box polypeptide 52	-2,7
Usp33	ubiquitin specific protease 33	-2,8
Agps	alkylglycerone phosphate synthase	-2,8
Pkn2	protein kinase N2	-2,8
Vps54	vacuolar protein sorting 54	-2,8
Rngtt	RNA guanylyltransferase and 5'-phosphatase	-2,8
Mbd4	methyl-CpG binding domain protein 4	-2,8
Fhl5	four and a half LIM domains 5	-2,8
Srp72	signal recognition particle 72	-2,8
Dhx36	DEAH (Asp-Glu-Ala-His) box polypeptide 36	-2,8
Fkbp5	FK506 binding protein 5	-2,9
Zrf2	zuotin related factor 2	-2,9
Evi5	ecotropic viral integration site 5	-2,9
Txn1	thioredoxin 1	-2,9
Lbr	lamin B receptor	-2,9
Ptma	prothymosin alpha	-2,9
Skp2	S-phase kinase-associated protein 2 (p45)	-2,9
Elovl7	ELOVL family member 7, elongation of long chain fatty acids (yeast)	-2,9
Rad51ap1	RAD51 associated protein 1	-2,9
Rap2c	RAP2C, member of RAS oncogene family	-2,9
Ddx26	DEAD/H (Asp-Glu-Ala-Asp/His) box polypeptide 26	-2,9
Donson	downstream neighbor of SON	-3,0
Cse1l	chromosome segregation 1-like (S. cerevisiae)	-3,0
Zfp403	zinc finger protein 403	-3,0
Vrk1	vaccinia related kinase 1	-3,0

Inpp5f	inositol polyphosphate-5-phosphatase F	-3,0
Ptma	prothymosin alpha	-3,0
Myh7	myosin, heavy polypeptide 7, cardiac muscle, beta	-3,0
Map3k1	mitogen activated protein kinase kinase kinase 1	-3,0
Timp3	tissue inhibitor of metalloproteinase 3	-3,0
Galnt6	UDP-N-acetyl-alpha-D-galactosamine:polypeptide N-acetylgalactosaminyltransferase 6	-3,1
Ltb4dh	leukotriene B4 12-hydroxydehydrogenase	-3,1
Sfrs3	splicing factor, arginine/serine-rich 3 (SRp20)	-3,1
Rasa1	RAS p21 protein activator 1	-3,1
Zfp326	zinc finger protein 326	-3,1
Ccnl1	cyclin L1	-3,1
Cdh17	cadherin 17	-3,1
Rab27b	RAB27b, member RAS oncogene family	-3,1
Vdp	vesicle docking protein	-3,2
Eif3s6	eukaryotic translation initiation factor 3, subunit 6	-3,2
Nol7	nucleolar protein 7	-3,2
Dixdc1	DIX domain containing 1	-3,2
Slc4a8	solute carrier family 4 (anion exchanger), member 8	-3,3
Fpgt	mRNA for putative GDP-L-fucose pyrophosphorylase	-3,3
Rnf2	ring finger protein 2	-3,3
Chm	choroidermia	-3,3
Terf1	telomeric repeat binding factor 1	-3,3
Ddx50	DEAD (Asp-Glu-Ala-Asp) box polypeptide 50	-3,3
Acbd5	acyl-Coenzyme A binding domain containing 5	-3,3
Psip1	PC4 and SFRS1 interacting protein 1	-3,3
Galnt7	UDP-N-acetyl-alpha-D-galactosamine: polypeptide N-acetylgalactosaminyltransferase 7	-3,3
Eea1	early endosome antigen 1	-3,3
Kif3a	kinesin family member 3A	-3,3
Mpp5	membrane protein, palmitoylated 5 (MAGUK p55 subfamily member 5)	-3,4
Prkdc	protein kinase, DNA activated, catalytic polypeptide	-3,4
Zfp281	zinc finger protein 281	-3,4
Clic3	chloride intracellular channel 3	-3,4
Myo5a	myosin Va	-3,5
Itgb7	integrin beta 7	-3,5
Slc35a3	solute carrier family 35 (UDP-N-acetylglucosamine (UDP-GlcNAc) transporter), member 3	-3,5
Rpp30	ribonuclease P/MRP 30kDa subunit (human)	-3,5
Lhfpl2	lipoma HMGIC fusion partner-like 2	-3,5
Abi2	abl-interactor 2	-3,5
Mbnl2	muscleblind-like 2	-3,5
Sec15l1	SEC15 homolog (S. cerevisiae)	-3,5
Tnxb	tenascin XB	-3,6
Mbtd1	mbt domain containing 1	-3,6
Taf15	TAF15 RNA polymerase II, TATA box binding protein (TBP)-associated factor	-3,6
Lamb3	laminin, beta 3	-3,6
Ltbp1	latent transforming growth factor beta binding protein 1	-3,6
Anxa7	annexin A7	-3,6
Galnact2	chondroitin sulfate GalNAcT-2	-3,6
Denr	density-regulated protein	-3,6
Chtf18	CTF18, chromosome transmission fidelity factor 18 homolog (S. cerevisiae)	-3,6
Egln3	EGL nine homolog 3 (C. elegans)	-3,7
Slbp	stem-loop binding protein	-3,7
Axot	axotrophin	-3,7
Ptbp2	polypyrimidine tract binding protein 2	-3,7
Zfml	zinc finger, matrin-like	-3,8
Sfrs7	splicing factor, arginine/serine-rich 7	-3,8
Slc22a4	solute carrier family 22 (organic cation transporter), member 4	-3,8
Gpsm2	G-protein signalling modulator 2 (AGS3-like, C. elegans)	-3,8
Ptpn18	protein tyrosine phosphatase, non-receptor type 18	-3,9
Myst4	MYST histone acetyltransferase monocytic leukemia 4	-4,0
Vdac2	voltage-dependent anion channel 2	-4,0
Cspg6	chondroitin sulfate proteoglycan 6	-4,0
Camk2g	calcium/calmodulin -dependent protein kinase II gamma	-4,0
Ddr2	discoidin domain receptor family, member 2	-4,1
Fdps	farnesyl diphosphate synthetase	-4,1
Chek1	checkpoint kinase 1 homolog (S. pombe)	-4,2
Mbnl2	muscleblind-like 2	-4,2
Etnk2	strain C3Hx101 putative ethanolamine kinase	-4,2
Nbn	nibrin	-4,3
Casp3	caspase 3, apoptosis related cysteine protease	-4,3
Zdhhc21	zinc finger, DHHC domain containing 21	-4,3
Pdgfrb	platelet derived growth factor receptor, beta polypeptide	-4,4
Zfp101	zinc finger protein 101	-4,4
Fmr1	fragile X mental retardation syndrome 1 homolog	-4,6
Cd2ap	CD2-associated protein	-4,7
Stk6	serine/threonine kinase 6	-4,7

Atr	protein kinase ATR	-4,8
Stk17b	serine/threonine kinase 17b (apoptosis-inducing)	-4,9
Sirt1	sirtuin 1	-5,0
Msln	mesothelin	-5,0
Sqle	squalene epoxidase	-5,1
Sema3a	sema domain, immunoglobulin domain (Ig), short basic domain, secreted	-5,1
Brip1	BRCA1 interacting protein C-terminal helicase 1	-5,2
Abcb1b	ATP-binding cassette, sub-family B (MDR/TAP), member 1B	-5,3
Smarca5	DNA-dependent ATPase SNF2H	-5,3
Gpr64	G protein-coupled receptor 64	-5,4
Ifit1	interferon-induced protein with tetratricopeptide repeats 1	-5,5
Dek	DEK oncogene	-5,5
Cdca1	cell division cycle associated 1	-5,6
Cacna1g	calcium channel, voltage-dependent, T type, alpha 1G subunit	-5,6
Rbl1	retinoblastoma-like 1	-5,7
Vldlr	clone:9630026O22 product:SIMILAR TO VERY LOW DENSITY LIPOPROTEIN RECEPTOR homolog	-5,7
Kpnb3	karyopherin (importin) beta 3	-5,8
Nkx2-3	NK2 transcription factor related, locus 3	-6,1
Trpm7	transient receptor potential cation channel, subfamily M, member 7	-6,7
Acsl3	clone:2610510B12 product:fatty acid Coenzyme A ligase, long chain 3	-6,7
Zfp53	zinc finger protein 53	-6,8
Cdc7	cell division cycle 7	-7,1
Ifi202b	interferon activated gene 202B	-7,1
Ccm1	cerebral cavernous malformations 1	-7,2
Fignl1	fidgetin-like 1	-7,3
Fshprh1	FSH primary response 1	-7,3
Mad2l1	mitotic checkpoint component Mad2	-7,5
Cdca3	cell division cycle associated 3	-7,6
Smarca1	SWI/SNF related, matrix associated, actin dependent regulator of chromatin, subfamily a, member 1	-7,8
Anpep	alanyl (membrane) aminopeptidase	-8,2
Sema3b	sema domain, immunoglobulin domain (Ig), short basic domain, secreted	-8,3
Cdc6	cell division cycle 6 homolog (S. cerevisiae)	-8,3
Shcbp1	Shc SH2-domain binding protein 1	-8,5
Kif23	kinesin family member 23	-8,8
Krt2-8	keratin complex 2, basic, gene 8	-9,9
Gbp4	guanylate nucleotide binding protein 3	-10,3
Nusap1	nucleolar and spindle associated protein 1	-10,6
Kntc1	clone:D330012D13 product:hypothetical protein, full insert sequence	-10,7
Cenpe	clone:C530022J18 product:hypothetical Lipocalin-related	-11,4

Gene	Description	PPARβ/δ
Sepp1	selenoprotein P, plasma, 1	9,7
Eif4a2	eukaryotic translation initiation factor 4A2	7,1
Fabp4	fatty acid binding protein 4, adipocyte	6,5
Hist1h2bc	histone 1, H2bc	5,5
BC013561	cDNA clone IMAGE:3492058, partial cds	5,4
Dcn	decorin	5,3
Maf	avian musculoaponeurotic fibrosarcoma (v-maf) AS42 oncogene homolog	5,2
Sesn3	sestrin 3	5,0
TC1463663	A48015 S-100 protein beta chain - mouse	5,0
Cirbp	cold inducible RNA binding protein	4,4
Spnb2	spectrin beta 2	4,1
MGI:1889205	plasma glutamate carboxypeptidase	3,9
Cltc	clathrin, heavy polypeptide (Hc)	3,8
Figf	c-fos induced growth factor	3,8
TC1536702	protein {Methanosarcina acetivorans C2A;}	3,8
Adamts1	a disintegrin-like and metalloprotease (reprolysin type)	3,7
Abcg5	ATP-binding cassette, sub-family G (WHITE)	3,6
Efna5	ephrin A5 (Efna5), transcript variant 1	3,6
Il15	interleukin 15	3,6
Slc40a1	solute carrier family 40 (iron-regulated transporter), member 1	3,5
Aldh3a2	aldehyde dehydrogenase family 3, subfamily A2	3,5
Spnb2	spectrin beta 2	3,5
Dtwd1	DTW domain containing 1	3,4
Mgp	matrix Gla protein	3,4
Ches1	checkpoint supressor 1	3,4
Actr2	ARP2 actin-related protein 2 homolog (yeast)	3,4
Hist1h2bk	histone 1, H2bk	3,3
9530028C05	similar to HISTOCOMPATIBILITY 2, CLASS II ANTIGEN E BETA	3,3
Slc8a1	solute carrier family 8 (sodium/calcium exchanger)	3,3
Mapk4	mitogen-activated protein kinase 4	3,3
Serpinb1b	serine (or cysteine) proteinase inhibitor, clade B, member 1b	3,3
Za20d2	zinc finger, A20 domain containing 2	3,2
Arl10c	similar to ADP-ribosylation factor Y57G11C.13 [Caenorhabditis elegans]	3,2
Serpinb1a	serine (or cysteine) proteinase inhibitor, clade B, member 1a	3,2
Ptp4a1	protein tyrosine phosphatase 4a1	3,2
Wisp2	WNT1 inducible signaling pathway protein 2	3,1
Htra3	serine protease HTRA3	3,1
Tspan13	tetraspanin 13	3,1
Ipo8	PREDICTED: importin 8	3,1
Stc2	stanniocalcin 2	3,0
Cri1	CREBBP/EP300 inhibitory protein 1	2,9
Npm1	nucleophosmin 1	2,9
Crot	carnitine O-octanoyltransferase	2,9
Cp	ceruloplasmin	2,9
MGI:2384914	Dip3 beta	2,9
Mtmr6	myotubularin related protein 6	2,9
Ggh	gamma-glutamyl hydrolase	2,9
Phyh	phytanoyl-CoA hydroxylase	2,9
Pdgfrl	platelet-derived growth factor receptor-like	2,9
Cys1	cystin 1	2,9
Acaa2	acetyl-Coenzyme A acyltransferase 2 (mitochondrial 3-oxoacyl-Coenzyme A thiolase)	2,8
Phr1	pam, highwire, rpm 1	2,8
Hnrph2	heterogeneous nuclear ribonucleoprotein H2	2,8
Slc22a5	solute carrier family 22 (organic cation transporter), member 5	2,8
Pten	phosphatase and tensin homolog	2,8
Snai2	snail homolog 2 (Drosophila)	2,8
Aldh1a7	aldehyde dehydrogenase family 1, subfamily A7	2,8
BC027183	mRNA similar to complement component 1, s subcomponent	2,8
Muc5b	mucin 5, subtype B, tracheobronchial	2,8
Ctla2a	cytotoxic T lymphocyte-associated protein 2 alpha	2,8
Phr1	pam, highwire, rpm 1	2,7
2-sep	septin 2	2,7
Dbp	D site albumin promoter binding protein	2,7
Rorc	RAR-related orphan receptor gamma	2,7
Ppfibp1	PTPRF interacting protein, binding protein 1 (liprin beta 1)	2,7
G0s2	G0/G1 switch gene 2	2,7
Pex13	peroxisomal biogenesis factor 13	2,7
Pscd3	pleckstrin homology, Sec7 and coiled-coil domains 3	2,7
Selenbp2	selenium binding protein 2	2,6
Itpr1	inositol 1,4,5-triphosphate receptor 1	2,6
A230083H22Rik	similar to BCL2/ADENOVIRUS E1B 19-KDA PROTEIN-INTERACTING PROTEIN 2	2,6
Zfp36l1	Mouse TIS11 primary response gene	2,6
Ak5	ADENYLATE KINASE ISOZYME 5 homolog	2,6
C1r	complement component 1, r subcomponent	2,6
Lox	lysyl oxidase	2,6
Gsta1	glutathione S-transferase, alpha 1	2,6
Rab5a	RAB5A, member RAS oncogene family	2,6
Nfia	nuclear factor I/A	2,6
Enpp1	ectonucleotide pyrophosphatase/phosphodiesterase 1	2,6
Mtpn	myotrophin	2,5
Ankhd1	GENE TRAP ANKYRIN REPEAT CONTAINING PROTEIN	2,5
Itch	ubiquitin protein ligase	2,5

Mrpl50	mitochondrial ribosomal protein L50	2,5
Mfap1	microfibrillar-associated protein 1	2,5
Ctla2b	Mouse ctla-2-beta mRNA, homolog. to cysteine protease proregion	2,5
Fzd4	frizzled homolog 4 (Drosophila)	2,5
Ostm1	osteopetrosis associated transmembrane protein 1	2,5
Rnf6	ring finger protein (C3H2C3 type) 6	2,5
Arid1b	6A3-5 PROTEIN upregulated in a proliferating, but not synthetic, rat smooth muscle cells	2,5
Rfk	riboflavin kinase	2,5
Spp1	secreted phosphoprotein 1	2,5
8-mrt	membrane-associated ring finger (C3HC4) 8	2,5
Ccng2	cyclin G2	2,5
Cd164	CD164 antigen	2,4
Falz	PREDICTED: fetal Alzheimer antigen	2,4
Olfr1198	olfactory receptor 1198	2,4
Insig2	insulin induced gene 2	2,4
Creg1	cellular repressor of E1A-stimulated genes 1	2,4
Cggbp1	CGG triplet repeat binding protein 1	2,4
Ttc3	tetratricopeptide repeat domain 3	2,4
Atg12l	autophagy-related 12-like (yeast)	2,4
Fdx1	ferredoxin 1	2,4
Col14a1	procollagen, type XIV, alpha 1	2,4
Csad	cysteine sulfinic acid decarboxylase	2,4
Sema3c	sema domain, immunoglobulin domain (Ig), short basic domain, secreted, (semaphorin) 3C	2,4
Olfr430	olfactory receptor 430	2,4
Edg2	endothelial differentiation, lysophosphatidic acid G-protein-coupled receptor, 2	2,4
Fras1	Fraser syndrome 1 homolog (human)	2,4
Olfr786	olfactory receptor 786	2,4
Ppp1r14c	protein phosphatase 1, regulatory (inhibitor) subunit 14c	2,4
Prnp	prion protein	2,4
Vps29	vacuolar protein sorting 29 (S. pombe)	2,4
Sumf1	sulfatase modifying factor 1	2,4
Osbpl1a	oxysterol binding protein-like 1A	2,4
Mod1	malic enzyme, supernatant	2,4
Syap1	synapse associated protein 1	2,4
Dock7	dedicator of cytokinesis 7	2,4
Olfr661	olfactory receptor 661	2,4
Hsdl2	hydroxysteroid dehydrogenase like 2	2,4
Tmed7	transmembrane emp24 protein transport domain containing 7	2,4
Ube1c	ubiquitin-activating enzyme E1C	2,4
Ccnc	cyclin C	2,4
Cetn2	centrin 2	2,4
Col15a1	procollagen, type XV	2,4
Csnk1a1	casein kinase 1, alpha 1	2,3
Cbx3	chromobox homolog 3 (Drosophila HP1 gamma)	2,3
MGI:1913996	dynein 2 light intermediate chain	2,3
Zfp580	zinc finger protein 580	2,3
Wnt16	wingless-related MMTV integration site 16	2,3
Slc35f5	solute carrier family 35, member F5	2,3
Plxdc2	plexin domain containing 2	2,3
Ccni	cyclin I	2,3
Cml1	camello-like 1	2,3
Ppid	peptidylprolyl isomerase D (cyclophilin D)	2,3
Anapc1	meiotic check point regulator	2,3
Chmp2b	chromatin modifying protein 2B	2,3
Pros1	protein S (alpha)	2,3
Slc1a1	solute carrier family 1 (neuronal/epithelial high affinity glutamate transporter, system Xag)	2,3
Arl1	ADP-ribosylation factor-like 1	2,3
Mxra8	matrix-remodelling associated 8	2,3
Tlr5	toll-like receptor 5	2,3
Synj2bp	synaptojanin 2 binding protein	2,3
Ube2d2	ubiquitin-conjugating enzyme E2D 2	2,3
Ttf1	transcription termination factor 1	2,2
Polr2b	polymerase (RNA) II (DNA directed) polypeptide B	2,2
Mfi2	antigen p97 (melanoma associated)	2,2
Sec61a2	Sec61, alpha subunit 2 (S. cerevisiae)	2,2
Sdpr	serum deprivation response	2,2
Pir	pirin	2,2
Ing4	inhibitor of growth family, member 4	2,2
Serpinb6a	serine (or cysteine) proteinase inhibitor, clade B, member 6a	2,2
Zranb3	zinc finger, RAN-binding domain containing 3	2,2
Taf13	TAF13 RNA polymerase II, TATA box binding protein (TBP)-associated factor	2,2
Nrn1	neuritin 1	2,2
Dscr5	Down syndrome critical region homolog 5 (human)	2,2
Mllt4	myeloid	2,2
Matn2	matrilin 2	2,2
Cfdp1	craniofacial development protein 1	2,2
Tulp4	tubby like protein 4	2,2
Rgag4	retrotransposon gag domain containing 4	2,2
Yipf4	Yip1 domain family, member 4	2,2
Hars2	histidyl tRNA synthetase 2	2,2
Hist1h4i	histone 1, H4i	2,1
Osbpl9	oxysterol binding protein-like 9	2,1
Ubl3	ubiquitin-like 3	2,1
Stambp	Stam binding protein	2,1
Bfar	bifunctional apoptosis regulator	2,1

Tmem57	transmembrane protein 57	2,1
Serpinb1c	serine (or cysteine) proteinase inhibitor, clade B, member 1c	2,1
Ctcf	CCCTC-binding factor	2,1
Huwe1	HECT, UBA and WWE domain containing 1	2,1
Tnfsf13	tumor necrosis factor (ligand) superfamily, member 13	2,1
Aggf1	angiogenic factor with G patch and FHA domains 1	2,1
Ythdf2	YTH domain family 2	2,1
H3f3b	H3 histone, family 3B	2,1
Tpd52l1	tumor protein D52-like 1	2,1
C4	complement component 4 (within H-2S)	2,1
Rpl31	ribosomal protein L31	2,1
Ramp1	receptor (calcitonin) activity modifying protein 1	2,1
Kazald1	Kazal-type serine protease inhibitor domain 1	2,1
Morf4l1	mortality factor 4 like 1	2,1
Trp53inp2	tumor protein p53 inducible nuclear protein 2	2,1
Pla2g4a	phospholipase A2, group IVA (cytosolic, calcium-dependent)	2,1
Rdh14	retinol dehydrogenase 14 (all-trans and 9-cis)	2,1
Pon3	paraoxonase 3	2,1
Magi2	membrane associated guanylate kinase, WW and PDZ domain containing 2	2,1
Msrb3	methionine sulfoxide reductase B3	2,1
Mgst2	microsomal glutathione S-transferase 2	2,1
Rnf139	ring finger protein 139	2,1
Pex7	peroxisome biogenesis factor 7	2,1
Cln5	adult male thymus cDNA, similar to CEROID-LIPOFUSCINOSIS NEURONAL PROTEIN 5	2,1
Rac1	RAS-related C3 botulinum substrate 1	2,0
Mdfic	MyoD family inhibitor domain containing	2,0
Tmsb4x	thymosin, beta 4, X chromosome	2,0
Rab7	RAB7, member RAS oncogene family	2,0
Snapc1	small nuclear RNA activating complex, polypeptide 1	2,0
Rnase4	ribonuclease, RNase A family 4 (Rnase4), transcript variant 1	2,0
Il11ra1	interleukin 11 receptor, alpha chain 1	2,0
Cbx3	chromobox homolog 3 (Drosophila HP1 gamma)	2,0
Nfe2l2	nuclear factor, erythroid derived 2, like 2	2,0
Sgcb	sarcoglycan, beta (dystrophin-associated glycoprotein)	2,0
Islr	immunoglobulin superfamily containing leucine-rich repeat	2,0
Loh11cr2a	loss of heterozygosity, 11, chromosomal region 2, gene A homolog (human)	2,0
Sox4	SRY-box containing gene 4	2,0
Fts	fused toes	2,0
Txndc9	thioredoxin domain containing 9	2,0
Igfbp2	insulin-like growth factor binding protein 2	2,0
Mkrn2	makorin, ring finger protein, 2	2,0
Laptm4a	lysosomal-associated protein transmembrane 4A	2,0
Ddef2	development and differentiation enhancing factor 2	2,0
Klf10	Kruppel-like factor 10	2,0
Pcdh7	protocadherin 7	2,0
Irf2bp2	PREDICTED: similar to interferon regulatory factor 2 binding protein 2	2,0
Hmgcs1	3-hydroxy-3-methylglutaryl-Coenzyme A synthase 1	2,0
Prkcbp1	adult male small intestine cDNA, CTCL TUMOR ANTIGEN SE14-3 [Homo sapiens]	2,0
Ncald	neurocalcin delta	2,0
Psme4	proteasome (prosome, macropain) activator subunit 4	2,0
Grb14	growth factor receptor bound protein 14	2,0
Mfhas1	similar to malignant fibrous histiocytoma amplified sequence 1	2,0
Aldh4a1	aldehyde dehydrogenase 4 family, member A1	-2,0
Whrn	whirlin (Whrn), transcript variant 2	-2,0
Junb	Jun-B oncogene	-2,0
Dusp8	dual specificity phosphatase 8	-2,0
Slc6a9	solute carrier family 6 (neurotransmitter transporter, glycine), member 9	-2,0
Sts	steroid sulfatase	-2,0
Cdca4	cell division cycle associated 4	-2,0
Nudc	nuclear distribution gene C homolog (Aspergillus)	-2,0
Nomo1	nodal modulator 1	-2,0
Socs3	suppressor of cytokine signaling 3	-2,0
Mvd	mevalonate (diphospho) decarboxylase	-2,0
Irf1	interferon regulatory factor 1	-2,0
Nfil3	nuclear factor, interleukin 3	-2,0
Flnc	PREDICTED: filamin C, gamma	-2,0
Hic1	hypermethylated in cancer 1	-2,0
Stat2	signal transducer and activator of transcription 2	-2,0
Gpr24	G protein coupled receptor 24	-2,0
Ppih	peptidyl prolyl isomerase H	-2,0
Mrpl37	mitochondrial ribosomal protein L37	-2,0
Tnfrsf12a	tumor necrosis factor receptor superfamily, member 12a	-2,0
Dlg5	discs, large homolog 5	-2,0
Sipa1	signal-induced proliferation associated gene 1	-2,0
Dusp1	dual specificity phosphatase 1	-2,0
Rcc2	regulator of chromosome condensation 2	-2,0
H2-Q1	histocompatibility 2, Q region locus 1	-2,1
Cdca7	cell division cycle associated 7	-2,1
Mesdc1	mesoderm development candidate 1	-2,1
Bax	Bcl2-associated X protein	-2,1
Thoc4	THO complex 4	-2,1
Wdr8	WD repeat domain 8	-2,1
Mast2	microtubule associated serine/threonine kinase 2	-2,1
Man2b1	mannosidase 2, alpha B1	-2,1
Praf1	polymerase (RNA) I associated factor 1	-2,1

Prim2	DNA primase, p58 subunit	-2,1
Grin2d	glutamate receptor, ionotropic, NMDA2D (epsilon 4)	-2,1
Smarca4	SWI/SNF related, matrix associated, actin dependent regulator of chromatin	-2,1
Gsdmdc1	gasdermin domain containing 1	-2,1
Actg2	actin, gamma 2, smooth muscle, enteric	-2,1
Snrpa1	small nuclear ribonucleoprotein polypeptide A'	-2,1
Scrib	scribbled homolog (Drosophila)	-2,1
Tubgcp2	tubulin, gamma complex associated protein 2	-2,1
Enah	enabled homolog (Drosophila)	-2,1
Chst1	carbohydrate (keratan sulfate Gal-6) sulfotransferase 1	-2,1
Itgb4	integrin beta 4	-2,1
Rbm14	RNA binding motif protein 14	-2,1
H2-Q2	histocompatibility 2, Q region locus 2	-2,1
Nxt1	NTF2-related export protein 1	-2,1
MGI:2384747	erythroid differentiation regulator 1	-2,1
Bcl3	B-cell leukemia/lymphoma 3 (Bcl3), mRNA [NM_033601]	-2,1
Pvalb	parvalbumin	-2,2
Ppm1g	protein phosphatase 1G (formerly 2C), magnesium-dependent, gamma isoform	-2,2
Gart	phosphoribosylglycinamide formyltransferase	-2,2
Hras1	Harvey rat sarcoma virus oncogene 1	-2,2
H2-Q7	histocompatibility 2, Q region locus 7	-2,2
Mvk	mevalonate kinase	-2,2
Prkd2	protein kinase D2	-2,2
Hmga1	high mobility group AT-hook 1	-2,2
Pcnt1	pericentrin 1	-2,2
Tnnc2	troponin C2, fast	-2,2
Slc16a3	solute carrier family 16 (monocarboxylic acid transporters), member 3]	-2,2
Myl9	PREDICTED: myosin, light polypeptide 9, regulatory	-2,2
Tnfaip2	tumor necrosis factor, alpha-induced protein 2	-2,2
Shmt2	serine hydroxymethyl transferase 2	-2,2
Phlda1	pleckstrin homology-like domain, family A, member 1	-2,3
Nola1	nucleolar protein family A, member 1 (H/ACA small nucleolar RNPs)	-2,3
H2-Q5	histocompatibility 2, Q region locus 5	-2,3
Pdxp	pyridoxal (pyridoxine, vitamin B6) phosphatase	-2,3
Arf4l	ADP-ribosylation factor 4-like (Arf4l), mRNA [NM_031160]	-2,3
Slc9a3r1	solute carrier family 9 (sodium/hydrogen exchanger), isoform 3 regulator 1	-2,3
Hba-a1	hemoglobin alpha, adult chain 1	-2,3
AY989880	MHC class I antigen	-2,3
Plac9	placenta specific 9	-2,3
Serpinf1	serine (or cysteine) proteinase inhibitor, clade F, member 1	-2,3
H2-Q10	histocompatibility 2, Q region locus 10	-2,3
Myo1c	myosin IC	-2,3
Ak2	mRNA for adenylate kinase isozyme 2	-2,3
Cmya4	cardiomyopathy associated 4	-2,3
Ifitm7	interferon induced transmembrane protein 7	-2,3
Tubb3	tubulin, beta 3	-2,3
Acta2	actin, alpha 2, smooth muscle, aorta	-2,3
Ii	Ia-associated invariant chain	-2,3
Dhcr24	24-dehydrocholesterol reductase	-2,4
Myd116	myeloid differentiation primary response gene 116	-2,4
Chmp4b	chromatin modifying protein 4B	-2,4
Ppil1	peptidylprolyl isomerase	-2,4
Mcm4	minichromosome maintenance deficient 4 homolog (S. cerevisiae)	-2,4
Nxn	nucleoredoxin	-2,4
Epha2	Eph receptor A2	-2,4
Csrp2	cysteine and glycine-rich protein 2	-2,4
Nasp	nuclear autoantigenic sperm protein (histone-binding)	-2,5
Rpa1	replication protein A1	-2,5
Eno1	enolase 1, alpha non-neuron	-2,5
Phgdh	3-phosphoglycerate dehydrogenase	-2,5
Smtn	smoothelin	-2,5
Fancg	Fanconi anemia, complementation group G	-2,5
Plk3	polo-like kinase 3 (Drosophila)	-2,5
Ruvbl2	RuvB-like protein 2	-2,5
Nol5a	nucleolar protein 5A	-2,6
Robo3	roundabout homolog 3 (Drosophila)	-2,6
Rnd1	Rho family GTPase 1	-2,6
Isgf3g	interferon dependent positive acting transcription factor 3 gamma	-2,6
Nsg1	neuron specific gene family member 1	-2,6
Lsm2	LSM2 homolog, U6 small nuclear RNA associated (S. cerevisiae)	-2,6
Pgea1	PKD2 interactor, golgi and endoplasmic reticulum associated 1	-2,6
Cdkn2d	cyclin-dependent kinase inhibitor 2D (p19, inhibits CDK4)	-2,6
Sh3bp1	SH3-domain binding protein 1	-2,7
Hist2h4	histone 2, H4	-2,7
Slc20a1	solute carrier family 20, member 1	-2,7
Igtp	interferon gamma induced GTPase	-2,7
Gne	glucosamine	-2,7
Gnb1l	guanine nucleotide binding protein (G protein), beta polypeptide 1-like	-2,7
Pmm1	phosphomannomutase 1	-2,7
Trim28	tripartite motif protein 28	-2,7
Mmp14	matrix metalloproteinase 14	-2,7
Cpz	carboxypeptidase Z	-2,8
Thop1	thimet oligopeptidase 1	-2,8
Cdk2	cyclin-dependent kinase 2	-2,8
Col5a2	procollagen, type V, alpha 2	-2,8

Hist1h1e	histone 1, H1e	-2,8
Col5a3	procollagen, type V, alpha 3	-2,8
Dnmt1	DNA methyltransferase (cytosine-5) 1	-2,8
Fosl1	fos-like antigen 1	-2,8
Hist1h4a	histone 1, H4a	-2,8
Nans	N-acetylneuraminic acid synthase (sialic acid synthase)	-2,9
Pbx4	pre-B-cell leukemia transcription factor 4	-2,9
Tmem48	transmembrane protein 48	-2,9
Bst2	bone marrow stromal cell antigen 2	-2,9
Syt10	synaptotagmin X	-3,0
Srm	spermidine synthase	-3,0
Trim27	tripartite motif protein 27	-3,0
Gjb5	gap junction membrane channel protein beta 5	-3,0
Lhx2	LIM homeobox protein 2	-3,1
Zmilch	Zwilch, kinetochore associated, homolog	-3,1
Prim1	DNA primase, p49 subunit	-3,1
Trip13	ES cells cDNA thyroid hormone receptor interactor 13	-3,1
Steap	six transmembrane epithelial antigen of the prostate	-3,1
Cad	carbamoyl-phosphate synthetase 2, aspartate transcarbamylase, and dihydroorotase	-3,2
Xrcc1	X-ray repair complementing defective repair in Chinese hamster cells 1	-3,2
Dnajc9	DnaJ (Hsp40) homolog, subfamily C, member 9	-3,2
Rfc2	replication factor C (activator 1) 2	-3,2
Oasl2	2'-5' oligoadenylate synthetase-like 2	-3,2
Cks1b	CDC28 protein kinase 1b	-3,3
Pkmyt1	protein kinase, membrane associated tyrosine/threonine 1	-3,3
Mcm6	minichromosome maintenance deficient 6	-3,3
Psmb8	proteosome (prosome, macropain) subunit, beta type 8	-3,3
Hist1h4d	histone 1, H4d	-3,3
Cotl1	coactosin-like 1 (Dictyostelium)	-3,3
Col18a1	procollagen, type XVIII, alpha 1	-3,3
Tubb6	tubulin, beta 6	-3,3
Arhgap22	Rho GTPase activating protein 22	-3,5
Nphp4	nephronophthisis 4 (juvenile) homolog (human)	-3,5
H2afx	H2A histone family, member X	-3,7
Glipr1	GLI pathogenesis-related 1	-3,8
H2-D4	histocompatibility 2, D region locus 4	-3,8
Pcna	proliferating cell nuclear antigen	-3,9
Rfc3	PREDICTED: replication factor C (activator 1) 3	-4,0
Gdf15	growth differentiation factor 15	-4,0
Lmod1	smooth muscle leiomodin mRNA	-4,0
Fbxo5	F-box only protein 5	-4,1
Sgol1	shugoshin-like 1 (S. pombe)	-4,2
Rfc5	replication factor C (activator 1)	-4,2
Cyba	cytochrome b-245, alpha polypeptide	-4,4
Cks2	CDC28 protein kinase regulatory subunit 2	-4,4
Rrm2	ribonucleotide reductase M2	-4,5
Ppp1r14a	protein phosphatase 1, regulatory (inhibitor) subunit 14A	-4,5
Gmnn	geminin	-4,7
Tnfaip8l1	tumor necrosis factor, alpha-induced protein 8-like 1	-4,7
Usp18	ubiquitin specific protease 18	-4,7
Nfkbil2	nuclear factor of kappa light polypeptide gene enhancer in B-cells inhibitor-like 2	-4,8
Ada	adenosine deaminase	-4,8
Rpa2	mRNA for 30-kDa subunit of replication protein A, complete cds	-4,9
Jag2	jagged 2	-5,1
Art3	ADP-ribosyltransferase 3	-5,1
Mcpt8	mast cell protease 8	-5,3
Asf1b	ASF1 anti-silencing function 1 homolog B (S. cerevisiae)	-5,3
Hmgb2	high mobility group box 2	-5,4
Tpx2	TPX2, microtubule-associated protein homolog (Xenopus laevis)	-5,7
Orc1l	origin recognition complex, subunit 1-like (S.cereviaiae)	-5,8
Cdc25c	cell division cycle 25 homolog C (S. cerevisiae)	-5,9
Tjp3	tight junction protein 3	-6,0
Ung	uracil DNA glycosylase	-6,4
Hist1h1b	histone 1, H1b	-6,5
Plk1	polo-like kinase 1	-7,4
Chaf1b	chromatin assembly factor 1, subunit B (p60)	-7,4
Ris2	retroviral integration site 2	-7,7
Prc1	protein regulator of cytokinesis 1	-7,7
Mcm3	minichromosome maintenance deficient 3	-7,8
Ube2t	ubiquitin-conjugating enzyme E2T	-8,1
Kif20a	mRNA for rabkinesin-6.	-8,2
Chaf1a	chromatin assembly factor 1, subunit A (p150)	-8,4
6720460F02Rik	RIKEN cDNA 6720460F02 gene	-8,5
E2f2	E2F transcription factor 2	-9,2

Gene	Description	PPARγ
1190002H23Rik	RIKEN cDNA 1190002H23 gene	10,9
2900024P20Rik	adult male hippocampus cDNA, RIKEN full-length enriched library, clone:2900024P20	5,4
Hipk2	18-day embryo whole body cDNA, RIKEN full-length enriched library, clone:1110014O20	5,2
Lgals4	lectin, galactose binding, soluble 4	5,1
Fvt1	follicular lymphoma variant translocation	3,6
Hspca	heat shock protein 1, alpha	3,3
Hnrph1	heterogeneous nuclear ribonucleoprotein H1	3,2
Sfrs5	splicing factor, arginine/serine-rich 5	3,1
Ctsl	cathepsin L	3,0
Ahsg	alpha-2-HS-glycoprotein	2,9
Jmjd1a	jumonji domain containing 1A	2,9
Rcor1	REST corepressor 1	2,8
Gas6	growth arrest specific 6	2,8
Fbxo32	F-box only protein 32	2,7
Clcn3	chloride channel 3	2,7
Tbc1d16	TBC1 domain family, member 16	2,7
Dci	dodecenoyl-Coenzyme A delta isomerase (3,2 trans-enoyl-Coenyme A isomerase)	2,6
Bicc1	bicaudal C homolog 1	2,6
Ik	IK cytokine	2,5
Igf2r	insulin-like growth factor 2 receptor	2,5
Glg1	golgi apparatus protein 1	2,5
Son	Son cell proliferation protein	2,5
Rhou	ras homolog gene family, member U	2,5
Spin	spindlin (Spin), transcript variant 1	2,5
Aplp2	amyloid beta (A4) precursor-like protein 2	2,5
Slc38a2	solute carrier family 38, member 2	2,5
Dstn	destrin	2,5
Pnrc2	proline-rich nuclear receptor coactivator 2	2,5
Ucp2	uncoupling protein 2 (mitochondrial, proton carrier)	2,5
Fndc3b	fibronectin type III domain containing 3B	2,5
Slc38a1	solute carrier family 38, member 1	2,4
Etfa	electron transferring flavoprotein, alpha polypeptide	2,4
M77003	glycerol-3-phosphate acyltransferase	2,4
Vps4b	vacuolar protein sorting 4b (yeast)	2,4
Snx2	sorting nexin 2	2,4
Dock1	PREDICTED: dedicator of cytokinesis 1	2,4
Sec8l1	SEC8-like 1 (S. cerevisiae)	2,4
Sertad2	SERTA domain containing 2	2,4
Cryz	crystallin, zeta	2,4
Pex11a	peroxisomal biogenesis factor 11a	2,3
Rbms1	RNA binding motif, single stranded interacting protein 1	2,3
Zfp96	zinc finger protein 96	2,3
Hsd17b4	hydroxysteroid (17-beta) dehydrogenase 4	2,3
Ifit3	interferon-induced protein with tetratricopeptide repeats 3	2,3
Ankfy1	ankyrin repeat and FYVE domain containing 1	2,3
Pgm5	phosphoglucomutase 5	2,3
Cyp26b1	cytochrome P450, family 26, subfamily b, polypeptide 1	2,3
Herc2	hect (homologous to the E6-AP (UBE3A) carboxyl terminus) domain and RCC1 (CHC1)-like domain	2,2
Lrrfip1	leucine rich repeat (in FLII) interacting protein 1	2,2
Rabggtb	RAB geranylgeranyl transferase, b subunit	2,2
Rnf14	ring finger protein 14	2,2
Rab14	RAB14, member RAS oncogene family	2,2
Laptm4b	lysosomal-associated protein transmembrane 4B	2,2
Rragc	Ras-related GTP binding C	2,2
Trim24	tripartite motif protein 24	2,2
Fbxo38	F-box protein 38	2,2
Hebp1	heme binding protein 1	2,2
Hs3st1	heparan sulfate (glucosamine) 3-O-sulfotransferase 1	2,2
Zfp238	zinc finger protein 238 (Zfp238), transcript variant 2	2,2
Aga	aspartylglucosaminidase	2,1
Bhlhb2	basic helix-loop-helix domain containing, class B2	2,1
Mppe1	metallophosphoesterase 1	2,1
Pkp2	plakophilin 2	2,1
Sdccag33	serologically defined colon cancer antigen 33	2,1
Hmg20a	high mobility group 20A	2,1
Ube2e3	ubiquitin-conjugating enzyme E2E 3, UBC4/5 homolog (yeast)	2,1
Nrbp2	nuclear receptor binding protein 2	2,1
Rbm6	RNA binding motif protein 6	2,1

Cct4	chaperonin subunit 4 (delta)	2,1
Yy1	YY1 transcription factor	2,1
Crat	carnitine acetyltransferase	2,1
Gtf2e2	general transcription factor II E, polypeptide 2	2,0
Nqo1	NAD(P)H dehydrogenase, quinone 1	2,0
Pex11a	peroxisomal biogenesis factor 11a	2,0
Btg1	B-cell translocation gene 1, anti-proliferative	2,0
Tcfcp2	transcription factor CP2	2,0
Fbxo9	f-box only protein 9	2,0
Sesn1	sestrin 1	2,0
Rbm16	2 days neonate thymus thymic cells cDNA, RIKEN full-length enriched library, clone:E430024N19	2,0
Ube2g1	ubiquitin-conjugating enzyme E2G 1 (UBC7 homolog, C. elegans)	2,0
Tnpo3	transportin 3	2,0
Ppgb	protective protein for beta-galactosidase	2,0
Rab12	RAB12, member RAS oncogene family	2,0
Copg2	coatomer protein complex, subunit gamma 2	2,0
Hadhsc	L-3-hydroxyacyl-Coenzyme A dehydrogenase, short chain	2,0
Trim25	tripartite motif protein 25	2,0
Pura	purine rich element binding protein A	2,0
Ncln	nicalin homolog (zebrafish)	-2,0
Ifi35	interferon-induced protein 35	-2,0
Rnu3ip2	RNA, U3 small nucleolar interacting protein 2	-2,0
Calr	calreticulin	-2,1
Prdx4	peroxiredoxin 4	-2,1
Pa2g4	proliferation-associated 2G4	-2,1
Upk3b	uroplakin 3B	-2,1
Fkbp11	FK506 binding protein 11	-2,2
Evpl	10 day old male pancreas cDNA, RIKEN full-length enriched library, clone:1810006M18	-2,4
Slc2a6	solute carrier family 2 (facilitated glucose transporter), member 6	-2,5
Psat1	phosphoserine aminotransferase 1	-2,5
Sytl1	synaptotagmin-like 1	-2,8
Uchl1	ubiquitin carboxy-terminal hydrolase L1	-3,1
C86302	expressed sequence C86302	-3,3
Ccnb2	cyclin B2]	-7,3
2010317E24Rik	RIKEN cDNA 2010317E24 gene	-7,3
Mcm10	minichromosome maintenance deficient 10 (S. cerevisiae)	-8,1
Cdca8	cell division cycle associated 8	-8,1

Gene	Description	PPARα	PPARβ/δ	PPARγ
Mlana	weakly similar to MELANOMA ANTIGEN RECOGNIZED BY T-CELLS 1 (MART-1)	16,2	6,1	7,6
Penk1	preproenkephalin 1	15,9	6,4	9,2
Prss12	protease, serine, 12 neurotrypsin	15,4	3,5	6,8
Col7a1	procollagen, type VII, alpha 1	4,1	-3,3	-3,9
Hunk	hormonally upregulated Neu-associated kinas	3,8	-4,6	-4,0
Epor	erythropoietin receptor	3,5	2,1	2,9
Arc	activity regulated cytoskeletal-associated protein	3,5	-3,7	-4,3
Mgst1	microsomal glutathione S-transferase 1	2,9	3,5	5,5
Atp1b1	ATPase, Na+/K+ transporting, beta 1 polypeptide	2,6	2,8	2,8
Nes	nestin	2,2	-2,1	-1,9
Cd24a	CD24a antigen	-2,0	2,6	2,0
Ckmt1	creatine kinase, mitochondrial 1	-2,1	-2,2	-2,9
Smad5	MAD homolog 5	-2,1	2,1	2,7
Tia1	cytotoxic granule-associated RNA binding protein 1	-2,1	3,3	5,5
Dnajc1	DnaJ (Hsp40) homolog, subfamily C, member 1	-2,2	2,6	3,3
Mcm7	minichromosome maintenance deficient 7 (S. cerevisiae)	-2,4	-3,8	-2,7
Atf1	activating transcription factor 1	-2,5	2,1	2,5
Hif1a	hypoxia inducible factor 1, alpha subunit	-2,6	2,9	6,8
Aqp5	aquaporin 5	-2,6	-2,2	-2,5
Rfc4	replication factor C (activator 1) 4	-3,1	-3,4	-3,0
Slc1a5	solute carrier family 1 (neutral amino acid transporter), member 5	-3,2	-3,0	-2,7
Asah1	N-acylsphingosine amidohydrolase 1 (Asah1)	-3,3	2,1	2,9
Itga6	integrin alpha 6	-3,4	2,6	5,6
Tk1	thymidine kinase 1	-3,8	-5,8	-7,0
Tjp1	tight junction protein 1	-4,1	3,6	3,8
Kcnmb4	potassium large conductance calcium-activated channel, subfamily M, beta member 4	-4,2	2,4	1,9
Bub1b	budding uninhibited by benzimidazoles 1 homolog, beta	-4,8	-6,7	-7,3
Pole	polymerase (DNA directed), epsilon	-5,5	-5,5	-4,7
Racgap1	Rac GTPase-activating protein 1	-6,5	-6,0	-4,8
Melk	maternal embryonic leucine zipper kinase	-7,6	-8,0	-7,1
Ube2c	ubiquitin-conjugating enzyme E2C	-8,9	-14,0	-15,8
Birc5	baculoviral IAP repeat-containing 5	-11,1	-9,7	-10,3
Spag5	sperm associated antigen 5	-14,3	-6,4	-5,1

Gene	Description	PPARα	PPARβ/δ
Acta1	actin, alpha 1, skeletal muscle	19,3	-1,9
Popdc2	popeye domain containing 2	13,7	-2,7
Clu	clusterin	13,4	3,6
Lpl	lipoprotein lipase	8,4	2,9
Ripk3	receptor-interacting serine-threonine kinase 3	7,3	-4,6
Ccl5	chemokine (C-C motif) ligand 5	6,5	-4,4
Hist1h2ba	histone 1, H2ba	6,4	2,6
Ephx2	epoxide hydrolase 2, cytoplasmic	5,3	3,2
Pde2a	phosphodiesterase 2A, cGMP-stimulated	4,8	2,2
Bambi	BMP and activin membrane-bound inhibitor	3,7	3,6
Tnc	tenascin C	3,4	2,4
Rab38	Rab38, member of RAS oncogene family	3,2	3,7
Pink1	PTEN induced putative kinase 1	2,7	2,9
Padi3	peptidyl arginine deiminase, type III (Padi3), mRNA	2,5	-5,0
Cish	cytokine inducible SH2-containing protein	2,5	-2,1
Sspn	sarcospan	2,5	2,2
Gsta4	glutathione S-transferase, alpha 4	2,5	2,9
Parva	parvin, alpha	2,2	-2,2
Cyp4b1	cytochrome P450, family 4, subfamily b, polypeptide 1	2,1	6,6
Ethe1	ethylmalonic encephalopathy 1	2,0	-2,4
Nfib	nuclear factor I/B	-2,0	2,2
Mllt3	myeloid/lymphoid or mixed lineage-leukemia translocation to 3 homolog	-2,1	2,2
Cd47	adult male liver tumor cDNA	-2,2	2,7
Lig1	ligase I, DNA, ATP-dependent	-2,3	-3,5
Casp7	caspase 7	-2,3	-2,0
Pole2	polymerase (DNA directed), epsilon 2 (p59 subunit)	-2,5	-2,7
Slc25a26	solute carrier family 25 (mitochondrial carrier; phosphate carrier), member 26	-2,8	2,3
Plscr4	phospholipid scramblase 4	-2,9	2,9
Mcts1	malignant T cell amplified sequence 1	-2,9	2,3
Nfkb2	nuclear factor of kappa light polypeptide gene enhancer in B-cells 2, p49/p100	-3,0	-2,1
Ppp3ca	protein phosphatase 3, catalytic subunit, alpha isoform	-3,1	2,9
Npc1	Niemann Pick type C1	-3,1	2,4
Recql4	RecQ protein-like 4	-3,1	-3,5
Hcfc1r1	host cell factor C1 regulator 1 (XPO1-dependent)	-3,2	2,1
Glis2	GLIS family zinc finger 2	-3,2	2,3
Fbln1	fibulin 1	-3,3	-2,8
Timeless	timeless homolog (Drosophila) (Timeless)	-3,3	-7,3
Ap3b2	AP-3 complex beta3B subunit	-3,5	2,1
Mcm5	minichromosome maintenance deficient 5, cell division cycle 46 (S. cerevisiae)	-3,5	-7,9
Galnt5	UDP-N-acetyl-alpha-D-galactosamine:polypeptide N-acetylgalactosaminyltransferase 5	-3,7	2,5
Tcf19	transcription factor 19	-3,8	-4,8
Dlx5	distal-less homeobox 5 (Dlx5), transcript variant 1	-3,8	2,4
Pask	PAS domain containing serine/threonine kinase	-3,9	-7,7
Cald1	caldesmon 1	-5,0	2,1
Stmn1	stathmin 1	-5,3	-8,8
Uhrf1	ubiquitin-like, containing PHD and RING finger domains, 1	-5,8	-13,2
Tacc3	transforming, acidic coiled-coil containing protein 3	-7,1	-8,6
Hsd17b7	hydroxysteroid (17-beta) dehydrogenase 7	-8,8	2,0

Gene	Description	PPARα	PPARγ
Slc1a6	solute carrier family 1 (high affinity aspartate/glutamate transporter), member 6	6,8	-2,3
Cpe	carboxypeptidase E	6,7	2,1
Nnmt	nicotinamide N-methyltransferase	3,0	-2,0
Tnnc1	troponin C, cardiac/slow skeletal	2,5	-2,3
Dhrs7	dehydrogenase/reductase (SDR family) member 7	2,5	2,1
Gprc5b	G protein-coupled receptor, family C, group 5, member B	2,4	3,3
Gata6	GATA binding protein 6	2,3	2,4
Fgfrl1	fibroblast growth factor receptor-like 1	2,1	1,9
Rhbdl4	rhomboid, veinlet-like 4 (Drosophila)	2,1	-2,1
Zfp191	zinc finger protein 191	-2,1	3,8
Kif22	kinesin family member 22	-2,5	-6,9
Scd2	stearoyl-Coenzyme A desaturase 2	-2,8	3,0
Ppfibp2	protein tyrosine phosphatase, receptor-type, F interacting protein, binding protein 2	-5,1	5,6

Gene	Description	PPARβ/δ	PPARγ
MGI:1929709	plasma membrane associated protein, S3-12	11,6	26,6
C1s	complement component 1, s subcomponent	5,4	7,3
Fabp3	fatty acid binding protein 3, muscle and heart	5,3	17,6
Cdh2	cadherin 2	4,3	3,5
S100b	S100 protein, beta polypeptide, neural	4,1	3,6
Cdh1	cadherin 1	3,9	5,2
Sdc2	syndecan 2	3,7	2,8
Thumpd3	THUMP domain containing 3	3,5	3,6
Impact	imprinted and ancient	3,5	6,8
Rgs2	regulator of G-protein signaling 2	3,4	4,0
Tspan12	tetraspanin 12	3,4	4,9
Antxr1	anthrax toxin receptor 1	3,4	3,6
Zkscan1	zinc finger with KRAB and SCAN domains 1 (Zkscan1), transcript variant 1	3,3	3,9
Luc7l2	LUC7-like 2 (S. cerevisiae)	3,3	3,2
Rab32	RAB32, member RAS oncogene family	3,2	2,8
Riok2	RIO kinase 2 (yeast)	3,2	3,4
Mgst3	glutathione S-transferase 3	3,2	3,6
Btbd1	BTB (POZ) domain containing 1	3,1	3,5
Ghr	growth hormone receptor	3,1	4,9
Agl	PREDICTED: amylo-1,6-glucosidase, 4-alpha-glucanotransferase	3,0	4,5
Zfp503	zinc finger protein 503	3,0	4,0
Aldh6a1	aldehyde dehydrogenase family 6, subfamily A1	3,0	3,5
Rpl23	ribosomal protein L23	2,9	3,0
Rnf103	ring finger protein 103	2,9	3,2
Dnase2a	deoxyribonuclease II precursor mRNA	2,9	2,8
Rin2	Ras and Rab interactor 2	2,8	3,2
Mgst3	microsomal glutathione S-transferase 3	2,8	3,6
Arid2	AT rich interactive domain 2 (Arid-rfx like)	2,8	4,1
Pdgfra	platelet derived growth factor receptor, alpha polypeptide	2,7	3,8
Ophn1	oligophrenin 1	2,7	3,4
Lrpprc	leucine-rich PPR-motif containing	2,7	3,6
Nrp1	neuropilin 1	2,7	3,7
Ech1	enoyl coenzyme A hydratase 1, peroxisomal	2,6	2,7
Slc16a1	solute carrier family 16 (monocarboxylic acid transporters), member 1	2,6	2,4
Scamp1	secretory carrier membrane protein 1	2,5	3,6
Nek7	NIMA (never in mitosis gene a)-related expressed kinase 7	2,5	2,9
Cdc42ep3	CDC42 effector protein (Rho GTPase binding) 3	2,5	2,6
Arid1b	6A3-5 PROTEIN upregulated in a proliferating, but not synthetic, rat smooth muscle cells	2,5	2,4
Jak1	Janus kinase 1	2,5	2,3
Aox1	aldehyde oxidase 1	2,5	3,1
Pcyox1	prenylcysteine oxidase 1	2,5	2,9
Cdw92	CDW92 antigen	2,4	2,5
Trim59	tripartite motif-containing 59	2,3	2,7
Col2a1	procollagen, type II, alpha 1	2,3	2,5
Acadm	acetyl-Coenzyme A dehydrogenase, medium chain	2,3	2,9
Ccnd2	cyclin D2	2,3	2,3
Rhoq	ras homolog gene family, member Q	2,3	3,7
Pts	6-pyruvoyl-tetrahydropterin synthase	2,3	2,6
Phf17	PHD finger protein 17	2,3	2,8
Rnf146	ring finger protein 146	2,3	2,2
Adamts15	a disintegrin-like and metalloprotease with thrombospondin type 1 motif, 15	2,3	3,2
Rcbtb1	regulator of chromosome condensation (RCC1) and BTB (POZ) domain containing protein 1	2,3	2,5
Fech	ferrochelatase	2,2	3,2
Tusc1	tumor suppressor candidate 1	2,2	2,3
Pparbp	peroxisome proliferator activated receptor binding protein (Pparbp)	2,2	2,6
Dscr5	Down syndrome critical region homolog 5 (human)	2,2	1,9
Kalrn	2 days neonate thymus thymic cells cDNA, KALIRIN-12A homolog [Rattus norvegicus]	2,2	2,5
Wwtr1	WW domain containing transcription regulator 1	2,2	2,7
Vps26	vacuolar protein sorting 26 (yeast)	2,2	3,2
Ddx42	DEAD (Asp-Glu-Ala-Asp) box polypeptide 42	2,2	2,3
Zadh2	zinc binding alcohol dehydrogenase, domain containing 2	2,2	2,5
Rerg	RAS-like, estrogen-regulated, growth-inhibitor	2,2	2,0
Ubl3	ubiquitin-like 3	2,1	1,8
Pcmt1	protein-L-isoaspartate (D-aspartate) O-methyltransferase 1	2,1	2,0
Ythdf2	YTH domain family 2	2,1	1,8
Kazald1	Kazal-type serine protease inhibitor domain 1	2,1	1,8
Ociad2	OCIA domain containing 2	2,1	3,1
Pon3	paraoxonase 3	2,1	1,7
Tmem23	transmembrane protein 23	2,0	2,5
Mut	methylmalonyl-Coenzyme A mutase	2,0	2,3
Nme3	expressed in non-metastatic cells 3	2,0	2,0
Ss18	synovial sarcoma translocation, Chromosome 18	2,0	2,3

Hadhb	hydroxyacyl-Coenzyme A dehydrogenase	2,0	2,0
Junb	Jun-B oncogene	-2,0	-1,9
Socs3	suppressor of cytokine signaling 3	-2,0	-1,8
Mvd	mevalonate (diphospho) decarboxylase	-2,0	-1,9
Nme4	expressed in non-metastatic cells 4, protein	-2,0	-2,1
Cgref1	cell growth regulator with EF hand domain 1	-2,0	-2,3
Ctps	cytidine 5'-triphosphate synthase	-2,0	-2,1
Bglap2	bone gamma-carboxyglutamate protein 2	-2,1	-2,3
MGI:2384747	erythroid differentiation regulator 1	-2,1	-1,9
Vars2	valyl-tRNA synthetase 2	-2,2	-2,1
Psmb9	proteosome (prosome, macropain) subunit, beta type 9 (large multifunctional protease 2)	-2,2	-2,3
Tubb4	tubulin, beta 4	-2,2	-2,0
Evpl	10 day old male pancreas cDNA, envoplakin	-2,3	-2,4
Ppil1	peptidylprolyl isomerase	-2,4	-1,9
Lmna	lamin A, transcript variant 2	-2,4	-2,5
Rpa1	replication protein A1	-2,5	-1,7
Ddx39	DEAD (Asp-Glu-Ala-Asp) box polypeptide 39	-2,5	-2,7
Oact1	O-acyltransferase (membrane bound) domain containing 1	-2,5	-2,5
Plaur	urokinase plasminogen activator receptor	-2,6	-2,9
Dut	deoxyuridine triphosphatase	-2,6	-2,4
Armet	arginine-rich, mutated in early stage tumors	-2,6	-2,8
Fthfd	formyltetrahydrofolate dehydrogenase	-2,7	-4,4
Dtymk	deoxythymidylate kinase	-2,8	-3,0
Lmnb2	lamin B2	-2,8	-2,4
Troap	adult male liver tumor cDNA, weakly similar to TROPHININ-ASSOCIATED PROTEIN (TASTIN)	-2,9	-3,9
C86302	expressed sequence C86302	-3,0	-3,3
Metrn	meteorin, glial cell differentiation regulator	-3,0	-2,0
Tap1	transporter 1, ATP-binding cassette, sub-family B	-3,0	-3,0
Prim1	DNA primase, p49 subunit	-3,1	-1,9
Mcam	melanoma cell adhesion molecule	-3,3	-2,9
Mfsd2	major facilitator superfamily domain containing 2	-3,4	-4,7
Ccna2	cyclin A2	-3,5	-2,0
Tyms	thymidylate synthase	-3,6	-3,4
Lrdd	leucine-rich and death domain containing	-3,7	-2,9
Nid2	nidogen 2	-3,7	-2,8
Oas1f	2'-5' oligoadenylate synthetase 1F	-3,7	-3,0
Psmc3ip	Mouse mRNA for TBPIP, complete cds	-3,8	-2,8
Traip	TRAF-interacting protein	-3,9	-4,5
Capg	capping protein (actin filament), gelsolin-like	-3,9	-5,2
Pold1	polymerase (DNA directed), delta 1, catalytic subunit	-4,0	-3,6
Krt2-7	adult male kidney cDNA similar to keratin K7, type II, epithelial [Homo sapiens]	-4,0	-4,8
Ccne1	cyclin E1	-4,1	-5,7
Pttg1	pituitary tumor-transforming 1	-4,3	-4,7
Ccnf	cyclin F	-4,4	-4,0
Tnfrsf18	tumor necrosis factor receptor superfamily, member 18	-5,1	-6,7
Nek2	NIMA (never in mitosis gene a)-related expressed kinase 2	-5,6	-7,0
Incenp	inner centromere protein	-5,7	-5,6
Cdc2a	cell division cycle 2 homolog A (S. pombe)	-5,9	-5,8
2010317E24Rik	RIKEN cDNA 2010317E24 gene	-5,9	-7,3
Mcm2	minichromosome maintenance deficient 2 mitotin (S. cerevisiae)	-6,3	-3,1
Rad51	RAD51 homolog	-7,5	-5,5
Cdca5	cell division cycle associated 5	-10,2	-15,9
Cenpa	centromere autoantigen A	-14,1	-12,1

chapter

٣

CHAPTER 3

The mitogen activated protein kinase kinase (MAPKK) MEK1 inhibits cardiac PPARα activity through nuclear export

Hamid el Azzouzi, Stefanos Leptidis, Leon J. De Windt

Submitted as:

Hamid el Azzouzi, Stefanos Leptidis, Leon J. De Windt. The mitogen activated protein kinase kinase (MAPKK) MEK1 inhibits cardiac PPARα activity through nuclear export.

ABSTRACT

Studies embarking on mitogen-activated protein kinase (MAPK) signaling cascades in the heart have indicated PPARα as a downstream effector that can be regulated through phosphorylation. The response of the postnatal heart to growth and stress stimuli includes activation of a network of signal transduction cascades, including the stress activated protein kinases such as p38 mitogen-activated protein kinase (MAPK), c-Jun NH2-terminal kinase (JNK) and the extracellular signal-regulated kinase (ERK1/2) pathways. In response to acute pressure overload stimulation induced by aortic banding, the mitogen-activated protein kinase kinase (MAPKK) MEK1 has been shown to be activated. Despite its importance, little is known about the relationship between MEK1-ERK1/2 pathway and cardiac PPAR signaling. Here we show that activation of the MEK1-ERK1/2 pathway leads to specific inhibition of PPARα transcriptional activity. Furthermore we show, for the first time, that this inhibitory effect is mediated by MEK1, and not by its downstream effector kinase ERK1/2, through a mechanism involving direct binding to PPARα and subsequent stimulation of PPARα export out of the nucleus.

INTRODUCTION

Peroxisome proliferator-activated receptor α (PPARα) is a nuclear receptor which is believed to act as a sensor of fatty acid and other metabolites to enable the cell to adapt to environmental changes through regulation of a large number of processes such as inflammation, differentiation and metabolism (1). PPARα is expressed in metabolically active tissues such as the liver, brown fat, kidney, skeletal muscle and heart (2). Transgenic mice with forced overexpression of PPARα in cardiac muscle display increased fatty acid oxidation rates, accumulation of triacylglycerides, decrease in glucose metabolism and eventually develop cardiomyopathy (3). In turn, mice deficient for PPARα have elevated free fatty acid levels as a consequence of inadequate fatty acid oxidation, rendering them hypoglycemic as a result of their reliance on glucose (4).The natural ligands for PPARα are fatty acids, such as medium and long chain fatty acids and eicosinoids. Synthetic ligands for PPAR comprise hypolipidemic, anti-inflammatory and insulin-sensitizing drugs. In the presence of a ligand, PPARs adopt an active conformation by forming an obligate heterodimer with the retinoid X receptor (RXR). Recruitment of additional co-activators leads to binding to peroxisome proliferator response elements (PPRE) in target genes, provoking PPAR-dependent gene expression.

During the development of cardiac hypertrophy, myocardial fatty acid oxidation (FAO) rats decrease and glucose utilization increases (5). During this transition, the reduced nuclear level of PPARα suggest that this phenomenon may be responsible for down-regulation of cardiac FAO genes in the hypertrophied heart (6). Hence, understanding the mechanisms that regulate the activity of PPARα is crucial to determine the precise contribution of altered FAO at the genesis and progression of heart failure.

Apart from the classical ligand-dependant regulation, several studies have reported the modulation of PPARα activity by phosphorylation. For example, insulin treatment induces phosphorylation, at the serine residues 12 and 21 in the transactivation domain, and subsequent activation of PPARα (7). PKA activators have also been shown to modulate the activity of PPARα through phosphorylation of several subdomains, including the DNA-binding domain and the ligand binding domain (8). The response of the postnatal heart to growth and stress stimuli includes activation of a network of signal transduction cascades, including the stress activated protein kinases such as p38 mitogen-activated protein kinase (MAPK), c-Jun NH2-terminal kinase (JNK) and the extracellular signal-regulated kinase (ERK1/2) pathways (9). Studies embarking on MAPK signaling in the heart have indicated PPARα as a downstream effector that can be regulated through phosphorylation (10). Moreover, members of the p38 kinase family have been shown to phosphorylate PPARα in ligand dependant manner and results in enhanced transcriptional activity (10). Transgenic mice with cardiac-restricted expression of an activated form of MEK1 developed concentric hypertrophy with preserved cardiac function (11), indicating an important role for MEK1-ERK1/2 signaling pathway during cardiac hypertrophy. It is interesting to note that activation of the MEK1-ERK1/2 pathway led to inhibition of PPARγ

transcriptional activity in cells (12,13), indicating a diverse effect of the different MAPK pathways on PPAR activity. Despite its importance, little is known about the relationship between MEK1-ERK1/2 pathway and cardiac PPAR signaling. Here we show that activation of the MEK1-ERK1/2 pathway leads to inhibition of PPARα transcriptional activity. Furthermore we show, for the first time, that the inhibitory effect is mediated by MEK1 through a mechanism involving direct binding to PPARα and subsequent export out of the nucleus.

MATERIALS AND METHODS

Cell culture. Low passage HEK293 and NKL-TAg cells were cultured in Dulbecco's modified Eagle's medium (Invitrogen) supplemented with 10% fetal bovine serum.

Cell transfection and Luciferase Assays. Transfections were performed in 24-well plates (1x104 cells/well). After 24 hours, transient transfections were performed as described(14) with FuGENE 6 reagent as per the manufacturer's recommendations. After 8 hours, cells were then overlaid with no-serum medium with or without the respective stimuli (Fig. 1A). After 24 hours, cells were then harvested and lysates were analyzed for firefly luciferase expression. In brief, 20 μl aliquots of cell lysates were mixed with 40 μl of luciferase reagent buffer (Promega Corp) and luminescence of the samples was integrated over a period of 10 seconds in a LUMAC Biocounter M1500P (Landgraaf). To asses transfection efficiency, a SV40 promoter driven Renilla luciferase vector was used (Dual Luciferase Assay, Promega Corp).

Plasmid Construction. The reporter plasmid containing the mCPT1 (mCPT1-luc) promoter linked to luciferase reporters was kindly provided by M. van Bilsen. Substitution of Serine 12, 21,76 with Alanine in pcDNA4/TO-PPARα was engineered by site-directed mutagenesis.

Immunoprecipitations, Western blotting. DNA binding assays were performed as described previously (15) either after transfection of pCDNA3.1-PPARα and/or pCDNA3.1-MEK1 , using FuGene 6 reagent (Roche) followed by purification by immunoprecipitation of polyclonal PPARα antibody (Santa Cruz) or MEK1 antibody (cell signaling) with the Catch and Release kit (Upstate). Proteins were extracted from cells using cell lysis buffer (20mM Tris pH8.0, 150mM NaCl, 1mM EDTA, 1mM EGTA, 1% Triton X-100) supplemented with a protease inhibitor cocktail (Complete Mini, Roche) for Catch and release kit and western blotting. Western blotting was performed as described previously (11).

Immunofluorescence. Paraformaldehyde-fixed HEK293 cells were were washed 3 times with PBS for 5 minutes, mounted with coverslips in Vectashield mounting medium H-1000

(vector Laboratories, Inc., CA USA), and analyzed by immunofluorescence microscopy using a Zeiss LSM 510 META instrument. Nuclei were counterstained with DAPI.

Cage-wheel exercise. Male WT mice were subjected to voluntary cage wheel exercise. Briefly, individual animals were individually housed in a cage equipped with an 11.5-cm-diameter running wheel with a 5.0-cm-wide running surface equipped with a digital magnetic counter activated by wheel rotation. Daily exercise values for time and distance run were recorded for individual exercised animals throughout the duration of the exercise period (4 weeks).

Statistical analysis. The results are presented as mean ± SEM. Statistical analyses were performed with InStat 3.0 (GraphPad Software, Inc, San Diego, CA). The analyses consisted of ANOVA, followed by Tukey's posttest when group differences were detected at the 5% significance level. Statistical significance was accepted at a p value <0.05.

RESULTS

Mek1 inhibits PPARα activity but not in an ERK1/2 dependent way.

It has been shown that phosphorylation of PPAR's attenuates their transcriptional activity in a sub-type specific way. To study the effect of the MEK1-ERK1/2 cascade on PPARα activity, we examined the transcriptional activity of PPARα in the presence of exogenous MEK1 constructs or their inhibitors. To this end we resorted to the use of a previously developed, ventricular muscle cell line, NKL-Tag. NKL-TAg cells actively proliferate without apparent senescence, while introduction of Cre recombinase results in the elimination of TAg expression, permanent exit from the cell cycle and expression of cardiac markers (16). As a functional verification of the transcriptional activity of PPARα, we performed transient transfection of a luciferase reporter driven by a mCPT promoter harboring a functional PPRE. Co-transfection of a PPARα expression vector and stimulation with Wy-14643 as synthethic ligand (24hr), resulted in increased luciferase activity (Fig. 1A), indicating enhanced transcriptional activity of PPARThis effect was totally abrogated when MEK1 was co-expressed (Fig. 1A). Addition of U0126, a specific inhibitor of MEK1, re-activated Wy-14643 mediated PPARα induction of the mCPT-luc promoter, indicating that the inhibitory effect involved MEK1 activation. A classical down stream effector of MEK1 is ERK1/2. Western Blot analysis showed increased phosphorylation of ERK1/2 after MEK1 activation. Moreover, addition of U0126 inhibited MEK1 induced phosphorylation of ERK1/2 (Fig. 1B), indicating the efficiency of used expression vectors and efficiency of U0126.

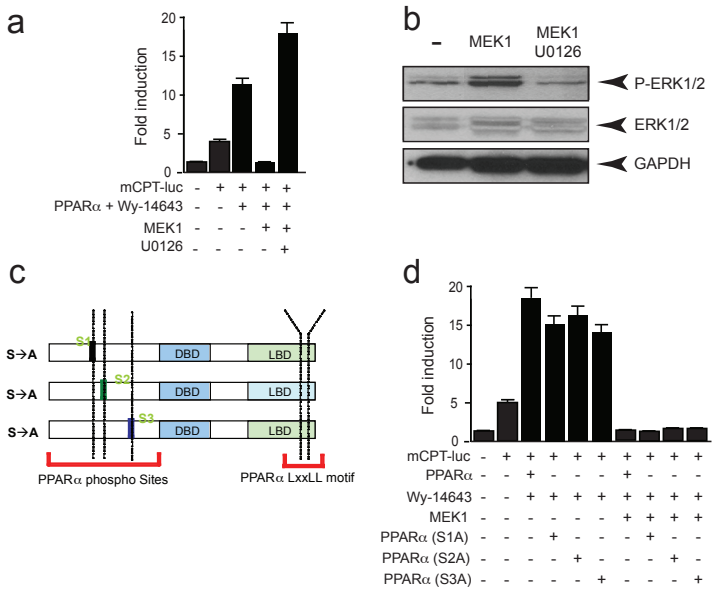

Figure 1. MEK1 expression inhibits PPARα transcriptional activity not via phosphorylation. (a) Luciferase measurements on of NkL-Tag cells transiently transfected with a mCPT promoter driven reporter as a functional readout for PPARα activity after co-transfection with PPARα-V5 and MEK1 for 24hr. (b) Western blot analysis using anti-fosforylated ERK1/2 (p-ERK1/2) antibody on lysates of NkL-Tag cells transiently transfected with MEK1 for 24 hr, indicating enhanced activation of ERK1/2 after MEK1 expression. (c) Schematic representation of the trans-activating domain of PPARα is shown along with three putative phosphorylation target sites for ERK1/2 and the LXXLL motif. (d) Luciferase measurements on of NkL-Tag cells transiently transfected with a mCPT promoter driven reporter and co-transfected with mutants of PPARα-V5 and MEK1 for 24 hr, indicating MEK1 induced inhibition of PPARα to be phosphorylation independent. *, indicates $P < 0.05$.

Protein-protein interactions with MEK1 are known to be mediated by the CRS/CD domain, which allows interaction with other regulatory proteins. Within the CRS domain interaction with MEK1 has been shown to be mediated by an LXXLL binding pocket (18). Characterization of the ligand binding domain of PPARα revealed an LXXLL binding pocket (Fig. 1C). We constructed a V5-tagged PPARα that has a truncation of the last 16 amino acids of the c-terminal AF2 domain, rendering it lacking the LXXLL binding pocket. Using this construct, coimmunoprecipitation with MEK1 failed (Fig. 2E), indicating this motif as a crucial structural motif for the protein-protein interaction between MEK1 with PPARα.Taken together, these findings reveal a novel mechanism for the regulation of cardiac PPARα activity via direct interaction and inactivation by MEK1.

Previous studies indicated that the PPAR trans-activating domain plays an important role in the regulation of the transcriptional activity of PPARα (17). Characterization of the trans-activating domain, amino acids 1-92, of PPARα revealed three putative phosphorylation target sites for ERK1/2 (Fig. 1C). To test whether ERK1/2-mediated phosphorylation of one or more putative phospho-acceptor sites on PPARa may underly the MEK1-ERK1/2-mediated inhibition of PPARa transcriptional activity, we employed site-directed mutagenesis to create different PPARα constructs harboring, at the indicated amino acids, a single serine to alanine conversion (Fig. 1C).

Surprisingly, MEK1 induced inhibition was not hampered by co-transfection of the mutated PPARα construct (Fig. 1D). As a second approach to exclude direct ERK1/2 phosphorylation events on PPARα, we set up an assay using the MAPK phosphatase MKP1, which provokes ERK1/2 dephosphorylation, to determine whether the MEK1 inhibitory effect is unrelated to activation of ERK1/2. As indicated by Western Blot, co-transfection of MKP1 led to dephosphorylation of ERK1/2 even in the presence of activated MEK1 (Fig. 2A). Interestingly, dephosphorylation of ERK1/2, by the transient co-transfection of MKP1, did not change the inhibitory effect of MEK1 on the transcriptional activity of PPARα (Fig. 2B).

Thus, these findings indicate a minor role for ERK1/2 phosphorylation events on putative phospho-acceptor sites in the trans-activating domain of PPARα as a mechanisms responsible for MEK1-ERK1/2 mediated inhibition of PPARα transcriptional activity.

Mek1 interacts with PPARα

Since the MEK1 inhibitory effect on PPARα activity could not be explained through the classical ERK1/2 pathway, we examined the possibility that the inhibitory effects are mediated by a direct protein-protein interaction with MEK1. HEK-293 cells were transiently co-transfected with a PPARα and a MEK1 construct. After 24 hr of stimulation with the synthethic ligand, Wy-14643, cells were then subjected to coimmunoprecipitation with PPARα antibody, leading to precipitation of MEK1 (Fig. 2C). The amount of transfected PPARα is indicated as loading control after coimmunoprecipitation (Fig. 2 C). Using the same conditions, we repeated the experiments using a MEK1 antibody to coimmunoprecipitate PPARα. Also under these conditions, PPARα was readily precipitated, indicating a direct interaction between PPARα and MEK1 (Fig. 2D). Beads only were used as a negative control for the specificity of PPARα binding to MEK1. Importantly, using a PPARβ/δ construct did not result in coimmunoprecipitation with MEK1 (data not shown), indicating the specificity of the interaction between MEK1 and PPARα.

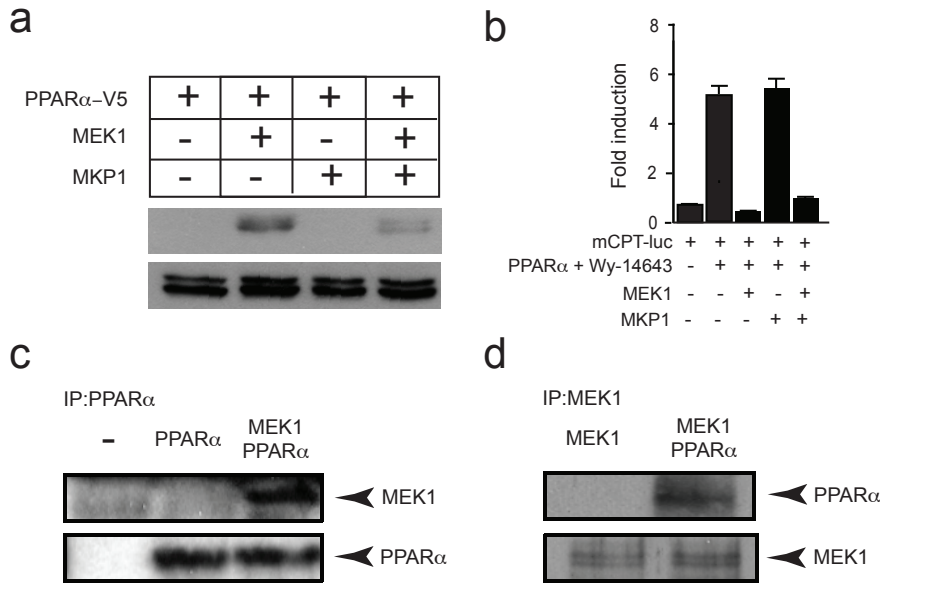

Figure 2. MEK1 interaction with PPARα. (a) Luciferase measurements on of NkL-Tag cells transiently transfected with a mCPT promoter driven reporter and co-transfected with PPARα-V5, MEK1 and MKP1, as indicated. (b) Western blot analysis using anti-fosforylated ERK1/2 (p-ERK1/2) antibody on lysates of NkL-Tag cells transiently transfected with MEK1 and MKP1, indicating decreased activation of ERK1/2 after co-expression of MKP1. (c) Western blot analysis on precipitates of HEK293 cells transiently co-transfected with PPARα-V5 and MEK1 for 24 hr and co-immunoprecipitated using anti-PPARα antibody. (d) Western blot analysis on precipitates of HEK293 cells transiently co-transfected with PPARα-V5 and MEK1 for 24 hr and co-immunoprecipitated using anti-MEK1 antibody. (e) Western blot analysis on precipitates of HEK293 cells transiently co-transfected with mutant PPARα-V5 and MEK1 for 24 hr and co-immunoprecipitated using anti-V5 antibody. *, indicates $P < 0.05$.

Mek1 binding to PPARα induces nuclear export

Since MEK1 has been shown to be unable to directly phosphorylate PPAR (12), we next considered subcellular localization as an important factor participating in the regulation of PPAR signaling (19). We therefore investigated whether the direct interaction serves as a new mechanism for regulating the subcellular localization of PPARα. To this end, HEK293 cells were transiently co-transfected with a PPARα-GFP with or without a MEK1 expression vector and stimulation with Wy-14643. After 24 hr, cells were fixed and PPARα localization was determined by GFP fluorescence. Over expressed PPARα-GFP was mainly localized to the nucleus in Wy-14643 stimulated cells (Fig. 3A).

In contrast, ectopic expression of an activated form of MEK1 resulted in a massive exclusion of PPARα from the nucleus towards a predominant cytoplasmic localization (Fig. 3A). Addition of U0126 inhibited the MEK1 induced translocation causing PPARα-GFP to be localized in the nucleus after stimulation with Wy-14643 (Fig. 3A).

It is important to mention that unstimulated PPARα-GFP remained largely in the cytosol (data not shown) and that the nuclear translocation was induced only after stimulation with Wy-14643. In light of our earlier results, we reasoned that MEK1 induced PPARα translocation was mediated through direct interaction of MEK1 with the LXXLL binding pocket of PPARα. We therefore designed a PPARα-GFP construct that harbored a truncation of the last 16 amino acids of the c-terminal AF2 domain of PPARα, lacking the necessary LXXLL binding pocket (PPARα-GFPΔLxxLL). Next, we repeated the experiment using PPARα-GFPΔLxxLL and analyzed subcellular localization, In this case, nuclear localization of PPAR was not affected by ectopic MEK1 expression (Fig. 3B). Again, this interaction proved to be PPARα specific, since co-transfection of MEK1 with PPARβ/δ-GFP did not result in nuclear extrusion (Fig. 3C).

In conclusion, the combined experiments demonstrates that the ERK1/2 selective MAPKK MEK1 binds to the LXXLL binding pocket of PPARα and forces translocation out of the nucleus to the cytosol as a novel mechanism whereby MEK1 signaling inhibits the transcriptional activity of PPARα.

Increased Mek1 activity during physiological hypertrophy inhibits PPARα activity.

It was already shown that MEK1/2 plays an important role in cardiac hypertrophy, since many hypertrophic stimuli also activate the MEK1 pathway [11]. Furthermore, Mek1 transgenic animals showed ventricular concentric hypertrophy with a 50-54% increase in septal thickness and left ventricular posterior wall thickness without signs of cardiomyopathy or lethality resembling a phenotype of physiological hypertrophy [11]. To further evaluate the effects of MEK1 signaling on PPARα activity during physiological hypertrophy, mice were subjected to cage wheel exercise, to stimulate physiological cardiac hypertrophy, after which MEK1 and PPARα activity was analyzed.

After 4 weeks of voluntary wheel exercise, mice were able to generate a cardiac growth response as evidenced by their HW/BW ratios (Fig. 4a,b). Next to the cardiac growth response, wheel exercise resulted in activation of MEK1 signaling in the heart, as indicated by an increase of phosphorylated ERK1/2 (Fig. 4c). As expected, enhanced MEK1 signaling during exercise induced hypertrophy resulted in reduced PPARα transcriptional activity inin the heart.

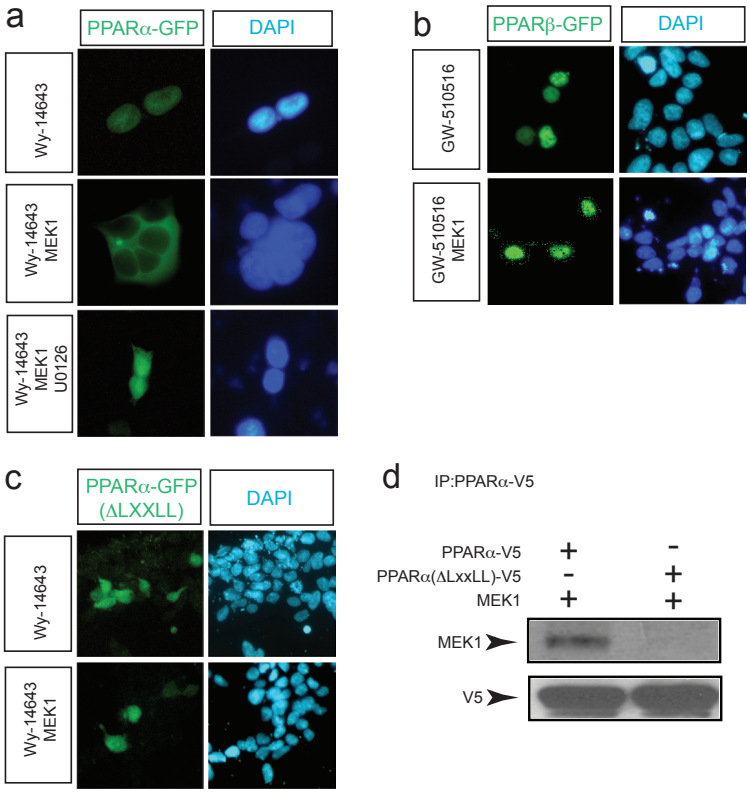

Figure 3. Mek1 interaction with PPARα induces nuclear export. (a) GFP fluorescence images of HEK293 cells transiently co-transfected with a PPARα-GFP with or without a MEK1 expression vector and stimulation with Wy-14643 for 24 hr, showing nuclear translocation of PPARα after co-transfection with MEK1. Addition of U0126 inhibited the MEK1 induced translocation. (b) GFP fluorescence images of HEK293 cells transiently co-transfected with a mutant PPARα-GFPΔLxxLL (lacking the LxxLL) motif with or without a MEK1 expression vector and stimulation with Wy-14643 for 24 hr. (c) GFP fluorescence images of HEK293 cells transiently co-transfected with a PPARβ/δ-GFP with or without a MEK1 expression vector and stimulation with Wy-14643 for 24 hr, indicating the MEK1 induced translocation to be PPARα specific.

RT-PCR analyses of PPARα target genes expression in exercised and sedentary mice hearts, showed decreased PPARα activity during physiological hypertrophy (Fig. 4d), with no effect on PPARα transcript abundance (data not shown). These data indicate that despite beneficial effect during pressure overload induced hypertrophy, PPARα signaling plays a minor role during physiological hypertrophy.

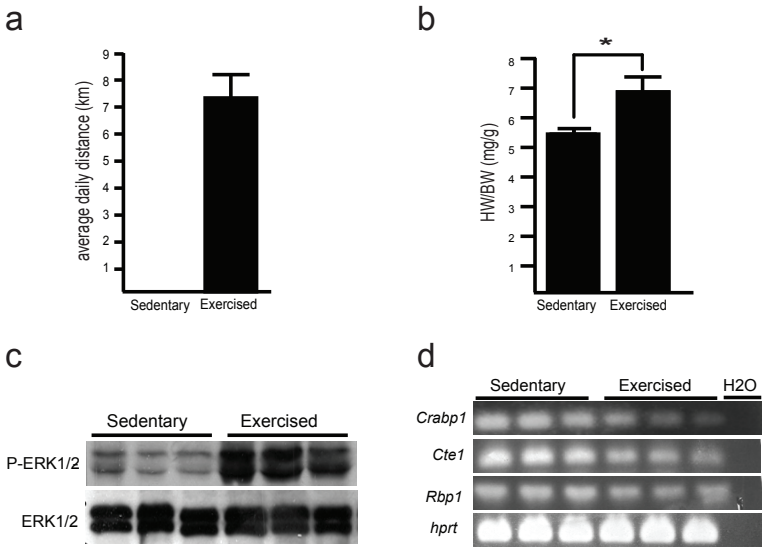

Figure 4. Activation of MEK1 during physiological hypertrophy inhibits PPARα activity. (a) Average daily distance that mice ran voluntarily. (b) Heart weight to body weight (HW/BW) ratios of indicated genotypes either sedentary or exercised (n=8 per group). (c) Western blot analysis using anti-fosforylated ERK1/2 (p-ERK1/2) antibody on lysates of heart sampels, indicating enhanced MEK1 activity during exercise induced hypertrophy. (d) RT-PCR analyses of PPARα and PPARα target genes expression in exercised and sedentary mice hearts, indicating decreased PPARα activity during physiological hypertrophy.

DISCUSSION

Mechanisms that regulate the ligand-independent activity of nuclear receptors, such as PPARs, are poorly understood and are often associated with kinase-dependent processes. Several consensus phosphorylation sites for PPARα have been identified including glycogen synthase kinase 3 (GSK3), protein kinase A (PKA), protein kinase C (PKC) and mitogen-activated protein kinase (MAPK). MAPK signaling pathways have been reported to be very important in the regulation of cellular differentiation, proliferation and stress responsiveness. Consisting of three major branches of sequentially signaling pathways, the MEK1 signaling pathway, which culminates in ERK1/2 activation, is hypothesized to regulate the growth and adaptation of the heart to both physiological and pathological stimuli (11).

Functional verification of the transcriptional activity of PPARα, after activation of the MEK1 pathway, resulted in a dramatic decrease of PPARα ability to activate a mCPT reporter. Although it was previously shown that activated ERK1/2 is able to phosphorylate PPARα (10), site-directed mutagenesis of all of the putative serine ERK1/2 phosphorylation target sites showed no difference to the MEK1 induced inhibition of PPARα transcriptional activity. Furthermore, inactivating ERK1/2 using the MAPK phosphatase MKP1 did not change the inhibitory effect of MEK1 on the transcriptional activity of

PPARα indicating an insignificant role for ERK1/2. This also indicated that the MEK1 induced inhibition of PPARα is unlikely to be phosphorylation mediated since it was shown that PPARα is phosphorylated exclusively on serine residues in vivo with no detectable threonine or tyrosine activity (20). In addition, MEK1 has been shown to be unable to phosphorylate PPAR (12).

An important factor that participates in the regulation of PPAR as well as MAPK signaling is their subcellular localization (19,21). Regarding the MAPK signaling, it has been shown that MEK1 resides in the cytosol of resting cells and translocates into the nucleus upon stimulation. Due to a nuclear export signal (NES), MEK1 is exported out of the nucleus (22). Unfortunately, little is known about the regulation of the intracellular distribution of PPAR's, though cytosolic localization of PPAR's has been reported as well as their bindings ability to the cytosolic/membrane proteins such as HSP90 (23-25). Interestingly, the presence of a CRS/CD domain in PPARα, which facilitates a protein-protein interaction with MEK1, indicated a possible direct interaction with MEK1. Indeed, co-immunoprecipitation studies showed a complex formation of PPARα with MEK1, but not with ERK1/2 (data not shown). In line, ectopic addition of MEK1 resulted in a massive extrusion of PPARα from the nucleus towards the cytoplasm even after continuous stimulation with its synthetic ligand. Furthermore, truncation studies showed that interaction of PPARα with MEK1 is mediated via a LXXLL binding pocket, given that deletion of this motif resulted in loss of the inhibitory effect of MEK1.

In this context one could assume that MEK1, via the inhibition of PPARα, has a role in the regulation of metabolic processes in the heart. Indeed, gene profiling studies executed on cardiomyocytes over expressing a constitutively active form of MEK1 (MEK-EE) demonstrated a significant decrease of genes coding for proteins involved in fatty acid metabolism (26). These included genes that would be localized to the mitochondria and involved in fatty acid translocation and oxidation (cpt1a, acadv1, Hadhsc), but also binding proteins that are involved in cellular transport of fatty acids (CD36). This effect was less clear for the regulation of genes involved the glycolysis/gluconeogenesis, where glucose transporter GLUT3 was up regulated but other components of the glycolysis were down-regulated. Nonetheless, this expression profile rendered the cardiomyocytes to be more resistant to energy deprivation following deoxyglucose exposure (11), indicating a preserved intrinsic reserve. Additionally, Analysis of cardiac substrate metabolism in PPARα knock-out hearts indicated a substrate switch from fatty acids to glucose and lactate but with an inability to respond to high energy demand, such as high workload, resulting in energetic and contractile failure mimicking end stage heart failure (27).

In response to acute pressure overload stimulation induced by aortic banding, MEK1 has been shown to be activated (28), further signifying that inhibition of PPARα activity by MEK1 could account for the metabolic switch that is known to occr during cardiac hypertrophy. In contrast, MEK1 transgenic mouse lines showed a mild concentric hypertrophy with thicker septum and left ventricular posterior wall with very few signs of histopathology or interstitial fibrosis (11). Moreover, echocardiography demonstrated an

enhanced contractile performance in these mice, suggesting compensated cardiac hypertrophy as seen in physiological hypertrophy. Indeed, exercise induced hypertrophy resulted in activation of the downstream effectors ERK1/2 indicating increased MEK1 activity, indicating that the preserved cardiac function, such as seen in MEK1 transgenic mouse lines, is likely to be PPARα independent. Thus, we present here a novel mechanism of down-regulation of PPARα activity through MEK1 induced redistribution from the nucleus to the cytosol. This ERK1/2 independent nuclear shuttling of PPARα by MEK1 provides an attractive explanation for the metabolic switch during cardiac hypertrophy and will lead to new insights into the different mechanisms between pathophysiological and physiological hypertrophy.

ACKNOWLEDGEMENTS
We are indebted to Marc van Bilsen (Maastricht University, The Netherlands) for providing PPAR expression and reporter vectors and Jeffery D. Molkentin (Cincinnati Children's Hospital Medical Center, USA) for providing MAPK expression vectors.

FUNDING SOURCES
This work was supported by grants 912-04-054, 912-04-017 and a VIDI award 917-863-72 from the Netherlands Organization for Health Research and Development; grant NHS2007B167 from the Netherlands Heart Foundation; and the European Union Contract No. LSHM-CT-2005-018833/EUGeneHeart (to L.J.D.W.).

AUTHOR CONTRIBUTIONS
H.E.A. and L.J.D.W. designed research; H.E.A. and S.L. performed research; H.E.A. and L.J.D.W. wrote the paper.

REFERENCES

1. Francis GS, Tang WH. Pathophysiology of congestive heart failure. Rev Cardiovasc Med 2003;4 Suppl 2:S14-20.
2. Wahli W, Braissant O, Desvergne B. Peroxisome proliferator activated receptors: transcriptional regulators of adipogenesis, lipid metabolism and more. Chem Biol 1995;2:261-6.
3. Burkart EM, Sambandam N, Han X, et al. Nuclear receptors PPARbeta/delta and PPARalpha direct distinct metabolic regulatory programs in the mouse heart. J Clin Invest 2007;117:3930-9.
4. Gelinas R, Labarthe F, Bouchard B, et al. Alterations in carbohydrate metabolism and its regulation in PPARalpha null mouse hearts. Am J Physiol Heart Circ Physiol 2008;294:H1571-80.
5. Sack MN, Rader TA, Park S, Bastin J, McCune SA, Kelly DP. Fatty acid oxidation enzyme gene expression is downregulated in the failing heart. Circulation 1996;94:2837-42.
6. Sack MN, Disch DL, Rockman HA, Kelly DP. A role for Sp and nuclear receptor transcription factors in a cardiac hypertrophic growth program. Proc Natl Acad Sci U S A 1997;94:6438-43.
7. Shalev A, Siegrist-Kaiser CA, Yen PM, et al. The peroxisome proliferator-activated receptor alpha is a phosphoprotein: regulation by insulin. Endocrinology 1996;137:4499-502.
8. Lazennec G, Canaple L, Saugy D, Wahli W. Activation of peroxisome proliferator-activated receptors (PPARs) by their ligands and protein kinase A activators. Mol Endocrinol 2000;14:1962-75.
9. Sugden PH. Signaling in myocardial hypertrophy: life after calcineurin? Circ Res 1999;84:633-46.
10. Barger PM, Browning AC, Garner AN, Kelly DP. p38 mitogen-activated protein kinase activates peroxisome proliferator-activated receptor alpha: a potential role in the cardiac metabolic stress response. J Biol Chem 2001;276:44495-501.
11. Bueno OF, De Windt LJ, Tymitz KM, et al. The MEK1-ERK1/2 signaling pathway promotes compensated cardiac hypertrophy in transgenic mice. Embo J 2000;19:6341-50.
12. Burgermeister E, Chuderland D, Hanoch T, Meyer M, Liscovitch M, Seger R. Interaction with MEK causes nuclear export and downregulation of peroxisome proliferator-activated receptor gamma. Mol Cell Biol 2007;27:803-17.
13. Burgermeister E, Seger R. MAPK kinases as nucleo-cytoplasmic shuttles for PPARgamma. Cell Cycle 2007;6:1539-48.
14. van Rooij E, Doevendans PA, de Theije CC, Babiker FA, Molkentin JD, de Windt LJ. Requirement of nuclear factor of activated T-cells in calcineurin- mediated cardiomyocyte hypertrophy. J Biol Chem 2002;277:48617-26.
15. Ye H, Cande C, Stephanou NC, et al. DNA binding is required for the apoptogenic action of apoptosis inducing factor. Nat Struct Biol 2002;9:680-4.
16. Rybkin, II, Markham DW, Yan Z, Bassel-Duby R, Williams RS, Olson EN. Conditional expression of SV40 T-antigen in mouse cardiomyocytes facilitates an inducible switch from proliferation to differentiation. J Biol Chem 2003;278:15927
17. Hi R, Osada S, Yumoto N, Osumi T. Characterization of the amino-terminal activation domain of peroxisome proliferator-activated receptor alpha. Importance of alpha-helical structure in the transactivating function. J Biol Chem 1999;274:35152-8.
18. Burgermeister E, Lanzendoerfer M, Scheuer W. Comparative analysis of docking motifs in MAP-kinases and nuclear receptors. J Biomol Struct Dyn 2003;20:623-34.
19. Varley CL, Stahlschmidt J, Smith B, Stower M, Southgate J. Activation of peroxisome prolifer-

ator-activated receptor-gamma reverses squamous metaplasia and induces transitional differentiation in normal human urothelial cells. Am J Pathol 2004;164:1789-98.
20. Burns KA, Vanden Heuvel JP. Modulation of PPAR activity via phosphorylation. Biochim Biophys Acta 2007;1771:952-60.
21. Marenda DR, Vrailas AD, Rodrigues AB, et al. MAP kinase subcellular localization controls both pattern and proliferation in the developing Drosophila wing. Development 2006;133:43-51.
22. Jaaro H, Rubinfeld H, Hanoch T, Seger R. Nuclear translocation of mitogen-activated protein kinase kinase (MEK1) in response to mitogenic stimulation. Proc Natl Acad Sci U S A 1997;94:3742-7.
23. Sumanasekera WK, Tien ES, Davis JW, 2nd, Turpey R, Perdew GH, Vanden Heuvel JP. Heat shock protein-90 (Hsp90) acts as a repressor of peroxisome proliferator-activated receptor-alpha (PPARalpha) and PPARbeta activity. Biochemistry 2003;42:10726-35.
24. Sumanasekera WK, Tien ES, Turpey R, Vanden Heuvel JP, Perdew GH. Evidence that peroxisome proliferator-activated receptor alpha is complexed with the 90-kDa heat shock protein and the hepatitis virus B X-associated protein 2. J Biol Chem 2003;278:4467-73.
25. Shibuya A, Wada K, Nakajima A, et al. Nitration of PPARgamma inhibits ligand-dependent translocation into the nucleus in a macrophage-like cell line, RAW 264. FEBS Lett 2002;525:43-7.
26. Badrian B, Bogoyevitch MA. Gene expression profiling reveals complex changes following MEK-EE expression in cardiac myocytes. Int J Biochem Cell Biol 2007;39:349-65.
27. Luptak I, Balschi JA, Xing Y, Leone TC, Kelly DP, Tian R. Decreased contractile and metabolic reserve in peroxisome proliferator-activated receptor-alpha-null hearts can be rescued by increasing glucose transport and utilization. Circulation 2005;112:2339-46.
28. Takeishi Y, Huang Q, Abe J, et al. Src and multiple MAP kinase activation in cardiac hypertrophy and congestive heart failure under chronic pressure-overload: comparison with acute mechanical stretch. J Mol Cell Cardiol 2001;33:1637-48.


chapter
4

CHAPTER 4

Conditional, heart-restricted deletion of PPAR-beta/delta provokes rapid and spontaneous cardiac remodeling

Hamid el Azzouzi, Heleen van den Bosch, Marc van Bilsen and Leon J. De Windt

ABSTRACT

PPARβ/δ is an abundant member of the peroxisome proliferator-activated receptors (PPARs) family, a nuclear receptor family of ligand activated transcription factors. Limited information is available on the function of PPARβ/δ in the adult myocardium. To circumvent the embryonic lethality associated with postnatal deletion of PPARβ/δ, we triggered conditional PPARβ/δ loss through the use of a tamoxifen-inducible Cre recombinase in the postnatal murine myocardium. Targeted PPARβ/δ deletion in adult mice provoked premature death within one week accompanied by rapid and dramatic biventricular enlargement, dramatic atrial enlargement, escorted by myocyte hypertrophy, myofiber disarray, ventricular fibrosis and strong induction of fetal gene transcripts and indications of severe disruption of fatty acid oxidation. Overall, these results indicate that PPARβ/δ loss suffices to impact both adult myocardial morphology and function.

INTRODUCTION

Long-chain fatty acids (FA) coordinately induce the expression of a panel of genes involved in cellular FA metabolism in cardiac muscle, thereby promoting FA oxidation in this organ (1). These effects are likely mediated by peroxisome proliferator-activated receptors (PPARs), members of the nuclear receptor family of ligand activated transcription factors (21, 22). Given their function as essential transcriptional mediators of adipogenesis, lipid metabolism, insulin sensitivity, and glucose homeostasis, PPARs are increasingly recognized as key players in inflammatory cells and in cardiovascular diseases (CVD) such as hypertension, atherosclerosis, cardiac hypertrophy, and congestive heart failure (2-4). In the presence of ligands, PPARs adopt an active conformation by forming an obligate heterodimer with the retinoid X receptor (RXR). Recruitment of additional co-activators provokes binding to peroxisome proliferator response elements (PPRE) in target genes, allowing PPAR-dependent gene expression (5). Despite the high levels of homologies at the protein level, the three PPAR isoforms, PPARα, PPARβ/δ and PPARγ, exert different functions relying on differentially distribution in distinct tissues, isoform specific phosphorylation, selective interactions with their specific ligand and co-activators, and, likely, isoform-selective target gene activation (2-4).

PPARα and PPARγ are characterized by their capacity to influence lipid metabolism, glucose homeostasis, cell proliferation, differentiation and apoptosis, as well as the inflammatory response (2-4). PPARα activation mediates different effects such as the stimulation of lipid oxidation and anti-inflammatory effect by squelching the inflammatory transcription factor NF-κB (6,7). Mice overexpressing PPARα in cardiac muscle display an increased fatty acid oxidation rates, accumulation of triacylglycerides, decrease in glucose metabolism and eventually develop cardiomyopathy (8,9). Not surprisingly, mice lacking PPARα have elevated free fatty acid levels as a consequence of inadequate fatty acids oxidation rendering them hypoglycemic as a result of their reliance on glucose (5). Elucidation of the role of PPARγ in cardiac muscle has been hampered by its low abundance and the absence of significant effects of PPAR ligands such as ciglitazone and rosiglitazone on regulation of target genes (1). Nevertheless, transgenic mice overexpressing PPARγ in the heart displayed increased cardiac FFA uptake without a concomitant reduction in glucose uptake, and ultimately developed severe heart failure (10).

Less is known about PPARβ/δ function in the heart. Heart muscle-restricted deletion of PPARβ/δ resulted in progressive myocardial lipid accumulation, cardiac hypertrophy and congestive heart failure (11). Based upon the analysis of the PPARβ/δ null mouse model, PPARβ/δ deficiency leads to multiple developmental and metabolic abnormalities including frequent embryonic lethality, impaired wound healing and skin abnormalities due to altered inflammatory responses in the skin (12,13). Conversely, selective overexpression of PPARβ/δ in the mouse heart provoked an increase in myocardial glucose utilization with no myocardial lipid accumulation and normal cardiac function (14,15).

To circumvent the embryonic lethality associated with postnatal deletion of PPARβ/δ, we triggered conditional PPARβ/δ loss through the use of a tamoxifen-inducible Cre recombinase in the postnatal murine myocardium. Targeted PPARβ/δ deletion in adult mice provoked premature death within one week accompanied by rapid and dramatic biventricular enlargement, dramatic atrial enlargement, escorted by myocyte hypertrophy, myofiber disarray, ventricular fibrosis and strong induction of fetal gene transcripts and indications of severe disruption of fatty acid oxidation. Overall, these results indicate that PPARβ/δ loss suffices to impact both adult myocardial morphology and function.

MATERIALS AND METHODS

Mice. Mice homozygous for PPAR-beta/delta-floxed alleles (PPARdF/F) and transgenic αMHC-MerCreMer (αMHC-MCM) mice were crossed to generate double-transgenic (αMHC-MCM-PPARdF/F) mice. Mice at xx weeks of age (αMHC-MCM-PPARdF/F and control PPARdF/F) were treated with vehicle or tamoxifen (20mg/kg/day) by daily intraperitoneal injections for consecutive 5 days. Tamoxifen was diluted in 10/90 % v/v ethanol/oil to a concentration of 1mg/100μl, for the vehicle group only ethanol/oil solution was injected.

Transthoracic Echocardiography. Echocardiographic measurements were performed on mice anesthetized with isoflurane as described before,(16) 1 week and 4 weeks after starting of tamoxifen treatment.

Immunolabeling and immunofluorescence microscopy. Hearts were arrested in diastole and perfusion fixed with 4% paraformaldehyde and embedded in paraffin, sectioned at 6 μm, and stained with hematoxylin and eosin (H&E) or Sirius red. Slides were visualized using a Nikon Eclipse E600 microscope.

Quantitative RT-PCR. One microgram of total RNA from mouse ventricular tissue was used as template for Superscript reverse transcriptase II (Promega). For real time RT-PCR, a BioRad iCycler (Biorad) and SYBR Green was used in combination with specific primer sets designed to detect transcripts for nppa, nppb, acta1, myh7, hadhac, cd36, glut1. (primer sequences available upon request) as described previously in detail (17).

Statistical analysis. The results are presented as mean ± SEM. Statistical analyses were performed with InStat 3.0 (GraphPad Software, Inc, San Diego, CA). The analyses consisted of ANOVA, followed by Tukey's posttest when group differences were detected at the 5% significance level. Statistical significance was accepted at a p value <0.05.

RESULTS

Deletion of PPARβ/δ causes rapid biventricular dilation and premature death

To investigate whether PPARβ/δ gene activation is required for normal myocardial homeostasis and to bypass the early embryonic lethality of PPARβ/δ-null mice, we first provoked deletion of a floxed PPARβ/δ (PPARdF/F) allele using a tamoxifen-inducible Cre recombinase protein fused to two mutant estrogen-receptor ligand-binding domains under control of the cardiac-specific α-myosin heavy chain promoter. We treated adult αMHC-MCM/PPARdF/F and PPARdF/F mice with vehicle or tamoxifen at the age of 8 weeks. We noted that within 5 days of start of tamoxifen delivery, αMHC-MCM/PPARdF/F mice displayed a weak condition and inactivity, compared to tamoxifen-treated PPARdF/F, or vehicle-treated αMHC-MCM/PPARdF/F control mice. Indeed, up to 25% of tamoxifen-treated αMHC-MCM/PPARdF/F mice died within one week after starting of treatment and this mortality rate increased up to 75% during the following two weeks (data not shown).

In addition, hearts from tamoxifen-treated αMHC-MCM/PPARdF/F mice displayed doubling in heart weight compared to their control littermates (Fig. 1a). To ascertain whether we indeed created mice with deficiency for ppard, we performed real time RT-PCR for all three endogenous PPAR isoforms. The data show that our genetic intervention did not intervene with ppara or pparg transcripts, but specifically indiced strong downregulation of ppard transcripts (Fig. 1b). A severe histopathology was evident after staining histological sections with H&E and Sirius Red. Cardiac tissue revealed an intricate phenotype with hypertrophied myofibers, myocyte disarray, strong inflammatory infiltration and interstitial fibrosis (Fig. 1d), hallmark features observed in experimental and clinical heart failure biopsies. Sirius red staining indicated massive interstitial and perivascular fibrosis in hearts from tamoxifen-treated αMHC-MCM/PPARdF/F mice (Fig. 1d).

Furthermore, measurements of heart-weight-to-body-weight (HW/BW) ratios indicated a similar increase in cardiac mass for from tamoxifen-treated αMHC-MCM/PPARdF/F mice (7.5±1.2 mg/g) compared to tamoxifen-treated PPARdF/F (6.2 ±0.9 mg/g) (Fig. 1c). These data demonstrate that adult-onset, cardiac-specific deletion of PPARβ/δ causes rapid cardiac remodeling, reduced survivability and multiple signs of end-stage heart failure.

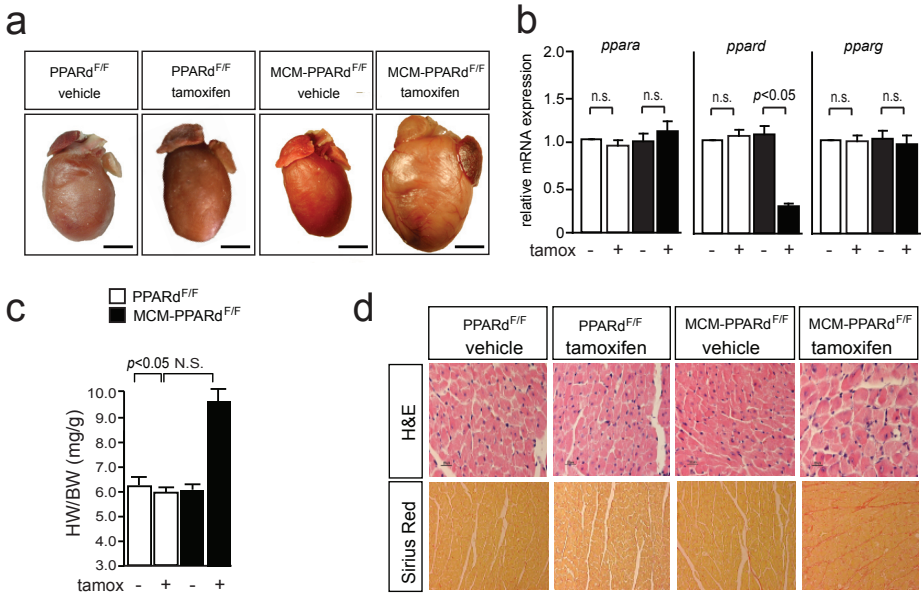

Figure 1. Deletion of PPARβ/δ provokes spontaneous cardiac remodeling. (a) Representative gross morphology of hearts dissected from 8 week-old mice of indicated genotypes, demonstrating visible cardiac enlargement by ppard deletion in the adult mouse heart (bar 5 mm). (b) Real-time PCR analysis of endogenous transcripts of ppara, ppard and pparg in the indicated genotypes, indicating specific deletion of endogenous ppard transcripts in the heart following tamoxifen treatment of MHC-MCM-PPARdF/F mice. (c) Heart weight to body weight ratio in the indicated genotypes indicates hypertrophic remodeling in MHC-MCM-PPARdF/F mice after tamoxifen treatment. (d) Representative histological images of hearts from mice with indicated genotypes (bar 2 mm). Sirius red staining indicates massive interstitial and perivascular fibrosis in hearts of MHC-MCM-PPARdF/F mice after tamoxifen treatment.

Targeted deletion of PPARβ/δ in the adult heart causes severe cardiac dysfunction and induction of fetal genes.

Cardiac geometry and function was assessed non-invasively by echocardiography at 2 weeks after tamoxifen treatment (Fig. 2). After 2 weeks, vehicle treated PPARdF/F and αMHC-MCM/PPARdF/F mice demonstrated normal cardiac geometry and function as indicated by fractional shortening (FS) (Fig. 2a), left ventricular internal dimensions (LVID) and left ventricular mass (Fig. 2a). As expected, tamoxifen-treated PPARdF/F mice showed no alterations in FS or other parameters. In contrast, at 2 week, αMHC-MCM/PPARdF/F animals demonstrated a rapid and significant decline in cardiac function, indicated by a 50% decrease in FS ($P<0.05$; Fig. 2b). At this time point after tamoxifen treatment, αMHC-MCM/PPARdF/F mice also showed a more pronounced deterioration in

cardiac geometry compared to vehicle treated αMHC-MCM/PPARdF/F mice, as demonstrated by a increase of 80-90% in LV internal diameters (LVIDs; Fig. 2c), indicating a rapid dilation of the left ventricle. These data indicate that PPARβ/δ depletion provokes progressive functional and geometrical deterioration consistent with a heart failure phenotype.

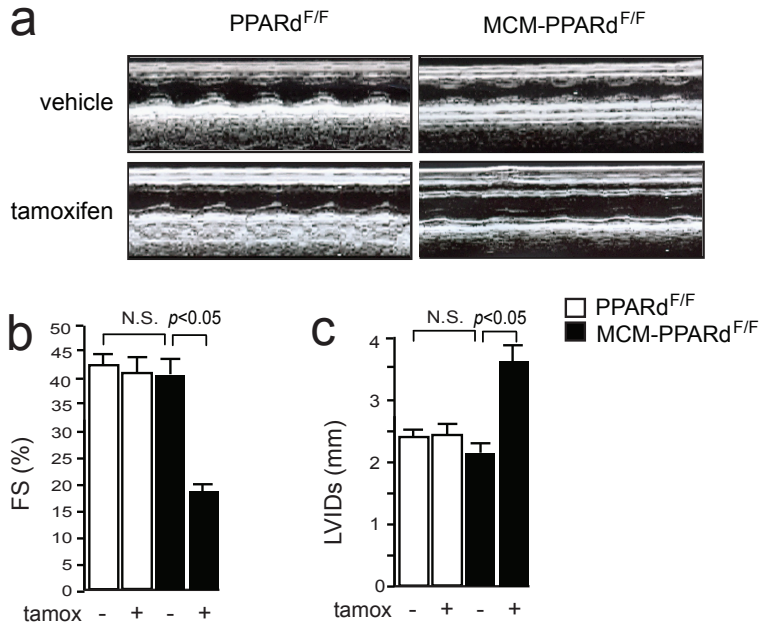

Figure 2. Deletion of PPARβ/δ causes severe cardiac dysfunction. (a) Representative M-mode images of mice with indicated genotypes. (b) Bar graph representation of Fractional Shortening (FS) in indicated genotypes indicates loss of contractility in hearts of MHC-MCM-PPARdF/F mice after tamoxifen treatment (n=6 per group). (c) Bar graph representation of ejection fraction (EF) in indicated genotypes indicates loss of cardiac output in hearts of MHC-MCM-PPARdF/F mice after tamoxifen treatment (n=6 per group).

Deletion of PPARβ/δ in adult mice also induced potent re-activation of embryonic genes such as acta1, nppb, myh7 and nppa in 8-week old αMHC-MCM/PPARdF/F hearts (Fig. 3). There was no substantial change in the expression of any of these genes in hearts of tamoxifen- or vehicle-treated control genotypes. Moreover, we noted a substantial decrease in transcript abundance for cd36 and hadha, and an increase in glut1 (Fig. 3). These data are indicative for a reduction in fatty acid transport capacity and oxiodation, and a concomitant increase in glycolysis. Conclusively, deletion of PPARβ/δ in the adult heart induces rapid and spontaneous cardiac dysfunction with strong induction of "fetal" hypertrophic marker genes.

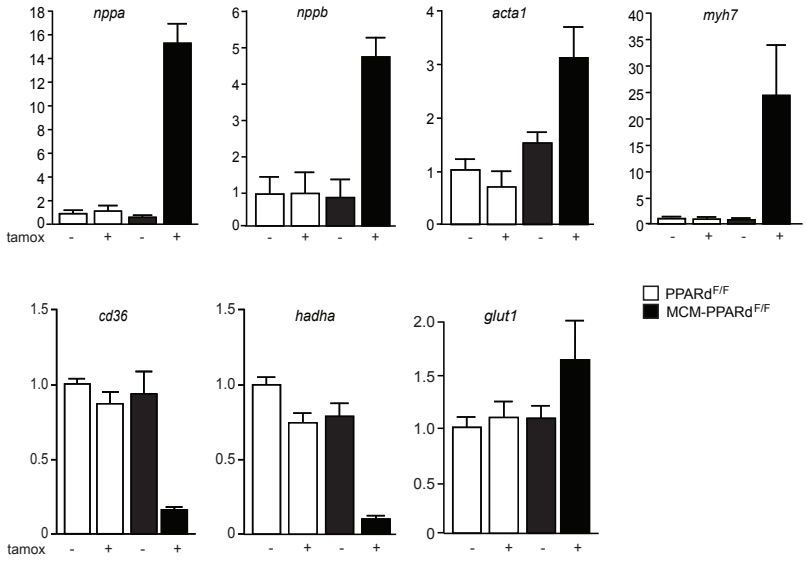

Figure 3. Targeted deletion of PPARβ/δ in the adult heart increases the expression of fetal and glycolytic genes, and decreases expression of fatty acid transport and oxidation genes. Analysis of expression of several fetal genes (nppa, nppb, myh7 and acta1) indicative of heart failure, glut1 (indicative of glycolysis), cd36 and hadha (indicative of fatty acid transport and oxidation) by quantitative RT-PCR in ventricular tissue of indicated genotypes. Error bars are mean ± SEM of n=3.

DISCUSSION

Despite major therapeutic advances, heart failure remains a leading cause of morbidity and mortality worldwide, which rivals or exceeds that of many forms of cancers (REF). Additionally, evidence is emerging that derangements in cardiac fuel metabolism, related to insulin resistance or diabetes, contribute to the development of diabetic cardiac dysfunction. Indeed, diabetes predisposes to heart failure, particularly in combination with other comorbid conditions such as hypertension and coronary artery disease (2, 3).

Numerous studies have identified decreased cardiac energy levels and flux as a consistent feature of HF, and have focused considerable attention on metabolic modulations as a therapeutic modality for HF (1,2). Although regulation of metabolism is modulated by a variety of influences, transcriptional regulation of genes involved in metabolism by the PPAR family of transcription factors has been intensively investigated. As PPARs are activated by lipid moieties, they provide attractive targets for therapeutic interventions. Despite their putative role in HF, only a few studies have sought to mutually compare PPAR subtype-specific activation of endogenous genes and their function in the heart (3).

All PPAR isoforms are present in the adult heart and isolated myocytes, with a relative abundance for PPARα and PPARβ/δ, with a quantitative minority for PPARγ (4). PPARα activation mediates different effects such as the stimulation of lipid oxidation and anti-inflammatory effect by squelching the inflammatory transcription factor NF-κB (5,6). Mice overexpressing PPARα in cardiac muscle display an increased fatty acid oxidation

rates, accumulation of triacylglycerides, decrease in glucose metabolism and eventually develop cardiomyopathy (7,8). Mice lacking PPARα have elevated free fatty acid levels as a consequence of inadequate fatty acids oxidation rendering them hypoglycemic as a result of their reliance on glucose (9). Elucidation of the role of PPARγ in cardiac muscle has been hampered by its low abundance and the absence of significant effects of PPAR ligands such as ciglitazone and rosiglitazone on regulation of target genes (4). Nevertheless, transgenic mice overexpressing PPARγ in the heart displayed increased cardiac FFA uptake without a concomitant reduction in glucose uptake, and ultimately developed severe heart failure (10).

Remarkably little is known about PPARβ/δ function in the heart, even though it expression level is likely as high as PPARα in the heart (4). Heart muscle-restricted deletion of PPARβ/δ from birth resulted in progressive myocardial lipid accumulation, cardiac hypertrophy and congestive heart failure (11). Based upon the analysis of the PPARβ/δ null mouse model, PPARβ/δ deficiency leads to multiple developmental and metabolic abnormalities including frequent embryonic lethality, impaired wound healing and skin abnormalities due to altered inflammatory responses in the skin (12,13). Conversely, selective overexpression of PPARβ/δ in the mouse heart provoked an increase in myocardial glucose utilization with no myocardial lipid accumulation and normal cardiac function (16,17).

To circumvent the embryonic lethality associated with postnatal deletion of PPARβ/δ, we triggered conditional PPARβ/δ loss through the use of a tamoxifen-inducible Cre recombinase in the postnatal murine myocardium. Targeted PPARβ/δ deletion in adult mice provoked premature death within one week accompanied by rapid and dramatic biventricular enlargement, dramatic atrial enlargement, escorted by myocyte hypertrophy, myofiber disarray, ventricular fibrosis and strong induction of fetal gene transcripts and indications of severe disruption of fatty acid oxidation. During the development of cardiac hypertrophy, myocardial fatty acid oxidation (FAO) rats decrease and glucose utilization increases (18). During this transition, the nuclear levels of PPARs are reduced, suggesting that this phenomenon may be responsible for downregulation of cardiac FAO genes in the hypertrophied heart (19).

Overall, our results indicate that PPARβ/δ is instructive in the metabolic switch from FAO to glycolysis, suggesting that any derangement in (PPARβ/δ) mediated FAO suffices to impact both adult myocardial morphology and function, and underscores the maladaptive nature of the metabolic switch that occurs in the genesis of heart failure.

ACKNOWLEDGMENTS

We are grateful to Jeroen Korving for technical assistance.

REFERENCES

1.Gilde AJ, van der Lee KA, Willemsen PH, et al. Peroxisome proliferator-activated receptor (PPAR) alpha and PPARbeta/delta, but not PPARgamma, modulate the expression of genes involved in cardiac lipid metabolism. Circ Res 2003;92:518-24.
2.Boudina S, Abel ED. Diabetic cardiomyopathy revisited. Circulation 2007;115:3213-23.
3.Madrazo JA, Kelly DP. The PPAR trio: Regulators of myocardial energy metabolism in health and disease. J Mol Cell Cardiol 2008.
4.Smeets PJ, Planavila A, van der Vusse GJ, van Bilsen M. Peroxisome proliferator-activated receptors and inflammation: take it to heart. Acta Physiol (Oxf) 2007;191:171-88.
5.Guerre-Millo M, Rouault C, Poulain P, et al. PPAR-alpha-null mice are protected from high-fat diet-induced insulin resistance. Diabetes 2001;50:2809-14.
6.Ding G, Cheng L, Qin Q, Frontin S, Yang Q. PPARdelta modulates lipopolysaccharde-induced TNFalpha inflammation signaling in cultured cardiomyocytes. J Mol Cell Cardiol 2006;40:821-8.
7.Hasegawa H, Takano H, Zou Y, et al. Pioglitazone, a peroxisome proliferator-activated receptor gamma activator, ameliorates experimental autoimmune myocarditis by modulating Th1/Th2 balance. J Mol Cell Cardiol 2005;38:257-65.
8.Finck BN, Han X, Courtois M, et al. A critical role for PPARalpha-mediated lipotoxicity in the pathogenesis of diabetic cardiomyopathy: modulation by dietary fat content. Proc Natl Acad Sci U S A 2003;100:1226-31.
9.Finck BN, Lehman JJ, Leone TC, et al. The cardiac phenotype induced by PPARalpha overexpression mimics that caused by diabetes mellitus. J Clin Invest 2002;109:121-30.
10.Ding G, Fu M, Qin Q, et al. Cardiac peroxisome proliferator-activated receptor gamma is essential in protecting cardiomyocytes from oxidative damage. Cardiovasc Res 2007;76:269-79.
11.Cheng L, Ding G, Qin Q, et al. Cardiomyocyte-restricted peroxisome proliferator-activated receptor-delta deletion perturbs myocardial fatty acid oxidation and leads to cardiomyopathy. Nat Med 2004;10:1245-50.
12.Peters JM, Lee SS, Li W, et al. Growth, adipose, brain, and skin alterations resulting from targeted disruption of the mouse peroxisome proliferator-activated receptor beta(delta). Mol Cell Biol 2000;20:5119-28.
13.Barak Y, Liao D, He W, et al. Effects of peroxisome proliferator-activated receptor delta on placentation, adiposity, and colorectal cancer. Proc Natl Acad Sci U S A 2002;99:303-8.
14.Burkart EM, Sambandam N, Han X, et al. Nuclear receptors PPARbeta/delta and PPARalpha direct distinct metabolic regulatory programs in the mouse heart. J Clin Invest 2007;117:3930-9.
15.He TC, Chan TA, Vogelstein B, Kinzler KW. PPARdelta is an APC-regulated target of nonsteroidal anti-inflammatory drugs. Cell 1999;99:335-45.
16.van Rooij E, Doevendans PA, Crijns HJ, et al. MCIP1 overexpression suppresses left ventricular remodeling and sustains cardiac function after myocardial infarction. Circ Res 2004;94:e18-26.
17.van Oort RJ, van Rooij E, Bourajjaj M, et al. MEF2 activates a genetic program promoting chamber dilation and contractile dysfunction in calcineurin-induced heart failure. Circulation 2006;114:298-308.
18.Sack MN, Rader TA, Park S, Bastin J, McCune SA, Kelly DP. Fatty acid oxidation enzyme gene expression is downregulated in the failing heart. Circulation 1996;94:2837-42.
19.Sack MN, Disch DL, Rockman HA, Kelly DP. A role for Sp and nuclear receptor transcription factors in a cardiac hypertrophic growth program. Proc Natl Acad Sci U S A 1997;94:6438-43.

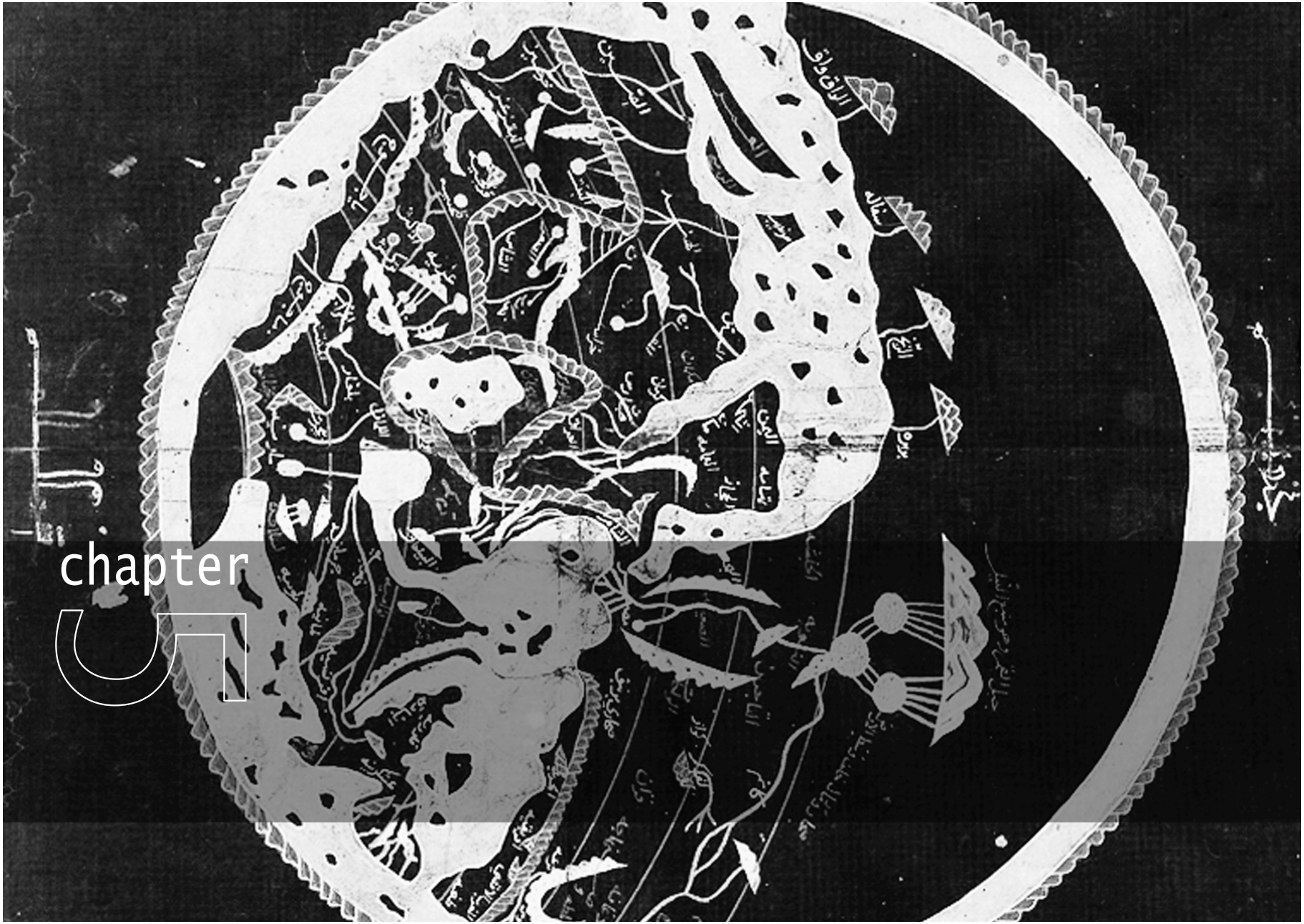

chapter 5

CHAPTER 5

MEF2 transcriptional activity maintains mitochondrial adaptation in cardiac pressure overload

Hamid el Azzouzi, Ralph J. van Oort, Roel van der Nagel,
Wim Sluiter, Martin W. Bergmann, Leon J. De Windt

In revision at J. Am. Coll. Cardiol, as:

Hamid el Azzouzi, Ralph J. van Oort, Roel van der Nagel, Wim Sluiter, Martin W. Bergmann, Leon J. De Windt. MEF2 transcriptional activity maintains mitochondrial adaptation in cardiac pressure overload.

ABSTRACT

The transcription factor myocyte enhancer factor 2 (MEF2) is a downstream target for several hypertrophic signaling pathways in the heart. Genetic mouse models lacking MEF2 isoforms have suggested that MEF2 activity in the postnatal heart evokes features of cardiac dilation, suggesting MEF2 as a valuable therapeutic target in the treatment of heart failure.In this study, we investigate the potential benefits of MEF2 inhibition in a mouse model of chronic pressure overloading. Therefore, we subjected wildtype and transgenic mice expressing a dominant negative form of MEF2 (DN-MEF2 Tg) in the heart to transverse aortic constriction (TAC). Histological analysis revealed no major differences in cardiac remodeling between DN-MEF2 Tg and wildtype mice after TAC. Surprisingly, echocardiographic analysis revealed that DN-MEF2 Tg mice displayed a decrease in cardiac function compared to control animals. Analysis of the mitochondrial respiratory chain showed that DN-MEF2 Tg mice displayed lower expression of NADH dehydrogenase subunit 6 (ND6), part of the large Complex I enzyme, only following pressure overload. The reduced expression of ND6 in DN-MEF2 Tg mice after pressure overload resulted in an increase in cell death secondary to overproduction of reactive oxygen species (ROS). Together, these data suggest that MEF2 transcriptional activity is required for proper mitochondrial function and its inhibition predisposes the heart to impaired mitochondrial function, overproduction of ROS, enhanced cell death and cardiac dysfunction following pressure overload.

INTRODUCTION

In response to stress, the heart compensates by hypertrophic growth, which frequently progresses to cardiac dilation and heart failure. The initial hypertrophic response is associated with activation of several intracellular signaling pathways (1,2). These pathways are interconnected and culminate in the nucleus on only a few transcriptional regulators. With the hope of revealing novel therapeutic targets in the treatment of heart failure, much effort has been dedicated to dissect the role of these select transcription factors. One common downstream transcriptional target for diverse stress cascades in the heart is myocyte enhancer factor 2 (MEF2).

The normal adult heart exhibits only basal MEF2 transcriptional activity, which is likely required for the maintenance of expression of genes involved in cardiomyocyte homeostasis, maintenance of the contractile apparatus and energy metabolism (3,4). MEF2 activity is upregulated by prohypertrophic signaling cascade constituents, such as calcineurin, calcium/calmodulin-dependent protein kinase (CaMK), protein kinase C (PKC), protein kinase D (PKD), big mitogen-activated protein kinase (MAPK)-1 (BMK-1), and p38 MAPK (2,3,5,6) (7,8).

Despite the considerable amount of evidence that suggest MEF2 factors to promote hypertrophic cardiac growth, this hypothesis has just recently been tested in a more direct approach. We and others have shown that overexpression of MEF2A or MEF2C in the postnatal murine heart minimally affects cardiac growth but evokes features of dilated cardiomyopathy (9,10). Furthermore, in vivo inhibition of MEF2 activity resulted in minimal reduction of calcineurin induced hypertrophy, but prevented wall thinning and chamber dilation and significantly improved cardiac function (10). These results imply that MEF2 triggers the molecular and genetic particulars underlying cardiac dilation and contractile loss, at least in certain experimental settings, which suggests that therapeutic MEF2 targeting may have future value to prevent chamber dilation and cardiac dysfunction in heart failure.

In this study, we directly tested the effects of MEF2 inhibition in cardiac hypertrophy and heart failure using a physiological model of pressure overload. To this end, conditional transgenic mice expressing dominant-negative MEF2 (DN-MEF2) in the heart were subjected to transverse aortic constriction (TAC), a surgical model for pressure overload. To our surprise, DN-MEF2 expressing mice did not display an improvement in heart function in response to TAC surgery, as assessed by echocardiography. In fact, cardiac function was worsened in DN-MEF2 Tg mice compared to wild-type mice following pressure overloading. OXHPOS expression analysis indicated that mice expressing DN-MEF2 had a lower expression level of NADH dehydrogenase subunit 6 (ND6), part of the larger mitochondrial Complex I. Furthermore, impaired expression of ND6 in mice expressing DN-MEF2 following pressure overload predisposed to exaggerated cell death due to overproduction of reactive oxygen species (ROS) compared to controlmice. The findings of this study indicate that MEF2 transcriptional activity in pressure overload

serves to compensate for increased energetic demand and protects against excessive ROS production and concomitant cell death.

EXPERIMENTAL PROCEDURES

Mice. Details on the generation of transgenic mice conditionally expressing DN-MEF2 and mice expressing Cre recombinase under control of the 5.5-kb murine cardiac α-myosin heavy chain promoter were described previously (10,11).

Aortic banding. Transverse aortic constriction (TAC) or sham surgery was performed in male mice, which were at least 10 weeks of age, by subjecting the aorta to a defined 27-gauge constriction between the first and second truncus of the aortic arch as described in detail previously (12).

Transthoracic echocardiography. Five weeks after surgery, cardiac remodeling and function was assessed by noninvasive echocardiography using a VisualSonics Vevo 770 high-resolution imaging system equipped with a 30 MHz RMV-707B scanning head. Echocardiographic measurements were performed on mice anesthetized with isoflurane. In M-mode, the following parameters were obtained with 3 or more readings per mouse: left ventricular posterior wall thickness, interventricular septum thickness, end-diastolic left ventricular internal diameter, end-systolic left ventricular internal diameter, left ventricular fractional shortening and ejection fraction. Doppler echocardiography was used to determine the pressure gradient between the proximal and distal sites of the transverse aortic constriction, and only mice with a pressure gradient >30 mm Hg were used in this study.

Immunolabeling and histological analysis. Hearts were arrested in diastole and perfusion fixed with 4% paraformaldehyde and embedded in paraffin. Sections were stained with hematoxylin and eosin (H&E), Sirius red, or FITC-labeled wheat germ agglutinin (WGA-FITC) or incubated with antibodies against 8-OHdG (7.5 μg/μl; Oxis International Inc., Portland, Oregon). Envision+ Kit (Dako Cytomation, glostrup, Denmark) was used as a secondary reagent. Stainings were developed using DAB (brown precipitate), and slides counterstained with hematoxylin and visualized using a Nikon Eclipse E600 microscope (Nikon, Melville, New York).

RNA quantification. Total RNA was isolated from heart tissue using TRIzol reagent (Invitrogen, Carlsbad, CA). One μg of RNA was reverse transcribed using M-MLV reverse transcriptase (Promega, Madison, WI). Real-time PCR using the BioRad iCycler (Bio-Rad, Hercules, CA) and fluorescence detection was performed in 96-well plates using SYBR Green and MyIQ optical software (Bio-Rad, Hercules, CA) as described in detail previously (10). Primer sequences are available upon request.

TUNEL staining. TUNEL assays were performed as described previously,(13) using the In Situ Cell Death Detection TMR-Red Kit (Roche) and using an antibody against α-actinin (Sigma) and TO-PRO3 (Molecular Probes) on 10 μm frozen, apical cross-sections of hearts.

Statistical analysis. The results are presented as mean ± SEM. Statistical analyses were performed with InStat 3.0 (GraphPad Software, Inc, San Diego, CA). The analyses consisted of ANOVA, followed by Tukey's posttest when group differences were detected at the 5% significance level. Statistical significance was accepted at a p value <0.05.

RESULTS

PPAR and MEF2 are transcriptional partners.

Earlier studies have had shown that CPT1β is a target gene for the action of peroxisome proliferator-activated receptors PPARα, and have localized a PPAR responsive element (PPRE) upstream of the first exon of this gene. Further analysis of this exon indicated an MEF2 binding site adjacent to a consensus PPRE. Next we showed synergistic activation of this reporter in the presence of PPARα and Wy-14643. Interestingly, site-directed mutagenesis of either the PPRE or MEF2 site or both completely abrogated the synergistic activation of this reporter plasmid (Fig. 1), indicating a functional interaction between PPARs and MEF2 in heart muscle cells.

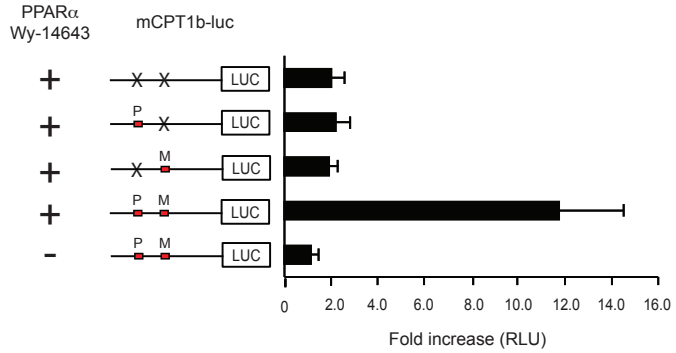

Figure 1. PPARα and MEF2 synergistically induce expression of the mCPT1 gene. (a) Luciferase measurements on NkL-Tag cells transiently transfected with a mCPT promoter driven reporter and PPARα-V5 for 24hr. As indicated, PPRE or/and MEF2 binding site-mutated mCPT-luc constructs showed decreased activation, demonstrating synergistic co-regulation of the mCPT by PPARα and MEF2.

Inhibition of MEF2 activity does not prevent pressure overload-induced cardiac hypertrophy

MEF2 transcription factors are activated by several intracellular hypertrophic signaling pathways (1). Using transgenic mice that express a dominant-negative form of MEF2 upon activation of Cre recombinase (FloxDN-MEF2 mice), we have recently demonstrated that inhibition of MEF2 transcriptional activity downstream of cardiac calcineurin signaling displayed a substantial reduction in cardiac dilation and improved contractility (10).

Accordingly, we used the same genetic loss-of-function approach to assess the role of MEF2 in pressure overload-induced cardiac remodeling, anticipating that heart-restricted MEF2 inhibition during pressure overload may also confer protection against this form of maladaptive remodeling. To this end, we subjected MHC-Cre/FloxDN-MEF2 and control MHC-Cre mice to transverse aortic constriction (TAC) or sham surgery, and analyzed cardiac remodeling and function 5 weeks after surgery. The hypertrophic response in MHC-Cre/FloxDN-MEF2 after TAC was indistinguishable from that of pressure-overloaded MHC-Cre mice (Fig. 2A and B). Heart-weight-to-body-weight (HW/BW) or heart-weight-to-tibia-length (HW/TL) ratios confirmed the increase in heart weight after pressure overload for both MHC-Cre and MHC-Cre/FloxDN-MEF2 mice compared to sham-operated mice (Fig. 2C and D). Furthermore, pressure overload was associated with pulmonary edema, as lung weight to body weight (LW/BW) increased to 7.2 ± 1.2 and 10.3 ± 1.8 (LW/BW) for MHC-Cre and MHC-Cre/FloxDN-MEF2 TAC mice. (Fig. 2E). The increase in these ratios for MHC-Cre/FloxDN-MEF2 TAC mice tended to be higher compared than MHC-Cre TAC mice (N.S.), which may suggest that cardiac function after TAC was worsened in these mice. Conclusively, inhibition of MEF2 activity does not inhibit the hypertrophic response following pressure overload.

H&E- and Sirius red-stained cardiac histological sections did not show any signs of histopathology in MHC-Cre/FloxDN-MEF2 and control MHC-Cre mice. Cardiomyocyte hypertrophy, myocyte disarray, and extensive areas of interstitial and perivascular fibrosis were evident in both pressure overloaded MHC-Cre/FloxDN-MEF2 and MHC-Cre mice hearts (Fig. 3A). As a more quantitative evaluation of individual myofiber hypertrophy, myofibril cross-sectional areas were quantified from WGA-stained sections. MHC-Cre/FloxDN-MEF2 and control MHC-Cre mice showed similar myofiber cross-sectional areas after TAC (Fig. 3B).

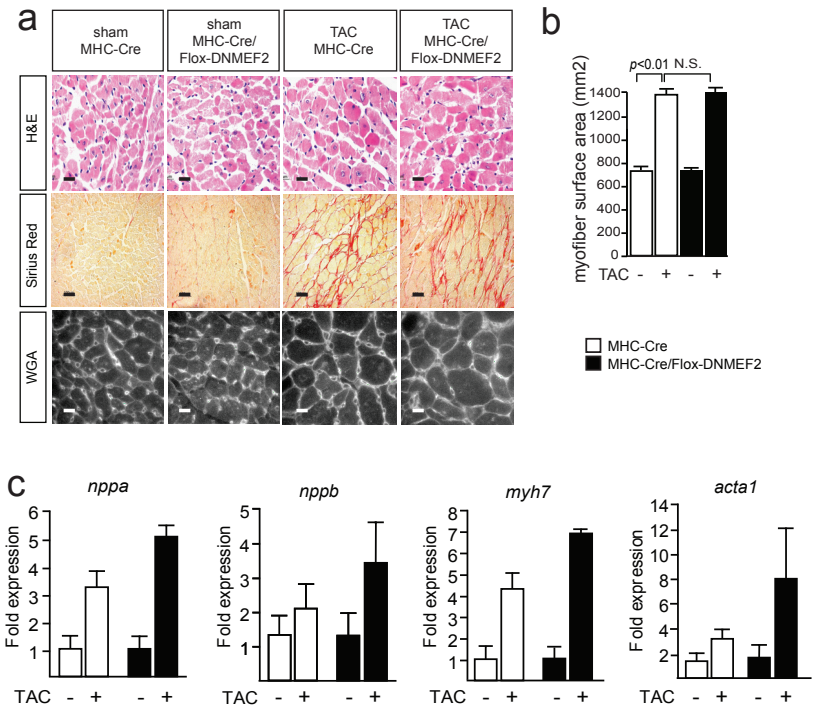

Figure 3. Gravimetrical, histological, functional and molecular analysis of MHC-Cre and MHC-Cre/FloxDNMEF2 mice after TAC. Representative histological images of hearts from mice of indicated genotypes (bar 0.2 mm). (a) H&E-stained images reveal remarkable myocyte hypertrophy and myofiber disarray in MHC-Cre and MHC-Cre/FloxDNMEF2 mice subjected to pressure overload. (b) Sirius red staining indicates massive interstitial and perivascular fibrosis in hearts of MHC-Cre and MHC-Cre/FloxDNMEF2 mice subjected to pressure overload. (c) Representative wheat germ agglutinin staining images of hearts from mice of indicated genotypes (bar 0.2 mm). (d) Quantification of myofiber cross-sectional area from indicated genotypes shows significant attenuation of myocyte hypertrophy in MHC-Cre and MHC-Cre/FloxDNMEF2 mice subjected to pressure overload (n=3 per group, with 100 fibers counted per animal). (e) Real time PCR analysis for hypertrophic markers, all of which were increased in MHC-Cre and MHC-Cre/FloxDNMEF2 mice subjected to pressure overload.

Reactivation of fetal gene expression is a hallmark of pathological hypertrophy and heart failure, and therefore the expression levels of a number of fetal genes were determined. Transcripts for nppa (atrial natriuretic factor), nppb (brain natriuretic peptide), myh7 (beta-myosin heavy chain) and acta1 (alpha-skeletal actin) were all strongly activated after TAC with no obvious difference between the two experimental groups (Fig. 3C). Overall, our pressure overload regimen induced pathological cardiac hypertrophy and dysfunction, which was similar when MEF2 activity was genetically attenuated. Heart geometry and function was also analyzed by noninvasive echocardiography after TAC (Fig. 4A).

In agreement with the increased HW/BW and HW/TL ratios, thickening of ventricular walls was evident in MHC-Cre mice, as left ventricular posterior wall thickness at diastole (LVPWd) amounted to 0.98 ± 0.05 mm for MHC-Cre TAC compared to 0.75 ± 0.05 mm for MHC-Cre sham mice ($p<0.05$, Table 1). MHC-Cre/FloxDN-MEF2 mice, in contrary, displayed signs of wall thinning instead of thickening after induction of pressure overload. During systole, both intraventricular septal wall thickness (IVS) and LVPW are significantly decreased in MHC-Cre/FloxDN-MEF2 TAC mice (1.08 ± 0.05 mm and 1.10 ± 0.05 mm for IVSs and LVPWs, respectively) compared to MHC-Cre TAC mice (1.41 ± 0.08 mm and 1.32 ± 0.05 mm for IVSs and LVPWs, respectively, $p<0.05$). Geometric changes of the heart were accompanied by an impaired cardiac function in MHC-Cre/FloxDN-MEF2 after TAC, as both fractional shortening (FS) and ejection fraction (EF) were significantly lower (18 ± 3% and 37 ± 5% for FS and EF, respectively) compared to MHC-Cre/FloxDN-MEF2 sham mice (32 ± 3% and 61 ± 4% for FS and EF, respectively, $p<0.05$, Table 1, Fig. 4B and C). Overall, these results indicate that inhibition of MEF2 activity does noprevent the development of cardiac hypertrophy and heart failure during pressure overload, and suggests accelerated adverse adaptation to pressure overload.

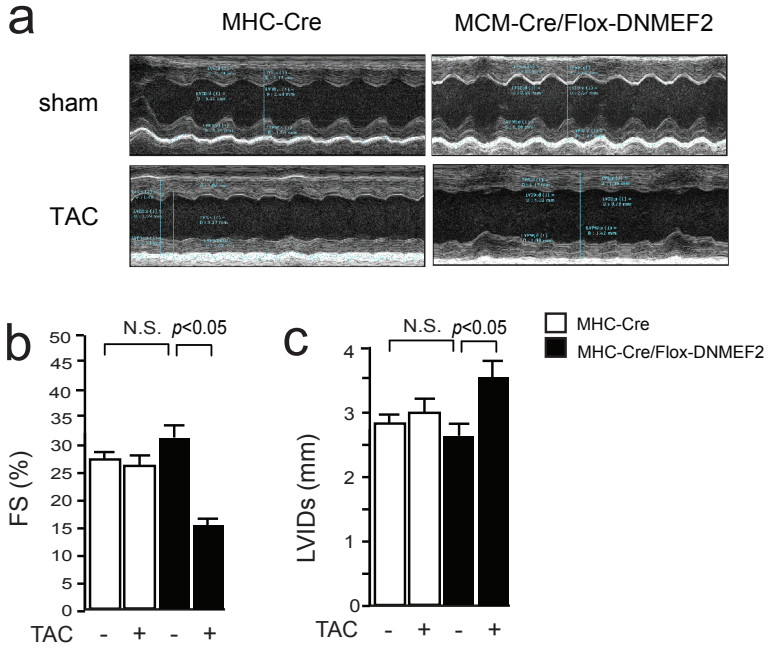

Figure 4. Inhibition of MEF2 accelerates pressure overload induced cardiac dysfunction. (a) Representative M-mode echocardiography images of MHC-Cre and MHC-Cre/Flox-DNMEF2 mice 5 weeks after TAC or sham surgery. (b) Fractional shortening (FS) and (c) ejection fraction (EF) indicate left ventricular dysfunction MHC-Cre/FloxDNMEF2 mice after TAC.

Table 1.

Echocardiographic characteristics in MHC-Cre and MHC-Cre/Flox-DN-MEF2 mice after sham operation and after transverse aortic constriction (TAC).

	Sham		TAC	
	MHC-Cre	*MHC-Cre/Flox-DN-MEF2*	*MHC-Cre*	*MHC-Cre/Flox-DN-MEF2*
n	5	5	8	8
BW, g	30.1 ± 3.8	33.8 ± 2.3	30.6 ± 2.2	25.6 ± 1.7
IVSs, mm	1.13 ± 0.09	1.32 ± 0.08	1.41 ± 0.08	1.08 ± 0.05 †
IVSd, mm	0.83 ± 0.06	0.92 ± 0.06	1.01 ± 0.05	0.84 ± 0.05
LVPWs, mm	1.15 ± 0.09	1.21 ± 0.04	1.32 ± 0.05	1.10 ± 0.05 †
LVPWd, mm	0.75 ± 0.05	0.85 ± 0.02	0.98 ± 0.05 *	0.87 ± 0.05
ESD, mm	2.89 ± 0.15	2.60 ± 0.20	3.00 ± 0.29	3.44 ± 0.18
EDD, mm	3.97 ± 0.13	3.82 ± 0.17	4.01 ± 0.24	4.16 ± 0.11
FS, %	27 ± 2	32 ± 3	27 ± 4	18 ± 3 *
EF, %	54 ± 4	61 ± 4	51 ± 6	37 ± 5 *
AoPg, mm Hg	3 ± 1	3 ± 1	48 ± 3 *	42 ± 2 *

Data are expressed as mean ± SEM. * Indicates $p<0.05$ vs. corresponding sham group. † Indicates $p<0.05$ vs. MHC-Cre TAC. AoPg = aortic pressure gradient; BW = body weight; EDD = end-diastolic diameter; EF = ejection fraction; ESD = end-systolic diameter; FS = left ventricular fractional shortening; IVS = intraventricular septal wall thickness; LVPW = left ventricular posterior wall thickness, TAC, transverse aortic constriction.

Inhibition of MEF2 during pressure overload causes mitochondrial defects.

Cardiac hypertrophy is thought to constitute a compensatory reaction to match the increased workload imposed upon the heart (14). In this compensation process mitochondrial energy supply should be able to match increased energy demand (15). During pathological hypertrophy, mitochondrial adaptation is inadequate, which may be a contributing factor to cardiac decompensation (15). Defects of the mitochondrial respiratory chain are an important, but poorly understood, cause of heart failure (16). Endocardial biopsies from patients with idiopathic hypertrophic cardiomyopathy showed a remarkable decrease in activity of either complex I, or complex IV, or both, relative to complex II + III activity (16).

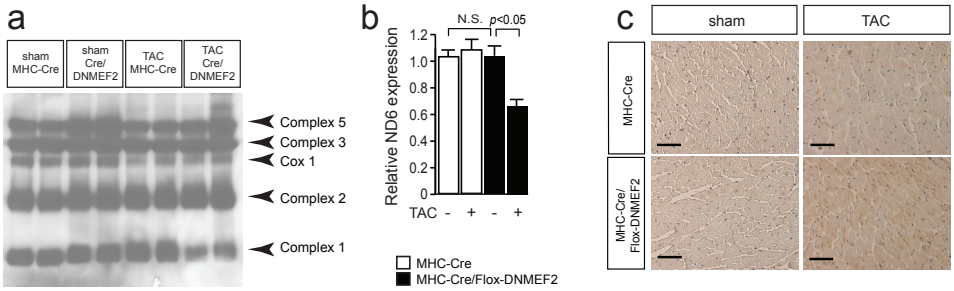

Figure 5. Inhibition of MEF2 during pressure overload causes mitochondrial defects. (a) western blot analysis using a mixture of monoclonal antibodies directed against various proteins in complexes of the electron transport chain (ETC), showing decreased expression of NADH dehydrogenase subunit 6 (ND6). (b) Real-time PCR analysis confirmed a significant decrease in mRNA levels of ND6 in MHC-Cre/FloxDNMEF2 compared to MHC-Cre after TAC. (c) Representative histological images of hearts of indicated genotypes (bar 0.2 mm) using 8-hydroxy-2'-deoxyguanosine (8-OHDG) as a marker for free radical DNA damage. Pressure overload elevated oxidative damage in both groups, with MHC-Cre/FloxDNMEF2 mice displaying more oxidative damage than MHC-Cre after TAC. Sham operated mice showed low amounts of 8-OHDG- positive nuclei.

As MEF2 is known to regulate the expression of genes involved in energy metabolism and of several nuclear encoded mitochondrial genes (REFs), we hypothesized that the accelerated decompensation observed in pressure overloaded MHC-Cre/FloxDN-MEF2 mice may be related to impaired mitochondrial adaptation. Using a mixture of monoclonal antibodies directed against various proteins in complexes of the electron transport chain (ETC), we found a specific decrease in expression of NADH dehydrogenase subunit 6 (ND6), part of mitochondrial complex 1, in MHC-Cre/FloxDN-MEF2 mice during pressure overload compared to MHC-Cre mice (Fig. 5A). Real-time PCR analyses confirmed a significant decrease in ND6 transcript abundance in MHC-Cre/FloxDN-MEF2 compared to MHC-Cre after TAC (Fig. 5B).

Mutations in ND6 have been shown to result in complex I dysfunction, provoking overproduction of ROS (17). To test whether the impaired expression of ND6 in pressure overloaded MHC-Cre/FloxDN-MEF2 mice may also cause excessive ROS production, we evaluated a downstream marker for oxidative stress related damage. The myocardium of all experimental genotypes were stained for 8-hydroxy-2'-deoxyguanosine (8-OHDG), a marker for free radical DNA damage. As expected, sham operated mice showed a very low number of 8-OHDG-positive nuclei (Fig. 5C).

In contrast, pressure overload dramatically elevated the number of 8-OHDG-positive nuclei in both groups, with MHC-Cre/FloxDN-MEF2 mice displaying more evidence of nuclear oxidative damage than pressure overloaded MHC-Cre mice (Fig. 5C).

Conclusively, these data directly demonstrate that MHC-Cre/Flox-DN-MEF2 mice, like their control counterparts, at baseline have no signs of oxidative stress, but dis-

play significantly more production of ROS and oxidative stress-induced damage following pressure overload compared to control mice. Moreover, these data also indicate that in MHC-Cre/Flox-DN-MEF2 mice TAC provokes excessive oxidative stress, damages crucial structures in the heart, and promotes adverse cardiac remodeling.

Inhibition of MEF2 during pressure overload increases ROS induced apoptosis in cardiomyocytes

A number of candidate pathological events have been identified for cardiac decompensation and heart failure, including a relative decrease in myocardial vascularization resulting in oxidative stress. Oxidative stress can become an additional physiological stressor for hemodynamically overloaded cardiomyocytes and can ultimately overwhelm protective cell survival pathways and result in apoptotic cardiomyocyte dropout with replacement fibrosis. Apoptotic loss of myocardium itself can increase hemodynamic stress through ventricular dilation and wall thinning and is therefore hypothesized to play an important role in the downward functional spiral that ultimately leads to overt heart failure.

To determine whether the increased ROS production in the MHC-Cre/FloxDN-MEF2 mice during pressure overload directly leads to myocyte loss, primary rat mocytes were either infected with AdGFP or Ad-DN-MEF2 for 24 hrs, stained with Annexin-V-PE to detect early loss of apoptotic-associated alterations in membrane asymmetry of phospholipids, and subjected to flow cytometry (Fig. 6A). H2O2 treatment induced apoptosis in the primary rat myocytes demonstrating the sensitivity of these cells to ROS induced apoptosis. No increase in the proportion of Annexin-V-PE positive cells was detected in H2O2-treated AdGFP-infected cells compared to H2O2-treated noninfected cells. In contrast, Ad-DN-MEF2 infected cells displayed a doubling in the proportion of Annexin-V-PE positive cells compared to control conditions (Fig. 6B).

ROS induced apoptosis leads to cleavage of PARP as a downstream target of the caspase pathway. Infecting primary rat myocytes with Ad-DN-MEF2 leads to an increase in cleaved PARP without the addition of H202, while Ad-GFP infection did not result in increased PARP cleavage only after co-stimuli with H202 (Fig. 6C). This clearly indicates than inhibition of MEF2 in myocytes induces apoptosis, probably via disruption of mitochondrial function eventually leading to the accumulation of ROS and the subsequent myocyte loss. Next, to more firmly confirm the apoptotic findings, we performed TUNEL labeling on sham and TAC subjected MHC-Cre and MHC-Cre/Flox-DNMEF2 hearts, and co-stained with phalloidin and DAPI to distinguish the cardiac cell types. Figure 6D demonstrates a representative confocal image of a merged TUNEL/phalloidin/DAPI positive cardiac myocyte. A very low incidence of TUNEL-positive cardiac myocytes was detectable in both sham-operated groups, a slight increase in TAC MHC-Cre hearts, and a substantially higher incidence in TAC MHC-Cre/Flox-DNMEF2 hearts (Figure 6E).

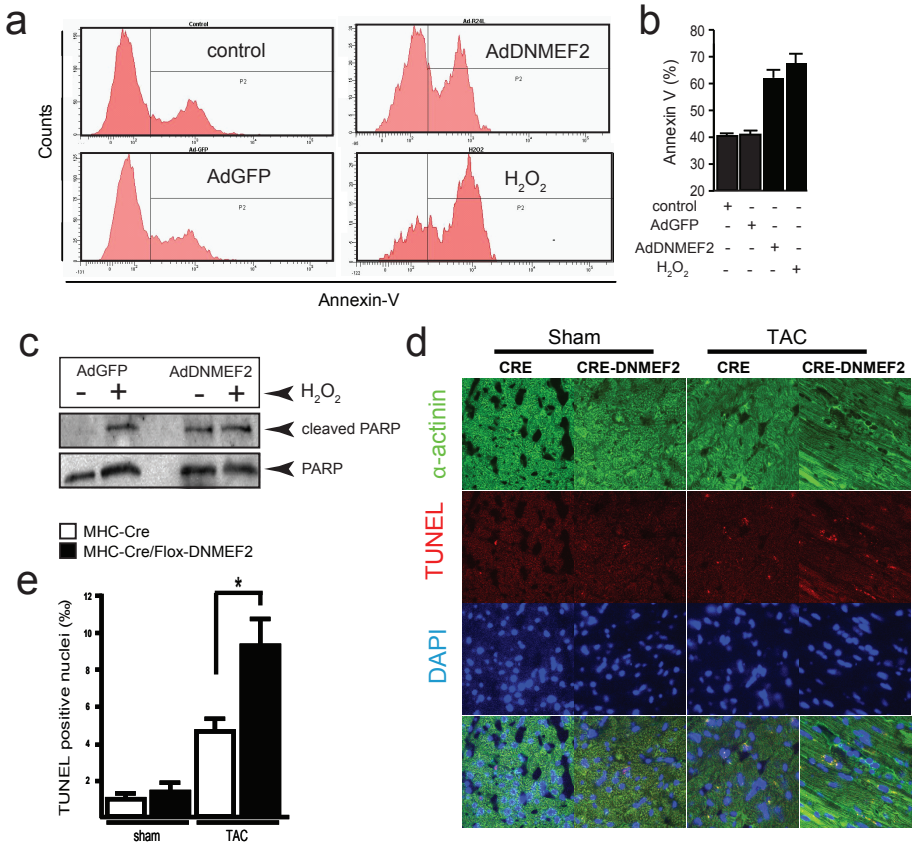

Figure 6. Inhibition of MEF2 results in ROS induced apoptosis apoptosis during pressure overload. (a) Representative pictures from flow cytometry experiments on primary rat cardiomyocytes, infected either with AdGFP, Ad-R24L or treated with H2O2 (500μM for 3h). (b) Average of the percentage AnnexinV-PE positive population is shown in the bargraph. Significantly more apoptotic cells were found after infection with Ad-R24L or after treatment with H2O2 as a positive controle (n=4 independent experiments per condition). (c) Western blot analysis using anti-Cleaved PARP and anti-PARP antibodies on lysates of isolated primary rat myocytes infected either with AdGFP or Ad-R24L and (un)treated with H2O2 (500μM for 3h) , showing increased cleaved PARP without the addition of H202, while Ad-GFP infection did not result in increased PARP cleavage only after co-stimuli with H202 . (d) Representative image of TUNEL labeling of MHC-Cre and MHC-Cre/Flox-DNMEF2 mice 5 weeks after TAC or sham surgery. (e) Bar graph indicates mean±SEM of the percentage of TUNEL positive cardiomyocytes in hearts of MHC-Cre and MHC-Cre/Flox-DNMEF2 mice subjected to sham or TAC surgery (n=3 per group), showing enhanced apoptosis in MHC-Cre/Flox-DNMEF2 hearts subjected to pressure overload. N.S., not significant; * indicates $p<0.05$.

DISCUSSION

Earlier work has demonstrated that MEF2 is involved in the development of postnatal heart disease. Although MEF2 was believed to be a prohypertrophic transcription factor, our recent data has demonstrated that MEF2 activation is more likely involved in provoking cardiac dilation instead of hypertrophy (9,10). It was, however, unknown if the heart is able to withstand stress induced by a pathophysiological trigger, such as pressure overload, when MEF2 transciptional activity is inhibited.

The results of this study demonstrate a protective role for MEF2 transcription factors in the response of the heart to pressure overload related to their role in adapting energy metabolism in the stressed myocardium. As determined by noninvasive echocardiography analysis, it was strikingly to notice a deterioration of cardiac function in mice expressing DN-MEF2 after TAC. Although histological analysis did not indicate any significant differences in cardiac remodeling between MHC-Cre/FloxDN-MEF2 and MHC-Cre animals 5 weeks after TAC, MHC-Cre/FloxDN-MEF2 mice displayed signs of wall thinning instead of thickening after induction of pressure overload. One could hypothesize that this difference in wall thickness is the result of inhibition of the hypertrophic response in MHC-Cre/FloxDN-MEF2 TAC mice, but this is unlikely with regard to the overall increase in heart size and weight in both groups after TAC. Furthermore, one would expect preserved cardiac function in MHC-Cre/FloxDN-MEF2 TAC mice if the hypertrophic response would have been inhibited, as wall thicknesses in these mice were comparable to sham control mice.

To characterize this phenomenon, we assessed whether changes in mitochondrial adaptation during pressure overload, since MEF2 has been linked to regulate the expression of genes involved in energy metabolism and of several nuclear encoded mitochondrial genes, could explain the worsened cardiac function in MHC-Cre/FloxDN-MEF2 mice. The progression to heart failure is associated with a decrease in the activity of mitochondrial respiratory pathways leading to diminished capacity for ATP production (15,16). Deficiencies of the mitochondrial respiratory chain are important since reduced capacity for energy generation leads to dysregulation of processes for cardiac pump function. Interestingly, MHC-Cre/FloxDN-MEF2 mice showed a significant decrease in ND6 expression during pressure overload compared to MHC-Cre mice. Being a subunit of the mitochondrial NADH ubiquinone oxireductase (Complex I), ND6 has been postulated to contribute in proton translocation (18). Absence of ND6 has been shown to result in failure to assemble the Complex I membrane arm that is essential for proton translocation (18,19).

Taken together, the basal decrease in ND6 expression may affect mitochondrial homeostasis in MHC-Cre/FloxDN-MEF2 mice, making these animals predisposed to development of cardiac decompensation. Despite its importance, the role of ND6 in the development of cardiac failure is poorly understood and has not been investigated in a cardiac setting. Nevertheless, mutations in ND6 induce a decrease in Complex I activity

and the respiratory rate, however, the energy levels did not change in cells harboring these mutations (20). Although different mutations have slightly different affects on Complex I activity, it was shown that Complex II-driven ATP generation was unaffected by the impaired Complex I activity due to the ND6 mutations (21). In addition, a compensatory mechanism such as, elevation of Complex II activity and mtDNA content was observed in leukocytes harboring ND6 mutations (22). Therefore ATP generation potential is unlikely to be affected in MHC-Cre/FloxDN-MEF2 mice after TAC.

Although ROS are generated as by-products in the mitochondria during normal oxidative metabolism, ND6 deficiencies cause Complex I dysfunction that lead to overproduction of ROS (23). Biochemical studies have shown that Complex I dysfunction, due to ND6 mutations, induces cytotoxicity that is not mediated by reduction in oxidative phosphorylation, but by increased production of ROS (24). Indeed, using a marker for free radical DNA damage, 8-hydroxy-2'-deoxyguanosine (8-OHDG), we show that MHC-Cre/FloxDN-MEF2 mice display more oxidative damage in the heart than MHC-Cre after TAC. It has been well documented that ROS accumulation leads to progressive cell death. Moreover, alterations in Complex I function due to ND6 mutations render the cells more susceptible to apoptosis and sensitive to diverse apoptotic stimuli than wild type cells (25-27). Furthermore, cells with an altered ND6 have increased cytochrome c release into the cytosol indicating that mitochondria are involved in the activation of the apoptotic cascade (28). Indeed, invitro analysis of primary rat myocytes infected with Ad-DN-MEF2 showed to have increased levels of cleaved PARP and an increase in apoptosis as postulated by the number of Annexin-V-PE positive cells through flow cyotmetry. These data were confirmed by increased TUNEL positive staining of cardiac muscle in vivo. These data indicated that, being a strong stimulus for apoptosis, pressure overload resulted in higher incidence of apoptosis in myocytes after inhibition of MEF2 explaining the worsened cardiac function in MHC-Cre/FloxDN-MEF2 mice.

The results of this study are in sharp contrast with a previous report from our group, where reduced MEF2 transcriptional activity in mice overexpressing an activated form of calcineurin in the heart resulted in inhibition of maladaptive cardiac remodeling (10). Pressure overload and the associated mechanical stress, however, triggers the release and/or expression of several growth factors and hormones, including endothelin 1, angiotensin II, insulin like growth factor, transforming growth factor-β, fibroblast growth factor, and cardiotrophin-1, resulting in the activation of a multiplicity of intracellular signaling cascades besides calcineurin signaling (2,29,30). At least three signaling pathways besides calcineurin can impinge upon MEF2 factors, including p38 MAPK, diverse forms of calcium/calmodulin-dependent protein kinase (CaMK), and certain forms of protein kinase C (2,5,6). Accordingly, nature and number of MEF2 target genes downstream of cardiac calcineurin activation may differ substantially from those target genes activated in the setting of pressure overload.

We postulate that in the setting of an active calcineurin transgene, any adverse metabolic effects may have a minimal role, if any, compared to the more complex setting of biomechanical stress.

Overall, these results indicate that inhibition of MEF2 activity does not prevent the development of cardiac hypertrophy and heart failure during pressure overload, and suggests accelerated adverse adaptation to pressure overload when MEF2 transcriptional activity was inhibited.

ACKNOWLEDGEMENTS

We are grateful to Martin Taube and Jeroen Korving for technical assistance. This work was supported by grants 912-04-054, 912-04-017 and a VIDI award 917-863-72 from the Netherlands Organization for Health Research and Development; grant NHS2003B258 from the Netherlands Heart Foundation; and by the European Union Contract No. LSHM-CT-2005-018833/EUGeneHeart (to L.J.D.W.).

REFERENCES

1. Frey N, Olson EN. Cardiac hypertrophy: the good, the bad, and the ugly. Annu Rev Physiol 2003;65:45-79.
2. Heineke J, Molkentin JD. Regulation of cardiac hypertrophy by intracellular signalling pathways. Nat Rev Mol Cell Biol 2006;7:589-600.
3. Passier R, Zeng H, Frey N, et al. CaM kinase signaling induces cardiac hypertrophy and activates the MEF2 transcription factor in vivo. J Clin Invest 2000;105:1395-406.
4. Naya FJ, Black BL, Wu H, et al. Mitochondrial deficiency and cardiac sudden death in mice lacking the MEF2A transcription factor. Nat Med 2002;8:1303-9.
5. McKinsey TA, Olson EN. Toward transcriptional therapies for the failing heart: chemical screens to modulate genes. J Clin Invest 2005;115:538-46.
6. Frey N, Katus HA, Olson EN, Hill JA. Hypertrophy of the heart: a new therapeutic target? Circulation 2004;109:1580-9.
7. Nadruz W, Jr., Kobarg CB, Constancio SS, Corat PD, Franchini KG. Load-induced transcriptional activation of c-jun in rat myocardium: regulation by myocyte enhancer factor 2. Circ Res 2003;92:243-51.
8. Molkentin JD, Markham BE. Myocyte-specific enhancer-binding factor (MEF-2) regulates alpha-cardiac myosin heavy chain gene expression in vitro and in vivo. J Biol Chem 1993;268:19512-20.
9. Xu J, Gong NL, Bodi I, Aronow BJ, Backx PH, Molkentin JD. Myocyte enhancer factors 2A and 2C induce dilated cardiomyopathy in transgenic mice. J Biol Chem 2006;281:9152-62.
10. van Oort RJ, van Rooij E, Bourajjaj M, et al. MEF2 activates a genetic program promoting chamber dilation and contractile dysfunction in calcineurin-induced heart failure. Circulation 2006;114:298-308.
11. Agah R, Frenkel PA, French BA, Michael LH, Overbeek PA, Schneider MD. Gene recombination in postmitotic cells. Targeted expression of Cre recombinase provokes cardiac-restricted, site-specific rearrangement in adult ventricular muscle in vivo. J Clin Invest 1997;100:169-79.
12. Rockman HA, Ross RS, Harris AN, et al. Segregation of atrial-specific and inducible expression of an atrial natriuretic factor transgene in an in vivo murine model of cardiac hypertrophy. Proc Natl Acad Sci U S A 1991;88:8277-81.
13. van Empel VP, Bertrand AT, van der Nagel R, et al. Downregulation of apoptosis-inducing factor in harlequin mutant mice sensitizes the myocardium to oxidative stress-related cell death and pressure overload-induced decompensation. Circ Res 2005;96:e92-e101.
14. Cooper Gt. Basic determinants of myocardial hypertrophy: a review of molecular mechanisms. Annu Rev Med 1997;48:13-23.
15. Goffart S, von Kleist-Retzow JC, Wiesner RJ. Regulation of mitochondrial proliferation in the heart: power-plant failure contributes to cardiac failure in hypertrophy. Cardiovasc Res 2004;64:198-207.
16. Zeviani M, Mariotti C, Antozzi C, Fratta GM, Rustin P, Prelle A. OXPHOS defects and mitochondrial DNA mutations in cardiomyopathy. Muscle Nerve 1995;3:S170-4
17. Ishikawa K, Takenaga K, Akimoto M, et al. ROS-generating mitochondrial DNA mutations can regulate tumor cell metastasis. Science 2008;320:661-4.
18. Bai Y, Attardi G. The mtDNA-encoded ND6 subunit of mitochondrial NADH dehydrogenase is essential for the assembly of the membrane arm and the respiratory function of the enzyme. Embo J 1998;17:4848-58.

19. Chomyn A. Mitochondrial genetic control of assembly and function of complex I in mammalian cells. J Bioenerg Biomembr 2001;33:251-7.
20. Yen MY, Lee JF, Liu JH, Wei YH. Energy charge is not decreased in lymphocytes of patients with Leber's hereditary optic neuropathy with the 11,778 mutation. J Neuroophthalmol 1998;18:84-5.
21. Baracca A, Solaini G, Sgarbi G, et al. Severe impairment of complex I-driven adenosine triphosphate synthesis in leber hereditary optic neuropathy cybrids. Arch Neurol 2005;62:730-6.
22. Yen MY, Lee HC, Liu JH, Wei YH. Compensatory elevation of complex II activity in Leber's hereditary optic neuropathy. Br J Ophthalmol 1996;80:78-81.
23. Robinson BH. Human complex I deficiency: clinical spectrum and involvement of oxygen free radicals in the pathogenicity of the defect. Biochim Biophys Acta 1998;1364:271-86.
24. Barrientos A, Moraes CT. Titrating the effects of mitochondrial complex I impairment in the cell physiology. J Biol Chem 1999;274:16188-97.
25. Battisti C, Formichi P, Cardaioli E, et al. Cell response to oxidative stress induced apoptosis in patients with Leber's hereditary optic neuropathy. J Neurol Neurosurg Psychiatry 2004;75:1731-6.
26. Danielson SR, Wong A, Carelli V, Martinuzzi A, Schapira AH, Cortopassi GA. Cells bearing mutations causing Leber's hereditary optic neuropathy are sensitized to Fas-Induced apoptosis. J Biol Chem 2002;277:5810-5.
27. Zanna C, Ghelli A, Porcelli AM, Martinuzzi A, Carelli V, Rugolo M. Caspase-independent death of Leber's hereditary optic neuropathy cybrids is driven by energetic failure and mediated by AIF and Endonuclease G. Apoptosis 2005;10:997-1007.
28. Ghelli A, Zanna C, Porcelli AM, et al. Leber's hereditary optic neuropathy (LHON) pathogenic mutations induce mitochondrial-dependent apoptotic death in transmitochondrial cells incubated with galactose medium. J Biol Chem 2003;278:4145-50.
29. Ruwhof C, van der Laarse A. Mechanical stress-induced cardiac hypertrophy: mechanisms and signal transduction pathways. Cardiovasc Res 2000;47:23-37.
30. Brancaccio M, Fratta L, Notte A, et al. Melusin, a muscle-specific integrin beta1-interacting protein, is required to prevent cardiac failure in response to chronic pressure overload. Nat Med 2003;9:68-75.

chapter

CHAPTER 6

General Discussion

Hamid el Azzouzi

Perturbations in myocardial energy metabolism play a role in the development of cardiomyopathy.

Despite major therapeutic advances, heart failure (HF) remains a leading cause of morbidity and mortality world wide, which rivals or exceeds that of many forms of cancers. Numerous studies have identified decreased cardiac energy levels and flux as a consistent feature of HF, and have focused considerable attention on metabolic modulations as a therapeutic modality for HF [1, 2]. The mammalian heart demonstrates tremendous energy source plasticity depending on the developmental stage, nutritional status or dietary composition, and cardiac demands. Because of limited oxygen and fatty acid availability, the fetal heart relies primarily on anaerobic glucose utilization pathways. Concomitant with the sudden increase in cardiac work and the abundance of fatty acids, the post-natal heart shows an increased reliance on mitochondrial fatty acid oxidation (FAO). Where fatty acid oxidation is the primary source of energy in the postnatal heart, impaired fatty acid oxidation and a shift to reliance on glucose metabolism are hallmarks of myocardial diseases such as cardiac hypertrophy and congestive heart failure [3] Although, altered metabolism was considered to be a byproduct of these pathological states, evidence is emerging that metabolic abnormalities contribute to the pathogenesis of cardiac disease. Several genetic studies have demonstrated that mitochondrial DNA disorders resulting in global impairment of mitochondrial respiratory function are associated with cardiac defects, including hypertrophic cardiomyopathy and conduction defects [4].

PPAR subtype specific target gene analysis reveal igf-1 as a downstream effector of PPARα anti-apoptotic signaling in the myocardium.

The peroxisome proliferator-activated receptor (PPAR) family of nuclear receptor transcription factors has been shown to regulate cardiac fuel metabolism at the gene expression level. Because of their responsiveness to fatty acid ligands and their regulation of the expression of genes involved in cellular lipid metabolism, they are unique in their ability to serve as transducers of developmental, physiological, and dietary cues to the control of cardiac fuel metabolism. Three different PPAR isotypes have been identified in mammals namely; PPARα, PPARβ/δ and PPARγ. Although, PPARs show high levels of homologies at the protein level, they exert different functions relying on differentially distribution in distinct tissues, isoform specific phosphorylation, selective interactions with their specific ligand and co-activators, and, likely, isoform-selective target gene activation.

As outlined in chapter 2, the use of animal models has indicated important roles for PPAR isoforms in cardiac pathology. Despite their important role in HF, only a few studies have sought to mutually compare PPAR subtype-specific activation of endogenous genes in the heart [5]. The disappointing results of recent clinical trials such as the DREAM (Diabetes REduction Assessment Medication) and the ADOPT (A Dia-

betes Outcome Progression Trial) trails have pointed out the need for the understanding of PPAR subtype-specific activation of endogenous genes in the heart. Due to there insufficient specificity, appliance of synthetic ligands have hampered PPAR subtype-specific target genes analyses [6].

Combining an in vitro system and siRNA based specific knockdown of each of the PPAR isoforms in cardiomyocytes, we show the differential and co-regulation of gene expression among the three PPAR isoforms in the cardiac muscle (Chapter2). This approach has yielded a significant amount of interesting PPAR subtype-specific unknown target genes in the cardiomyocyte and depicted the number and overlap between the target genes of the three PPAR isoforms. Furthermore, PPARγ seems to have a considerably less target genes in the heart compared to PPARα and PPARβ/δ. Indeed, it was shown by Gilde and colleagues that cardiomyocytes express only functional amounts of PPARα and PPARβ/δ, but not PPARγ [7].

Since cardiomyocyte apoptosis plays an important role in the depressed cardiac function after global cardiac Ischemia/reperfusion injury, it was interestingly to see that PPARα had a profound role in the differential regulation of genes involved in apoptosis in the cardiomyocyte compared to PPARβ/δ and PPARγ. Although an emerging body of evidence suggests that PPARα agonists protect the heart from apoptosis [8], the mechanisms involved in this cardioprotection were not well understood. As Igf-1 has been shown to decrease myocyte apoptosis after myocardial infarction in mice [9], it was interesting to demonstrate that administration of Wy-14643 resulted in upregulation of igf-1 expression and subsequent protection against ischemia/reperfusion induced apoptosis. The two main IGF-1 signaling pathways that are well described comprise the activation of phosphatidylinositol 3-kinase (PI 3-kinase) pathway and the MAP-kinase pathway [9]. Where the latter has been linked to metabolism, cell growth and proliferation, it is the phosphatidylinositol 3-kinase (PI 3-kinase) pathway that promotes survival of cardiac myocytes both in vitro and in vivo [10, 11]. Moreover, increased cardiomocyte loss during pressure overload in PPARKO mice was accompanied with a decreased expression of igf-1 in PPARKO compared to WT.

Interaction with MEK causes inhibition of PPARα through nuclear export.

Although our data suggest an important role for the anti-apoptotic properties of PPARα signaling in the heart muscle, the metabolic transition during pressure overload is accompanied with reduced nuclear levels of PPARα. In chapter 3 we analyzed the mechanisms that control the activity of PPARα, through inhibition, at the onset of heart failure. Activation of the MEK1 pathway resulted in a dramatic decrease in transcriptional activity of PPARα, indicating an upstream regulation by MAPK signaling. Using MKP1 (MAPK phosphatases) to inhibit ERK1/2 activation did not change the inhibitory effect of MEK1 on the transcriptional activity of PPARα indicating an insignificant role for ERK1/2. In

contrast to our findings, Shalev and colleagues showed an increased PPARα activity after treatment with insulin in hepatocytes. Herein, this increase is subscribed to an insulin mediated ERK1/2-MAPK activity, since co-transfection of MKP1 with PPARα resulted in a decrease in ligand inducible reporter activity [12]. Although the different findings could reside in the use of hepatocytes and the use of insulin as a stimulus to activate the MAPK pathway, it is interesting to note that although the phosphorylation sites are in the A/B ligand-independent domain of PPARα (AF-1), insulin treatment had only an effect on the ligand-dependent domain (AF-2). Furthermore, activity of heterologous PPARα A/B-Gal4 construct is not affected by the MEK inhibitor PD98059; also, introducing mutations into these constructs had no effect on the A/B domain [13].

Indeed we show that MEK 1/2 induced inhibition is phosphorylation independent and that the inhibitory effect is mediated by MEK1/2 through a mechanism involving direct binding to PPARα and subsequent export out of the nucleus. Many agents that induce cardiac hypertrophy can also activate the MEK1/2 pathway [14]. In fact, Mek1 transgenic animals showed ventricular concentric hypertrophy with a 50-54% increase in septal thickness and left ventricular posterior wall thickness without signs of cardiomyopathy or lethality resembling a phenotype of physiological hypertrophy. Interestingly, mice subjected to cage wheel exercise indeed showed an increase in MEK1/2 activity and also an impaired PPARα activity compared to sedentary animals indicating a minor role for PPARα during physiological hypertrophy. The fact that PPARβ/δ is unaffected by MEK1/2 activation suggests a more prominent role for PPARβ/δ during physiological hypertrophy.

Taken together, although we show that PPARα signaling has a beneficial effect during pressure overload induced hypertrophy (chapter2), other mechanisms might be involved during physiological hypertrophy that render the cardiomyocyte less dependent on PPARα signaling.

Role of PPARβ/δ signaling in cardiac remodeling.

Whereas PPARα and PPARγ have been studied extensively, relatively little is known about PPARβ/δ. In contrast, PPARβ/δ shows an almost ubiquitous tissue expression with an almost 50-fold higher expression level in the heart compared to PPARα or PPARγ [7]. Even though, it was suggested to have a housekeeping role [15], recent studies have now indicated its basic function relates to transcriptional programs which enhance fatty acid catabolism and energy uncoupling. PPARβ/δ deficiency in mouse models led to multiple developmental and metabolic abnormalities [16, 17] and disrupted fatty acid oxidation in skeletal muscle cells [18, 19]. To investigate whether PPARβ/δ gene activation is required for normal myocardial homeostasis and to bypass the early embryonic lethality of PPARβ/δ-null mice, we first provoked deletion of a floxed PPARβ/δ (PPARdF/F) allele using a cardiac-specific tamoxifen-inducible Cre recombinase protein. Strikingly, within

5 days of start of tamoxifen treatment, αMHC-MCM/PPARdF/F mice displayed a weak condition and inactivity. Indeed, echocardiography demonstrated a rapid and significant decline in cardiac function, indicated by a 50% decrease in cardiac contraction, compared to vehicle treated αMHC-MCM/PPARdF/F mice. As measurements of heart-weight-to-body-weight (HW/BW) ratios indicated an increase in cardiac mass for tamoxifen-treated αMHC-MCM/PPARdF/F mice, cardiac tissue also revealed an intricate phenotype with hypertrophied myofibers and myocyte disarray.

These data indicate that PPARβ/δ depletion provoke progressive functional and geometrical deterioration. Moreover, deletion of PPARβ/δ in adult mice induced potent re-activation of embryonic genes as consistent with a heart failure phenotype.

MEF2 as a co-regulator of PPARα.

As transcriptional regulation is vital for homeostasis and adaptation of physiological processes to external signals, transcriptional control of metabolism is conserved from simple prokaryotes to complex eukaryotes such as humans. Transcription factors, however, do not function alone and require co-regulators to modify and epigenetically remodel chromatin structure and form basal transcriptional complexes to allow transcriptional regulation. Next to well documented PPAR co-regulators such as CBP/p300 and PGC-1α, myocyte enhancer factor-2 (MEF2) has been documented to be involved in the transcriptional regulation of skeletal muscle metabolism [20]. Furthermore, it was shown that PGC-1α and PGC-1β can both drive a switch from glycolytic to oxidative fibers by co-activating the MEF2D transcription factor [21].

It was interesting to see that the basal expression of the mCPT1-luc construct, mediated by PPARα, was similar in several cell lines derived from different tissues but not in C2C12 myotubes. Using these myotubes, PPARα induced activation of mCPT1-luc was up to 38-fold compared to other cell lines [22]. The presence of myogenic proteins in C2C12 and the high induction of mCPT1 in response to PPARα activation indicated a mechanism of synergy between myogenic proteins and PPARα. Indeed we show in chapter 5 that PPARα and MEF2 synergistically induce expression of the mCPT1 gene, indicating a concurrence of myogenic and metabolic signals. Although many studies have implicated MEF2 as a downstream target for several hypertrophic signaling pathways in the heart, mice expressing a dominant negative form of MEF2 (DNMEF2) showed impaired cardiac function when subjected to pressure overload (chapter 5). Interestingly, transgenic expression of PGC-1β in skeletal muscle led to the co-activation of MEF2 and PPARα eventually resulting in mitochondrial biogenesis [20]. Although there was no difference in mitochondrial biogenesis (unpublished data), analysis of the mitochondrial respiratory chain showed that mice expressing DNMEF2 had a lower expression level of NADH dehydrogenase subunit 6 (ND6), during pressure overload compared to there WT counterpart.

Furthermore, the decreased ND6 expression eventually led to a distorted mitochondrial function thereby overproducing reactive oxygen species (ROS), rendering the cells susceptible to apoptosis.

While three PPAR isoforms are expressed in the heart muscle, the combined findings from our studies provide evidence that the individual PPAR isoforms have a unique role in the regulation of cardiac homeostasis. This unique function is furthermore substantiated by the fact that for example, the phenotype of PPARα null mice is distinct from PPARβ/δ mutant mice. Although PPAR share many aspects such as protein homology, we here provide for the first time an insight in isoform specific targetgenes in the cardiomyocte and consequently new mechanisms of PPAR function in the heart. In addition, we show that transcriptional co-regulators of PPAR have an important role in the indirect regulation of PPAR function. Further studies will be needed to study PPARs in cardiac as well as whole body energy homeostasis.

REFERENCES

1. Braissant, O., et al., Differential expression of peroxisome proliferator-activated receptors (PPARs): tissue distribution of PPAR-alpha, -beta, and -gamma in the adult rat. Endocrinology, 1996. 137(1): p. 354-66.
2. Brun, R.P., et al., Differential activation of adipogenesis by multiple PPAR isoforms. Genes Dev, 1996. 10(8): p. 974-84.
3. Sack, M.N., et al., A role for Sp and nuclear receptor transcription factors in a cardiac hypertrophic growth program. Proc Natl Acad Sci U S A, 1997. 94(12): p. 6438-43.
4. Tiemann, K., et al., Real-Time Contrast Echo Assessment of Myocardial Perfusion at Low Emission Power: First Experimental and Clinical Results Using Power Pulse Inversion Imaging. Echocardiography, 1999. 16(8): p. 799-809.
5. Nielsen, R., et al., Peroxisome proliferator-activated receptor subtype- and cell-type-specific activation of genomic target genes upon adenoviral transgene delivery. Mol Cell Biol, 2006. 26(15): p. 5698-714.
6. Seimandi, M., et al., Differential responses of PPARalpha, PPARdelta, and PPARgamma reporter cell lines to selective PPAR synthetic ligands. Anal Biochem, 2005. 344(1): p. 8-15.
7. Gilde, A.J., et al., Peroxisome proliferator-activated receptor (PPAR) alpha and PPARbeta/delta, but not PPARgamma, modulate the expression of genes involved in cardiac lipid metabolism. Circ Res, 2003. 92(5): p. 518-24.
8. Yeh, C.H., et al., Inhibition of NF-kappa B activation can attenuate ischemia/reperfusion-induced contractility impairment via decreasing cardiomyocytic proinflammatory gene up-regulation and matrix metalloproteinase expression. J Cardiovasc Pharmacol, 2005. 45(4): p. 301-9.
9. Liu, T., et al., Developing a strategy to define the effects of insulin-like growth factor-1 on gene expression profile in cardiomyocytes. Circ Res, 2001. 88(12): p. 1231-8.
10. Foncea, R., et al., Insulin-like growth factor-I rapidly activates multiple signal transduction pathways in cultured rat cardiac myocytes. J Biol Chem, 1997. 272(31): p. 19115-24.
11. Fujio, Y., et al., Akt promotes survival of cardiomyocytes in vitro and protects against ischemia-reperfusion injury in mouse heart. Circulation, 2000. 101(6): p. 660-7.
12. Shalev, A., et al., The peroxisome proliferator-activated receptor alpha is a phosphoprotein: regulation by insulin. Endocrinology, 1996. 137(10): p. 4499-502.
13. Jaaro, H., et al., Nuclear translocation of mitogen-activated protein kinase kinase (MEK1) in response to mitogenic stimulation. Proc Natl Acad Sci U S A, 1997. 94(8): p. 3742-7.
14. Bueno, O.F. and J.D. Molkentin, Involvement of extracellular signal-regulated kinases 1/2 in cardiac hypertrophy and cell death. Circ Res, 2002. 91(9): p. 776-81.
15. Kliewer, S.A., et al., Differential expression and activation of a family of murine peroxisome proliferator-activated receptors. Proc Natl Acad Sci U S A, 1994. 91(15): p. 7355-9.
16. Ding, G., et al., PPARdelta modulates lipopolysaccharide-induced TNFalpha inflammation signaling in cultured cardiomyocytes. J Mol Cell Cardiol, 2006. 40(6): p. 821-8.
17. Hasegawa, H., et al., Pioglitazone, a peroxisome proliferator-activated receptor gamma activator, ameliorates experimental autoimmune myocarditis by modulating Th1/Th2 balance. J Mol Cell Cardiol, 2005. 38(2): p. 257-65.
18. Finck, B.N., et al., A critical role for PPARalpha-mediated lipotoxicity in the pathogenesis of diabetic cardiomyopathy: modulation by dietary fat content. Proc Natl Acad Sci U S A, 2003. 100(3): p. 1226-31.

19. Finck, B.N. and D.P. Kelly, Peroxisome proliferator-activated receptor alpha (PPARalpha) signaling in the gene regulatory control of energy metabolism in the normal and diseased heart. J Mol Cell Cardiol, 2002. 34(10): p. 1249-57.
20. Arany, Z., et al., Transverse aortic constriction leads to accelerated heart failure in mice lacking PPAR-gamma coactivator 1alpha. Proc Natl Acad Sci U S A, 2006. 103(26): p. 10086-91.
21. Lin, J., et al., Peroxisome proliferator-activated receptor gamma coactivator 1beta (PGC-1beta), a novel PGC-1-related transcription coactivator associated with host cell factor. J Biol Chem, 2002. 277(3): p. 1645-8.
22. Baldan, A., et al., Functional interaction between peroxisome proliferator-activated receptors-alpha and Mef-2C on human carnitine palmitoyltransferase 1beta (CPT1beta) gene activation. Nucleic Acids Res, 2004. 32(16): p. 4742-9.

Samenvatting in het Nederlands

Hamid el Azzouzi

Samenvatting

Ondanks de verbeterde behandeling en preventie van cardiovasculaire aandoeningen, heeft hartfalen nog steeds een leidende rol in het aantal doodsoorzaken in de industrieele landen. Hartfalen is een aandoening waarbij het hart niet meer in staat is om voldoende bloed het lichaam in te pompen als gevolg van een reactie op stress signalen. Invloeden zoals chronische verhoogde bloeddruk , hartinfarct en genetische afwijkingen kunnen leiden tot groei van de individuele hartspiercel, dit wordt ookwel hypertrofie genoemd.

De groei van het hart lijkt in eerste instantie een aanpassing te zijn van het hart aan overbelasting, bijvoorbeeld vanwege een verhoogd bloedruk. Door een nog onbekende mechanisme resulteert hypertrofie, in een latere stadium, in dilatatie en uiteindelijk in hartfalen. Helaas, ondanks vele onderzoek is er niet veel bekend over de signalen en mechanisme dat hartfalen induceert. Voor de pompfunctie voorziet het hart zichzelf van energie door voornamelijk de oxidatie van langketenige vetzuren en, in mindere mate, door glucose oxidatie. Het is dan ook markant dat vele onderzoek heeft aangetoond dat gedurende hypertrofie er een verschuiving van energie substraat plaats vind in het hart, waarbij het hart voornamelijk glucose metaboliseerd voor zijn energie verbruik.

Geheel in de trend dat waargenomen wordt tijdens hypertrofie, lijkt deze metabole verschuiving op een neonatale conditie van het hart. Steeds meer raakt men ervan overtuigd dat deze verschuiving geen bijkomstigheid is maar ook bijdraagt aan de pathogenese van het hartfalen. Een belangrijke functie in de regulatie van metabolisme in het hart wordt vervuld door de PPAR famillie van nucleaire recpetoren. De PPAR famillie bestaat uit 3 isovormen, PPARα, PPARβ/δ en PPARγ. Zoals de meeste nucleaire recpetoren kunnen PPAR's door liganden geactiveerd worden om vervolgens verbindingen aan te gaan met andere eiwitten en zo expressie van specifieke genen te kunnen beïnvloeden. PPARα en PPARγ zijn naast vetzuur metabolisme en glucose homeostase ook bekend om hun regulatie van andere cellulaire processen zoals cel proliferatie, differentiatie, apoptosis en inflammatoire respons. Daarnaast lijkt hartspier beperkte deletie van PPARβ/δ te resulteren in vetzuur accumulatie, cardiale hypertrofie en hartfalen. Ondanks hun belangrijke rol in de homeostase van het hart, is de bijdrage door de individuele PPAR isovorm tijdens de progressie van hartfalen nog onbekend.

In hoofdstuk 2 worden PPAR isovorm-specifieke doelgroepgenen in de hartspiercel bepaald. Door middel van op siRNA gebaseerd technologie worden hartspier-cellijnen gemaakt die één specifieke PPAR isovorm missen, en in combinatie met microarray wordt het gehele genoom gescand ter identificatie van PPAR isovorm-specifieke doelgroepgenen. Naast vele onbekende isovorm-specifieke doelgroepgenen wordt er ook een beeld geschapen van de verschillen en overeenkomsten in gen regulatie tussen de drie PPAR isovormen. Interessant is het feit dat PPARα een duideljke anti-apoptostische profiel laat zien qua genregulatie.

Omdat apoptose een belangrijke rol heeft in hartfalen en eerdere studies hebben aangetoond dat PPARα activatie anti-apoptostische effecten heeft in het hart, wordt er een meachanisme onderzocht waarbij igf-1 een hoofdrol speelt. Inderdaad leidt activatie van PPARα zowel in-vitro als in-vivo tot verhoogd expressie van igf-1. Vervolgens laten we zien dat PPARα activatie tot apoptose verlaging leid in muizen harten onderworpen aan ishemia/reperfusie geïnduceerde schade en dat dit effect geheel wordt teniet gedaan in muizen harten die geen PPARα tot expressie brengen (PPARα knock-out). Histologische en hemodynamische analyses laten zien dat inductie van chronische overdruk belasting in PPARα knock-out geen verschil vertonen in hypertrofie met wildtype dieren. Echter, analyse van hart functie met echoacrdiografie, laat wel degelijk een verslechtering zien in hart contractie van PPARα knock-out dieren na overdruk belasting vergeleken met wildtype dieren. TUNEL analyse laat zien dat op cardiomyocyte niveau, het aantal apoptose gevallen zijn toegenomen in PPARα knock-out dieren na inductie van chronische overdruk belasting in vergelijking met wildtype dieren. Alle bevindigen bij elkaar laten, voor het eerst, een mechanisme zien waarbij PPARα activatie tot remming van celdood en verbetering van hartfunctie leidt.

Een kenmerk van groei van de hartspiercel is de activatie van een netwerk van stress geactiveerde signaal transductie, zoals de p38 mitogen-activated protein kinase (MAPK), c-Jun NH2-terminal kinase (JNK) en de extracellular signal-regulated kinase (ERK1/2) cascades. In hoofdstuk 3, wordt het effect van MEK1 signalering op PPARα onderzocht. Door gebruik te maken van een mCPT1-luciferase construct laten we zien dat activatie van MEK1 leidt tot remming van de transcriptionele activiteit van PPARα. Aangezien MEK1 activatie leidt tot fosforylatie van ERK1/2, hebben we gekeken of ERK1/2 PPARα activiteit remt door fosforylatie. Site-directed mutagenese van alle eventuele serine ERK1/2 fosforylatie residuen in PPARα, laat zien dat er geen verschil is in de MEK1 geïnduceerde inhibitie. Bovendien leidt inactivatie van ERK1/2 door MKP1(MAPK phosphatases), ook niet tot remming van MEK1 geïnduceerde inhibitie van de transcriptionele activiteit van PPARα. Naast de insignificante rol van ERK1/2, laten beide bevindingen zien dat MEK1 geïnduceerde inhibitie fosforylatie onafhankelijk is.

Naast de aanwezigheid van een CRS/CD domein in PPARα, dat interactie met MEK1 mogelijk maakt, lieten co-immunoprecipitatie experimenten zien dat PPARα een complex vormt met MEK1. Door gebruikt te maken van een PPARα gekoppeld aan GFP, laten we zien dat MEK1 expressie leidt tot binding en onttrekking van PPARα uit de kern naar het cytoplasma. Geheel in lijn met andere studies leidt truncatie van de LXXLL residue tot abrogatie van MEK1 binding aan PPARα. Aangezien bovenstaande bevindingen niet gelden voor PPARβ/δ lijkt de MEK1 geïnduceerde effect PPARα specifiek te zijn. Aangezien transgene muizen met hart-specifieke expressie van actieve MEK1 leidt tot concentrische hypertrophy zonder gehavend hart functie, hebben we gekeken naar PPARα activiteit gedurende fysiologische hypertrophy.

Samenvatting

Muizen die onderworpen zijn aan rennen in een kooi-wiel, ontwikkelen fysiologische hypertrophy met verhoogd MEK1 activiteit zien en verlaagd PPARα activiteit. In tegenstelling tot onze bevindingen in hoofdstuk 2 lijkt PPARα een rol te hebben in pathologische hypertrophy, maar dat andere mechanismen actief zijn gedurende fysiologische hypertrophy maar die de cardiomyocyte onafhankelijk maken van PPARα.

Integenstelling met PPARα en PPARγ is de expressiepatroon van PPARβ/δ veelal door het het gehele lichaam aanwezig. Daarnaast komt PPARβ/δ het hoogst tot expressie in het hart. In hoofdstuk 4 laten we zien dat specifieke afwezigheid van PPARβ/δ in hart dramatische gevolgen heeft de hart functie. Omdat PPARβ/δ null dieren al in complicaties gedurende de embrynale stadium laten zien, maken we gebruik van een Tamoxifen induceerbare hart-specifieke deletie van PPARβ/δ. Al na 5 dagen van afwezigheid van PPARβ/δ vertonen de desbetreffende dieren een vermoeide en zieke fenotype. Vedere analyse van de harten van deze dieren laat zien dat er een vergroting van het hart heeft opgetreden en dat er vervolgens een verergering heeft opgetreden in hartfunctie. Verder laten de dieren een verlaagd expressie van genen betrokken in vetzuur metabolisme en een verhoogd expressie van een glucose transporter zien. Dit alles duidt op een rol voor PPARβ/δ in het homeostase van het hart , maar vooral het belang van een functionele vetzuur metabolisme voor de hart functie.

Een bekende feit van transcriptiefactoren is dat ze samen met andere co-regulatoren complexen vormen om transcriptie mogelijk te maken. Naast bekende co-regulators zoals CBP/p300 en PGC-1α, is MEF2 betrokken bij trancriptionele regulatie van metabolisme in skeletspieren. Analyse van de mCPT1 promoter laat zien dat er een geconserveerde PPAR en MEF2 bindingsplaatsen naast elkaar liggen. Functionele analyse van deze bindingsplaatsen door middel van mutagenese laat zien dat beide bindingsplaatsen van belang zijn voor expressie van mCPT1. Door gebruik te maken van een transgene muizen die een dominante negatieve MEF2 (DNMEF2) tot expressie brengen, laten we in hoofdstuk 5 zien dat MEF2 een belangrijke rol speelt in de homeostase van het hart gedurende hypertrofie. Na 5 weken van aanhoudende hoge bloeddruk, laten we via echoacrdiografie zien dat na hypertrofie er veslechtering optreedt van hartfunctie bij de transgene muizen in verglijking met wildtype muizen. Aangezien histologische en hemodynamische analyses geen verschil lieten zien, hebben we, naar aanleiding van eerdere studies, gekeken naar verschillen in mitochondriale respiratoire keten.

DNMEF2 transgene muizen die blootgesteld zijn aan chronische hoge bloedruk lieten een verlaagd expressie zien van NADH dehydrogenase subunit 6 (ND6) in verglijking met wildtype dieren. Verlaagd expressie van ND6 resulteerde vervolgens tot inefficiënte mitochondrial functie waarbij er radicalen (ROS) vrijkomen met als gevolg dat de cardiomyocyten vatbaarder zijn voor apoptose. Hieruit blijkt dat naast regulatie van vetzuur metabolisme, de PPAR co-regulator MEF2 een belangrijk rol speelt in de (co)-regulatie van metabolisme in het hart gedurende pathologische hypertrophy.

In hoofdstuk 6 bediscussiëren we de belangrijkste bevindingen van dit proefschrift en de toekomstige richting voor het PPAR signalering onderzoek. Onze data benadrukken de belangrijkste bijdrage van de PPAR signalering gedurende hypertrofie en hart falen en onthullen de identiteit van PPAR gerelateerde genen in de hartspier. Dit alles kan een mogelijke bijdarge leveren aan de ontwikkeling van toekomstige therapeutische medicijnen voor de behandeling van hart en spier ziekten.

"Misschien is niets geheel waar, en zelfs dat niet"
Multatuli (1820-1887)

Acknowledgements

As with all things in life, great achievements are rarely accomplished on your own, therefore would like to thank all of the following people (those I can recall).

Leon:
What started with an unusual interview has led to a great experience the past years. Although my project wasn't in line with other projects you always found a way to keep me enthusiastic, and there I went with a full sprit and confidence that we are about to solve the missing link. As each morning the question… any new data?... is followed by great discussions and laughter, science was a hobby. I have learned many things from you, scientific and non-scientific, and it's therefore I am glad to say that I had a great teacher and a friend rather than a boss….N'uff said!

Dr. Marc van Bilsen:
As my second co-promoter I would like to thank you for the discussions and help the past years. The long trip all the way to Maastricht was paralleled by great scientific knowledge.

Prof. H. Clevers.
I would like to thank you for being my promoter and for the clever advise to not proceed with the ChIP-on-chip assay.

Prof. Arie Verkleij:
Thou it was at the end of the project, I would like to thank you for the discussions we had. Your knowledge about the topic has amazed me and I hope to benefit from your insights in the years to come.

The Group:
Paula (poolshark): As with a good receipt you brought the missing ease in the group. You have shown us that good science is always accompanied by bit of fun. I have enjoyed your presence and your witty comments and I wish you all the pleasure and affection with the new member in your little family. I only wonder how you will manage to get your last name on her jersey?
Meriem: Together we started our project and got to work with and bear each other's stress. I have got to know as a person who didn't hesitate to help and support. Not only am I very proud of you to have finished an excellent promotion, but much more that you have endured my way of doing science while using your materials (sorry for the everlasting mess).
Monika: I wanted to write this in your languish but I reasoned that it would be too polished. Starting as a technician you were already an example of great help and kindness, but when you became a Phd student it didn't change much. I am confident that you will be a great scientist and a great supplier of bird-milk.
Jenny: You joined the group in a very stressful time and together we had to learn a difficult

surgical technique. Despite this, you always kept your cheerful laughter and fanatical support for the team. Maybe one day FC Utrecht will get in the top five.
Kanita: As last but definitely not least you came in the group and were appreciated by all of us. Although your kindness is obviously, your passion for science is remarkable and yet I have to say to you that not all hairpins are microRNAs.
Roel: Although not a member of the group anymore and as modesty is your hallmark, I only become to realize what a great surgeon you are when I had the opportunity to learn from you. I also have to say that I enjoyed the philosophical discussion that we had followed by loud cursing, as we would of course forget to label our tubes while talking.
Ralph: As the senior Phd student in our group, I enjoyed our scientific discussions. Although we had some laughs about it, your punctuality is an example of doing science. I am confidant that you will do great science in the USA, and of course we will keep contact dusss.....
Eva and Vannessa: Unfortunalty, when I started both of you were finishing you're Phd and I didn't get the chance to get to know you better. Yet, both of you helped me starting up and explained a lot. Good luck to both of you!
Abdel-Azziz: I really enjoyed the soccer games and seeing you playing made me hesitate whether you're better off as a scientist, I think a carrier in sport would have been as great. On the other hand an excellent promotion showed a right decision and great potential.
I want to thank all the other colleagues that I have got to know during the past years including Bart, Melany, Joost, Mara, Anna (Faro), Simona and of course members of the Bakkers groep; Jeroen, Sonja, Ruben, Manon, Emma, Kelly, Anne, Merlijn and Karel

French delegation:
Anne-Sophie: As one of the first members in the group, I must admit that without you're help I wouldn't have come so far. It's amazing how a person can answer so many questions daily and never lose her patience. I can't even recall one moment that we disagreed on something... although I really dislike those ginger snacks.
Anne: As my former neighbor in the office I got to know you closely and we soon had our ways of making jokes. Of course, having so much fun in a scientific environment couldn't stay unnoticed and we got separated, only to start having more fun in the lab were we also were neighbors ☺I really appreciated your guidance and help during the whole period. It was a great privilege to have worked with both of you.

Greek delegation:
Stephanos: You came in our group to do a six-month project and it was amazing to see how a person could fit in a group within an hour. The longer period you stayed, than was planned, eventually resulted in a perfect mix of laughter and excellent science. I am certain that you will be an exceptional scientist.
Pantelis: Although not a member of the group and very busy, you always took time to help. Next to your remarkable passion for soccer and clandestine affection for pool, I also ap-

preciated your admirable scientific insights. Yet I regret to have introduced you to squash, since I only found myself awfully loosing the game. I have enjoyed working with both of you, but much more to get to know you guys as good friends.

Family:
Although not present at the daily practice, their contribution to this work is greatly appreciated. I would like to thank my sisters for there relentless support and I appreciate their interest in sometimes boring explanations of what I do. A special appreciation for my brother Samir, whose patience to join me and wait for me while working in the weekend was of great help in the past years. I hope you want to wait once more since I would be greatly honored to have you as my paranimf. Ibrahim, as the little brother (only in age) your support and help is greatly appreciated. The design of this thesis and many of my figures show a great talent and I hope we can work together in the future.

The small gang:
To my wife, your support from the beginning, I still remember it well, made me decide to stay in science. As science has unusual working hours you kept supporting me and even tried to understand and help. As I am a person of many words I would like to say.. Thank you!! and I am looking forward for the years to come. Yassin (4): your presence has greatly influenced me. Your energy in the things you do always amazed me and what's more showed me that one can't get tired of things if one likes doing them. Tasnim (2 months): Unaware of the things happening around you still managed to achieve something impossible without your presence, the deadline of submission. I would not have made it if it weren't that I had to finish before your birth.

My Parents:
Father: As you are a man of a view words, there are not many people I know that can compete with your knowledge. I have always found great inspiration in you and your mere presence has thought me what's really important in life. Mother: The same holds for you also, your concerns about health and amount of work always filled me compassion. I know that your concerns are not easily vanished but I promise that I always will be the little boy you still remember.

Hubrecht Instituut:
I would like to the people that made working in the Hubrecht a memorable time including Thea, Anneke, Romke, Jules, Richard, Susann, Sofia, Ira and Janny and the rest without naming them. Special thanks to the animal caretakers (Miep, Petra, Benaissa and Mark), for their great patience and help.

Curriculum Vitae

Hamid el Azzouzi werd geboren op 20 april 1977 te Gzenaya (Marokko). In 1998 behaalde hij het VWO (Atheneum) diploma aan het Openbare Scholengemeenschap Schoonoord te Zeist, en ging hij Biologie studeren aan de Universiteit Utrecht. In het kader van deze studie deed hij 2 onderzoeksstages. Zijn eerste stage was bij de afdeling Moleculaire Celbiologie, Instituut Biomembranen, Universiteit Utrecht onder begeleiding van Dr. Paul van Bergen en Henegouwen. Zijn tweede stage werd uitgevoerd bij de afdeling Virologie, aan de faculteit Diergeneeskunde in Utrecht, onder begeleiding van Dr. R. de Groot. In oktober 2003 behaalde hij het doctoraal examen voor Biologie. In april 2004 is hij als assistent in opleiding begonnen aan het Hubrecht Instituut te Utrecht, onder leiding van Dr. Leon de Windt . De resultaten van dat onderzoek staan beschreven in dit proefschrift.

List of Publications

Papers:

Smits SL, van Vliet AL, Segeren K, **el Azzouzi H**, van Essen M, de Groot RJ. Torovirus non-discontinuous transcription: mutational analysis of a subgenomic mRNA promoter. J Virol. 2005;103:228-231.

Horsthuis T, Houweling AC, Habets PE, de Lange FJ, **el Azzouzi H**, Clout DE, Moorman AF, Christoffels VM. Distinct regulation of developmental and heart disease-induced atrial natriuretic factor expression by two separate distal sequences. Circ Res. 2008;102:849-859.

El Azzouzi H, De Windt LJ. Heart spotting. Basic Res Cardiol. 2008;103:228-231

Armand AS, Bourajjaj M, Martínez-Martínez S, **el Azzouzi H**, da Costa Martins PA, Hatzis P, Seidler T, Redondo JM, De Windt LJ. Cooperative synergy between NFAT and MyoD regulates myogenin expression and myogenesis. J Biol Chem. 2008;283:29004-10.

el Azzouzi H,* van Oort RJ, * van der Nagel, R*, Sluiter W, Bergmann MW, De Windt LJ. MEF2 transcriptional activity maintains mitochondrial adaptation in cardiac pressure overload. In revision at J. Am. Coll. Cardiol.
*authors contributed equally

Bertrand AT*, **el Azzouzi H***, van Empel VPM*, van der Nagel R, Crijns HJ, Hofstra L, Doevendans PA, De Windt LJ. Nuclear accumulation of Apoptosis-Inducing Factor fails to induce cardiac muscle apoptosis. J Biol Chem. In Revision
*authors contributed equally

el Azzouzi H, Leptidis S, Bourajjaj M, van der Nagel R, van Bilsen M, De Windt LJ. PPAR gene profiling uncovers insulin-like growth factor-1 (IGF1) as a PPAR-alpha target gene in cardioprotection. Submitted

El Azzouzi H, Leptidis S, De Windt LJ. The mitogen activated protein kinase kinase (MAPKK) MEK1 inhibits cardiac PPARα activity through nuclear export. Submitted

Bookchapters:

El Azzouzi H, Bourajjaj M, da Costa Martins P, De Windt LJ. Apoptosis in cardiovascular pathogenesis. In: Essentials of Apoptosis. A Guide for Basic and Clinical Research. Eds. XM Yin and Z Dong (Eds). 2008 Humana Press Inc (US).